EFFECT OF PERMAFROST THAW ON METHANE AND CARBON DIOXIDE EXCHANGE IN TWO WESTERN ALASKA PEATLANDS

by

Carmel Eliise Johnston

A thesis submitted in partial fulfillment
of the requirements for the degree

of

Master of Science

in

Land Resources and Environmental Sciences

MONTANA STATE UNIVERSITY
Bozeman, Montana

August 2013

©COPYRIGHT

by

Carmel Eliise Johnston

2013

All Rights Reserved

APPROVAL

of a thesis submitted by

Carmel Eliise Johnston

This thesis has been read by each member of the thesis committee and has been found to be satisfactory regarding content, English usage, format, citation, bibliographic style, and consistency and is ready for submission to The Graduate School.

Dr. Stephanie Ewing

Approved for the Department of Land Resources and Environmental Sciences

Dr. Tracy Sterling

Approved for The Graduate School

Dr. Ronald W. Larsen

STATEMENT OF PERMISSION TO USE

In presenting this thesis in partial fulfillment of the requirements for a master's degree at Montana State University, I agree that the Library shall make it available to borrowers under rules of the Library.

If I have indicated my intention to copyright this thesis by including a copyright notice page, copying is allowable only for scholarly purposes, consistent with "fair use" as prescribed in the U.S. Copyright Law. Requests for permission for extended quotation from or reproduction of this thesis in whole or in parts may be granted only by the copyright holder.

Carmel Eliise Johnston

August 2013

ACKNOWLEDGEMENTS

I would like to thank my advisor, Dr. Stephanie Ewing for her guidance, motivation, and for allowing me to have the incredible opportunity to conduct novel research in one of the most beautiful places on Earth. Her dedication to the development and improvement of myself as a student, researcher, and a person has pushed me to be better than I thought I could. Her commitment to producing quality research and a thought provoking classroom while maintaining a well-balanced lifestyle has been nothing short of inspirational. I would also like to extend my gratitude to my committee members Dr. Jennifer Harden and Dr. Paul Stoy for showing a steadfast commitment to my education and growth as a researcher. They have always helped me to see the bigger picture, which can be easy to lose when focusing on the details.

Thanks to my Ewing Lab mates, Christine Miller and Adam Sigler, and Stoy Lab friends, Aiden Johnson and Christopher Welch, for their collaboration, letting me think out loud, and for their love and friendship. Thank you to two summers of field crews who helped collect a whole heck of a lot of data and instigated a couple of crazy adventures: Christopher Dorich, Claire Treat, Rebecca Finger, Nicole McConnell, Lily Cohen, Lillian Aoki, Anna Lello-Smith, and Carme Estruch.

Lastly, thank you to my family and friends, who may not care for all the gory details of permafrost thaw but still listened to me anyway. Their love, support, and encouragement right to the end is much appreciated.

TABLE OF CONTENTS

TABLE OF CONTENTS-CONTINUED

TABLE OF CONTENTS-CONTINUED

LIST OF TABLES

LIST OF TABLES-CONTINUED

Table Page

LIST OF FIGURES

LIST OF FIGURES CONTINUED

LIST OF FIGURES CONTINUED

LIST OF FIGURES CONTINUED

LIST OF FIGURES CONTINUED

LIST OF FIGURES CONTINUED

Figure Page

GLOSSARY

CO_2 : Carbon dioxide
CH_4: Methane
NEE: Net ecosystem exchange
ER: Ecosystem respiration

ABSTRACT

Methane (CH_4) causes about 20% of greenhouse gas radiative forcing despite its relatively short lifetime (~10 y) and low concentration (1800 ppb) in the atmosphere. Wetlands are the largest natural source of CH_4, amounting to 22% of CH_4 production globally, with emission of CH_4-C by both diffusion and ebullition pathways. Permafrost peatlands store about 10% of permafrost C and 5% of global belowground C; hence CH_4-C emission with peatland permafrost thaw is of concern. We quantified temporal and spatial aspects of CH_4 and CO_2 emissions from northern peatlands using two approaches: (1) a ~1000 y thaw chronosequence in remote western Alaska (Innoko Flats Wildlife Refuge; May-September, 2011), and (2) lateral transects in intermediate age (~20-500 y) collapse-scar bog features at a well-instrumented site near Fairbanks, Alaska (Alaska Peatland Experiment (APEX)/Bonanza Creek Long Term Experimental Research site; June-September, 2012). At Innoko Flats, peak CH_4 production was observed in features aged 30-590 y since thaw, which had warmer soils than younger sites and shallower water tables than older sites. Average surface flux at these 30-590 y sites (+2.52 ± 0.98 mg CH_4-C m^{-2} hr^{-1}) was greater than estimated ebullition flux (0.13 ± 0.05 mg CH_4-C m^{-2} hr^{-1}) based on an observed rate of 0.78 ± 0.33 mL m^{-2} hr^{-1}. Net ecosystem exchange of CO_2-C (NEE) did not differ among chronosequence features, and offset CH_4-C emissions by a factor of 2 to 400 when considered as 100-y global warming potential. At APEX, bogs reflecting <100 y since most recent thaw showed high variability in CH_4 exchange, but rates were generally consistent with levels at the Innoko 30-590 y sites (mean of 5.42 ± 1.16 mg CH_4-C m^{-2} hr^{-1}). APEX bogs showed greater balance between CH_4-C efflux and CO_2-C influx, with CH_4-C fluxes offsetting 80-140% of NEE during the growing season when considered as 100-y global warming potential. We argue that CH_4 contributes most significantly to post-thaw C loss over timescales of decades to centuries in these northern peatlands.

CHAPTER 1

1.0 INTRODUCTION

1.1 Effect of Global Temperature Change on Permafrost Carbon

Permafrost soils cover 16% of Earth's surface, but store over half of the world's total belowground carbon (C) (Tarnocai *et al.* 2009; Hugelius *et al.* in revision). These soils have acted as sinks for atmospheric C over several millennia and particularly since the last interglacial period (MacDonald *et al.* 2006; Froese *et al.* 2008), resulting in large stores of terrestrial C over long timescales (Grosse *et al.* 2011). Like other pathways of natural sequestration, however, these rates of C uptake are generally slow compared to anthropogenic CO_2 production (Harden *et al.* 1992). Moreover, most permafrost soils are found at high latitudes where rates of climate warming are greatest (Qin *et al.* 2007), and are now increasingly vulnerable to thaw and accelerated loss of C as CO_2 and CH_4, resulting in a positive feedback to warming (Osterkamp 2005; Jorgenson and Osterkamp 2005; Schuur *et al.* 2008, 2013; Jorgenson *et al.* 2010, 2013).

In northern peatlands, permafrost degradation reorganizes peat hydrology, thermal regimes, and plant species assemblages (Jorgenson *et al.* 2013). Wetter soil conditions commonly associated with lowland permafrost thaw can make permafrost more vulnerable, even in regions with colder mean annual air temperatures (Jorgenson *et al.* 2010; Schuur *et al.* 2008). Meanwhile, if conditions become drier due to altered drainage with thaw, fire intensity and frequency can increase (Frolking *et al.* 2011) and lead to deeper thaw (O'Donnell *et al.* 2011a). Mineral substrate may drive these outcomes by controlling drainage patterns and hence hydrologic reorganization upon thaw (Jorgenson *et al.* 2013; Johnson *et al.* in revision.)

Over the last half century, Alaska has undergone significant climatic change (Hinzman *et al.* 2005, 2006; Osterkamp *et al.* 2009), leading to transformation of permafrost dominated landscapes (Jorgenson *et al.* 2013). On the Tanana Flats, near Fairbanks, AK, 49% of the area is affected by thermokarst bog formation (Jorgenson *et al.* 2001). More generally, the area of near-surface permafrost in Arctic and boreal systems has decreased steadily over the past 100 years, and nearly all permafrost is projected to be gone by the year 2100 (Lawrence *et al.* 2008; Heginbottom *et al.* 2013).

Over timescales of decades to centuries, boreal forests have been acting as slight net sinks for C from the atmosphere to land, but periods of disturbance such as drought and severe fire activity can make these systems net sources of C (Harden *et al.* 2000). Development of drought conditions reduces the success of black spruce and *Sphagnum*, decreasing long-term ecosystem carbon storage in the adjacent landscape (Myers-Smith *et al.* 2008). Additionally, warming and/or increased fire disturbance can promote permafrost degradation and bog expansion (Myers-Smith *et al.* 2008), leading to hydrologic reorganization and increased C loss (Jorgenson *et al.* 2001, 2013). In general, the disturbance caused by climate warming may result in significant redistribution of C among major reservoirs such as terrestrial soils, the Arctic ocean, and the atmosphere, contributing to the change in net C source/sink characteristic of these high-latitude soils

(Grosse *et al.* 2011). Consistent with chronic loss of permafrost area, permafrost soils also may become a net source of C by the end of this century (Koven *et al.* 2011).

1.2 Importance of Methane and Emissions

Methane is an important greenhouse gas whose balance in the atmosphere is strongly affected by wetlands, including northern peatlands (Gorham 2013). Methane contributes about 20% of greenhouse gas forcing despite its relatively short lifetime (~10 y) and low concentration (1800 ppb) in the atmosphere (Qin *et al.* 2007). Wetlands are the largest natural source of CH_4, contributing 22% of CH_4 production globally. Northern peatlands contribute ~13% (15-50 Tg y^{-1}) of global CH_4 emissions and host about 10% of permafrost C (Tarnocai *et al.* 2009). Hence, despite covering only a small proportion of the Earth's surface (~3%; Frolking *et al.* 2011; Roulet *et al.* 2007; Limpens *et al.* 2008), these regions have the potential to be a large biogeochemical feedback to the climate system (Olefeldt *et al.* 2012).

To understand the balance of CH_4 in the atmosphere and its response to permafrost degradation, we must first characterize the belowground production of CH_4 and controls on its subsequent release. However, we do not fully understand the hydrologic and biogeochemical processes controlling CH_4 exchange in most environments, including northern peatlands (Frolking *et al.* 2011; Jorgenson *et al.* 2010; Turetsky *et al.* 2002). Soil temperature and soil moisture are known to have a strong influence on CH_4 release, and can explain up to 75% of the variance in CH_4 flux in high-latitude wetlands regardless of vegetation type (Torn and Chapin 1993; Olefeldt *et al.*

2012). Other factors may include vegetation type (vascular vs non-vascular) and microbial community (Torn and Chapin 1993).

Methane emissions from wetlands are transported to the atmosphere by diffusive and ebullitive pathways (Figure 1; Oleson *et al.* 2013). In these carbon-rich, anoxic environments, 18-50% of CH_4 release may occur as ebullition (release of subsurface bubbles; (Christensen and Panikov 2003; Goodrich *et al.* 2011; Whalen 2005). Ebullition events can be difficult to quantify because their magnitude and frequency reflect both biotic and physical controls. Biotic controls include suites of organisms (Waldrop *et al.* 2012) and locally specific consortia of methanogens and methanotrophs (Zak and Kling 2006). Ebullition fluxes are additionally complicated by the physical controls imposed by water table height, atmospheric pressure, floating moss mats and plant mediated transport to the atmosphere (Strack *et al.* 2005; Strack and Waddington 2007; Tokida *et al.* 2007a; Cronk and Fennessy 2001). The result of these combined biotic and physical controls is highly episodic releases of CH_4, resulting in highly stochastic observed fluxes (Goodrich *et al.* 2011). In one small ombrotrophic peatland in Japan, Tokida *et al.* (2007b) observed a large burst of CH_4 immediately upon thaw of surface ice cover. At another northern peatland in northeast Greenland, Mastepanov *et al.* (2008) documented a large burst of CH_4 during the late autumn freeze-up period. These events were similar in magnitude to peak growing season emissions, showing that processes occurring in the cold and shoulder seasons are important to consider when evaluating total CH_4 exchange. With snow and ice melt in spring, accumulated bubbles can be released directly into the atmosphere, causing a burst of CH_4 (Tokida *et al.* 2007b). As the active layer beings to freeze from the top down in fall, CH_4 produced or accumulated in this layer may be squeezed out through frost activity (Mastepanov *et al.* 2008).

Ultimately, permafrost thaw influences carbon dioxide (CO_2) and CH_4 emissions by transforming the belowground habitat, including increasing the availability of belowground C stores to microbial metabolism and changing the oxidative state of the belowground environment through inundation and drainage (Jorgenson *et al.* 2001; Jorgenson and Osterkamp 2005; O'Donnell *et al.* 2011b). Understanding the effect of permafrost thaw on biotic and abiotic conditions that control trace gas exchange and thus global warming potential over longer timescales is critical for predicting outcomes of climate warming. The relative contribution of CH_4 and CO_2 exchange both determine the C balance of an ecosystem – particularly if that ecosystem is hydrologically isolated - and provide a metric of net C uptake or release with permafrost thaw.

1.3 Brief Overview of Research Questions and Approach

My work investigated the effects of thaw on trace gas exchange in the context of changes in total C stocks, physical collapse, inundation, and plant community succession that accompany thaw trajectories in lowland settings. To examine the effects of lowland permafrost thaw on C release over decadal to millennial timescales, I quantified CH_4 and CO_2 exchange in two studies on related landscapes: a chronosequence of thermokarst bog and fen features developed within a degrading peatland in western Alaska (Innoko Flats Wildlife Refuge), and a series of a lateral transects across recent collapse-scar features (Alaska Peatland Experiment/Bonanza Creek LTER). Both efforts were in collaboration with research teams undertaking a broader suite of measurements, under grants with the National Science Foundation (NSF) and the United States Geological Survey (USGS).

This investigation began with the observation that thaw of permafrost in northern peatlands has the potential to release a substantial pool of carbon. A positive feedback to climate warming may result, depending on the character and rate of C exchange, as well as ecosystem response. Consequently we asked:

Q_1: In northern peatlands, what is the balance and magnitude of CO_2 and CH_4 exchange as a function of time since permafrost thaw?

Our approach to addressing this question was shaped by two related hypotheses:

$H_{1.1}$: In northern lowlands with poorly drained soils (frozen peatlands), permafrost thaw leads to inundation and C release as CH_4.

$H_{1.2}$: In northern lowlands, warming will increase the release of CH_4 relative to CO_2 uptake (net C source) over decades to millennia.

Consequently we developed the following objective:

O_1: Quantify seasonal CO_2 and CH_4 exchange in a ~1000-y chronosequence within a degrading peatland, accounting for known controlling variables (water table height, subsurface temperature, peat C stock) in the context of topographic relationships.

Therefore at Innoko Flats, I worked with field crews to quantify CH_4 and CO_2 at three time points during the 2011 growing season, focusing on a ~1000-y chronosequence of thaw features. I coupled these measurements with assessment of landscape feature age and other data collected by the research team -- continuously logged soil temperature and water table measurements, ground level elevation surveys and inventories of C stocks -- to determine the effect of temperature and water table position on C fluxes.

At Innoko Flats we found that methane efflux increased with time since thaw initiation, with highest methane efflux occurring after 30-590 y of thaw. When we evaluated methane and CO_2 flux together, we found that all sites were net C sinks -- CO_2 uptake outweighed CH_4 efflux in terms of global warming potential, by a factor of two to 400. Based on our findings at Innoko we asked:

Q_2: How does CH_4 exchange within similar thaw features of intermediate age (decades to centuries) vary with thaw feature position and mode of exchange (diffusion vs. ebullition)?

Our approach to addressing this question in the subsequent year (2012) was shaped by the following hypotheses:

$H_{2.1}$: Thaw features of comparable age will have comparable methane efflux and CO_2 exchange.

$H_{2.2}$: Edges of comparable thaw features will produce greater methane efflux than centers due to wetter conditions.

Consequently we developed our study objective at APEX:

O_2: Quantify seasonal diffusive CO_2 and CH_4 flux, and subsurface CH_4 production, in thaw features of similar age (20-50 y) as a function of position (edge, center, intermediate location).

In conversation with investigators at APEX/Bonanza Creek, I undertook a targeted gas flux study during the summer of 2012. In this work, I investigated the effect of position on measures of CH_4 flux in thaw features initially estimated to be 27 y to 42 y post thaw, comparable in age to sites where maximum CH_4 flux had been observed at Innoko Flats. I worked with field crews to quantify CH_4 and CO_2 fluxes throughout the growing season, and undertook two different methods of measuring ebullition events to see how those events varied with position across replicates of intermediate aged bogs. This work showed that APEX features comparable in age to Innoko intermediates had comparable methane fluxes with similar seasonal patterns. However, position within these thaw features was not an important predictor of methane efflux. Seasonal patterns emerged for individual features when positions were combined. Unlike observations at the Innoko sites, gas flux results suggested that thaw at the APEX sites had a potential net warming effect: when considered as global warming potential, methane efflux generally equaled or exceeded CO_2 uptake. These results provide evidence of the circumstances of change in C balance over decadal to millennial timescales in these lowland settings.

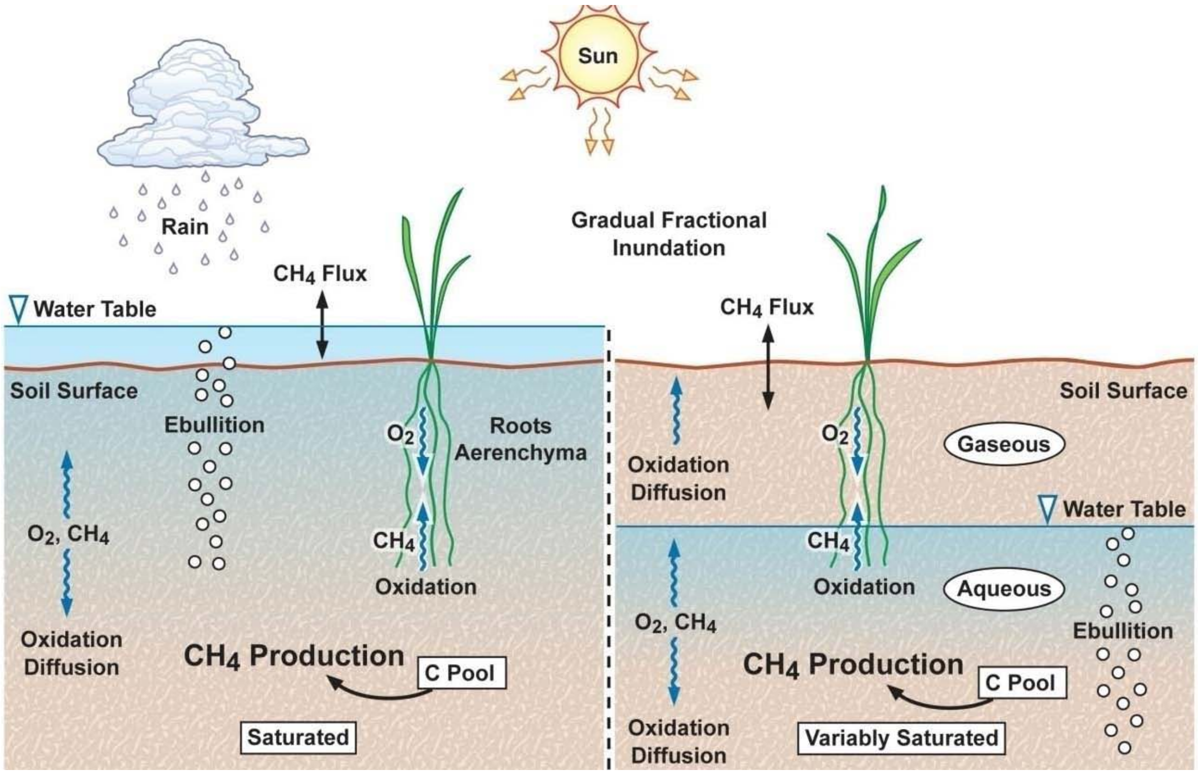

Figure 1: A conceptual description of methane dynamics in the Community Land Model version 4.5 (CLMv4.5) following Oleson *et al.*. (2013) and related references. A schematic representation of biological and physical processes integrated in CLM that affect the net CH_4 surface flux are displayed for inundated (left) and non-inundated (right) conditions.

1.4 References

Christensen T R and Panikov N 2003 Biotic controls on CO_2 and CH_4 exchange in wetlands – a closed environment study *Biogeochemistry* **64** 337–54

Cronk J and Fennessy M 2001 *Wetland plants: biology and ecology* (CRC Press LLC)

Froese D G, Westgate J A, Reyes A V., Enkin R J and Preece S J 2008 Ancient permafrost and a future, warmer Arctic. *Science* **321** 1648

Frolking S, Talbot J, Jones M C, Treat C C, Kauffman J B, Tuittila E and Roulet N 2011 Peatlands in the Earth's 21st century climate system *Environmental Review* **19** 371–96

Goodrich J P, Varner R K, Frolking S, Duncan B N and Crill P M 2011 High-frequency measurements of methane ebullition over a growing season at a temperate peatland site *Geophysical Research Letters* **38** 1–5

Gorham E 2013 Northern peatlands: role in the carbon cycle and probable responses to climatic warming *Ecological Society of America* **1** 182–95

Grosse G, Harden J, Turetsky M, McGuire A D, Camill P, Tarnocai C, Frolking S, Schuur E A G, Jorgenson T, Marchenko S, Romanovsky V, Wickland K P, French N, Waldrop M, Bourgeau-Chavez L L and Striegl R G 2011 Vulnerability of high-latitude soil organic carbon in North America to disturbance *Journal of Geophysical Research* **116** 1–23

Harden J W, Mark R K M, Sundquist E T and Stallard R F 1992 Dynamics of soil carbon during deglaciation of the laurentide ice sheet. *Science (New York, N.Y.)* **258** 1921–4

Harden J W, Trumbore S E, Stocks B J, Hirsch A, Gower S T, O'Neill K P and Kasischke E S 2000 The role of fire in the boreal carbon budget *Global Biogeochemical Cycles* **6** 174–84

Hinzman L D, Bettez N D, Bolton W R, Chapin F S, Dyurgerov M B, Fastie C L, … Yoshikawa K 2005 Evidence and Implications of Recent Climate Change in Northern Alaska and Other Arctic Regions *Climatic Change* **72** 251–98

Hinzman L D, Viereck L A, Adams P C, Romanovsky V E and Yoshikawa K 2006 Climatic and Permafrost Dynamics of the Alaskan Boreal Forest *Alaska's Changing Boreal Forest* ed F S C III, M W Oswood, K V Cleve, L A Viereck and D Verbyla (Oxford, United Kingdom) pp 39–61

Hugelius G, Tarnocai C, Bockheim J, Camill P, Elberling B, Grosse G, Harden J, Johnson K, Jorgenson T, Koven C, Kuhry P, Michaelson G, Mishra U, Palmtag J, Ping C-L, O'Donnell J, Schirrmeister L, Schuur E, Sheng Y, Smith L, Strauss J and Yu Z Short communication: A new dataset for estimating organic carbon storage to 3 m depth in soils of the northern circumpolar permafrost region *Earth System Science Data Discussions* **6**

Johnson K D, Harden J W, McGuire A D, Clark M, Yuan F and Finley A Permafrost and organic layer interactions over a climate gradient in a discontinuous permafrost zone *Environmental Research Letters* in review

Jorgenson M T, Harden J, Kanevskiy M, Donnell J O, Wickland K, Ewing S, Manies K, Zhuang Q, Shur Y, Striegl R and Koch J 2013 Reorganization of vegetation , hydrology and soil carbon after permafrost degradation across heterogeneous boreal landscapes *Environmental Research Letters* **8** 1–13

Jorgenson M T and Osterkamp T E 2005 Response of boreal ecosystems to varying modes of permafrost degradation *Canadian Journal of Forestry Research* **35** 2100–11

Jorgenson M T, Racine C H, Walters J C and Osterkamp T E 2001 Permafrost degradation and ecological changes associated with a warming climate in central alaska *Climate Change* **48** 551–79

Jorgenson M T, Romanovsky V, Harden J, Shur Y, O'Donnell J A, Schuur E A G, Kanevskiy M and Marchenko S 2010 Resilience and vulnerability of permafrost to climate change *Canadian Journal of Forestry Research* **40** 1219–36

Koven C D, Ringeval B, Friedlingstein P, Ciais P, Cadule P, Khvorostyanov D, Krinner G and Tarnocai C 2011 Permafrost carbon-climate feedbacks accelerate global warming. *Proceedings of the National Academy of Sciences of the United States of America* **108** 14769–74

Lawrence D M, Slater A G, Romanovsky V E and Nicolsky D J 2008 Sensitivity of a model projection of near-surface permafrost degradation to soil column depth and representation of soil organic matter *Journal of Geophysical Research* **113** 1–14

Limpens J, Berendse F, Blodau C, Canadell J G, Freeman C, Holden J, Roulet N, Rydin H and Schaepman-Strub G 2008 Peatlands and the carbon cycle: from local processes to global implications – a synthesis *Biogeosciences* **5** 1475–91

MacDonald G M, Beilman D W, Kremenetski K V, Sheng Y, Smith L C and Velichko A a 2006 Rapid early development of circumarctic peatlands and atmospheric CH_4 and CO_2 variations. *Science (New York, N.Y.)* **314** 285–8

Mastepanov M, Sigsgaard C, Dlugokencky E J, Houweling S, Ström L, Tamstorf M P and Christensen T R 2008 Large tundra methane burst during onset of freezing *Nature* **456** 628–30

Myers-Smith I H, Harden J W, Wilmking M, Fuller C C, McGuire A D and Chapin III F S 2008 Wetland succession in a permafrost collapse : interactions between fire and thermokarst *Biogeosciences* **5** 1273–86

O'Donnell J A, Harden J W, McGuire A D and Romanovsky V E 2011a Exploring the sensitivity of soil carbon dynamics to climate change, fire disturbance and permafrost thaw in a black spruce ecosystem *Biogeosciences* **8** 1367–82

O'Donnell J A., Harden J W, McGuire A. D, Kanevskiy M Z, Jorgenson M T and Xu X 2011b The effect of fire and permafrost interactions on soil carbon accumulation in an upland black spruce ecosystem of interior Alaska: implications for post-thaw carbon loss *Global Change Biology* **17** 1461–74

Olefeldt D, Turetsky M R, Crill P M and McGuire a D 2012 Environmental and physical controls on northern terrestrial methane emissions across permafrost zones *Global Change Biology* **19** 589–603

Oleson K W, Lawrence D M, Bonan G B, Drewniak B, Huang M, Koven C D, Levis S, Li F, Riley W J, Subin Z M, Swenson S C, Thornton P E, Bozbiyik A, Fisher R, Heald C L, Kluzek E, Lamarque J-F, Lawrence P J, Leung L R, Lipscomb W, Muszala S, Ricciuto D M, Sacks W, Sun Y, Tang J and Yang Z-L 2013 Technical Description of Version 4.5 of the Community Land Model (CLM) *NCAR/TN-503+STR* pp 1-434

Osterkamp T 2005 The recent warming of permafrost in Alaska *Global and Planetary Change* **49** 187–202

Osterkamp T E, Jorgenson M T, Schuur E A G, Shur Y L, Kanevskiy M Z and Vogel J G 2009 Physical and ecological changes associated with warming permafrost and thermokarst in Interior Alaska *Permaforst and Periglacial Processes* **256** 235–56

Potter C S 1997 An ecosystem simulation model for methane production and emission from wetlands *Global Biogeochemical Cycles* **11** 495

Qin D, Manning M, Marquis M and Averyt K 2007 *Climate Change 2007: The Physical Science Basis* (Cambridge University Press)

Roulet N T, Lafleur P M, Richard P J H, Moore T R, Humphreys E R and Bubier J L 2007 Contemporary carbon balance and late Holocene carbon accumulation in a northern peatland *Global Change Biology* **13** 397–411

Schuur E A. G, Abbott B W, Bowden W B, Brovkin V, Camill P, Canadell J G, … Zimov S A. 2013 Expert assessment of vulnerability of permafrost carbon to climate change *Climatic Change* **119** 359–74

Schuur E A G, Bockheim J G, Canadell J G, Euskirchen E, Field C B, Goryachkin S V., Hagemann S, Kuhry P, Lafleur P M, Lee H, Mazhitova G, Nelson F E, Rinke A, Vladimir E, Shiklomanov N, Tarnocai C, Venevsky S, Vogel J G and Zimov S A 2008 Vulnerability of permafrost carbon to climate change : implications for the global carbon cycle *Bioscience* **58** 701–14

Strack M, Kellner E and Waddington J M 2005 Dynamics of biogenic gas bubbles in peat and their effects on peatland biogeochemistry *Global Biogeochemical Cycles* **19** GB 1003

Strack M and Waddington J M 2007 Response of peatland carbon dioxide and methane fluxes to a water table drawdown experiment *Global Biogeochemical Cycles* **21** GB1007

Tarnocai C, Canadell J G, Schuur E A G, Kuhry P, Mazhitova G and Zimov S A 2009 Soil organic carbon pools in the northern circumpolar permafrost region *Global Biogeochemical Cycles* **23** 1–11

Tokida T, Miyazaki T, Mizoguchi M, Nagata O, Takakai F, Kagemoto A and Hatano R 2007a Falling atmospheric pressure as a trigger for methane ebullition from peatland *Global Biogeochemical Cycles* **21** GB2003

Tokida T, Mizoguchi M, Miyazaki T, Kagemoto A, Nagata O and Hatano R 2007b Episodic release of methane bubbles from peatland during spring thaw. *Chemosphere* **70** 165–71

Torn M and Chapin III F S 1993 Environmental and biotic controls over methane flux from arctic tundra *Chemosphere* **26** 357–68

Turetsky M R, Wieder R K and Vitt D H 2002 Boreal peatland C fuxes under varying permafrost regimes *Soil Biology and Biochemistry* **34** 907–12

Waldrop M P, Harden J W, Turetsky M R, Peterson D G, McGuire A D, Briones M J, Churchill A C, Doctor D H and Pruett L E 2012 Bacterial and enchytraeid abundance accelerate soil carbon turnover along a lowland vegetation gradient in interior Alaska *Soil Biology and Biochemistry* **50** 188–98

Whalen S C 2005 Biogeochemistry of methane exchange between natural wetlands and the atmosphere *Environmental Engineering Science* **22** 73–94

Zak D R and Kling G W 2006 Microbial Community Composition and Function across an Arctic Tundra Landscape *Ecological Society of America* **87** 1659–70

CHAPTER 2

2.0 EFFECT OF PERMAFROST THAW ON CO_2 AND CH_4 EXCHANGE IN A WESTERN ALASKA PEATLAND CHRONOSEQUENCE

Contribution of Authors and Co-Authors

Manuscript in Chapter 2

Author: Carmel Eliise Johnston

Contributions: Carmel Johnston was responsible for data collection, data analysis, and original composition of manuscript.

Co-Author: Dr. Stephanie A. Ewing

Contributions: Dr. Stephanie A. Ewing was responsible for project conceptualization and methodologies, securing funding, undertaking field logistics, leading field campaigns, data collection, data analysis, and original manuscript writing and editing.

Co-Author: Dr. Jennifer W. Harden

Contributions: Dr. Jennifer W. Harden was responsible for leading project conceptualization and initiation, securing funding, field design, data collection, radiocarbon data analysis, ^{210}Pb dating analysis, and manuscript writing and editing.

Co-Author: Dr. Paul C. Stoy

Contributions: Dr. Paul Stoy contributed methodologies for data collection and analysis, data analysis, and editing of manuscript.

Co-Author: Dr. Ruth K. Varner

Contributions: Dr. Ruth Varner contributed equipment and methodologies for data collection, sample analysis, data analysis, and editing of manuscript.

Contribution of Authors and Co-Authors- Continued

Co-Author: Dr. Kimberly P. Wickland

Contributions: Dr. Kimberly Wickland contributed equipment and methodologies for data collection and analysis, data for dissolved methane profiles and percent respired methane, and editing of manuscript.

Co-Author: Dr. Joshua C. Koch

Contributions: Dr. Joshua Koch contributed data collection expertise, collection and analysis of water quality samples and survey data, and editing of manuscript.

Co-Author: Dr. Christopher Fuller

Contributions: Dr. Christopher Fuller contributed radiocarbon data analysis, ^{210}Pb dating analysis, and editing of manuscript.

Co-Author: M. Torre Jorgenson, M.S.

Contributions: M. T. Jorgenson was responsible for project conceptualization and initiation, securing funding, field design, data collection and sensor deployment, primary logistical support, data collection, and editing of manuscript.

Manuscript Information Page

Carmel E. Johnston, Stephanie A. Ewing, Jennifer W. Harden, Paul C. Stoy, Ruth K. Varner, Kimberly P. Wickland, Joshua Koch, Christopher Fuller, Mark T. Jorgenson
Environmental Research Letters
Status of Manuscript:
____ Prepared for submission to a peer-reviewed journal
_X_ Officially submitted to a peer-review journal
____ Accepted by a peer-reviewed journal
____ Published in a peer-reviewed journal

IOP Publishing: Environmental Research Letters
May 31, 2013
Focus on the Impact of Climate Change on Wetland Ecosystem Carbon Dynamics

2.1 Abstract

Permafrost soils store over half of global belowground carbon (C), and northern hemisphere frozen peatlands store about 10% of permafrost C. Many high latitude lowland peatlands are undergoing thaw and inundation, which may increase the surface-atmosphere flux of methane (CH_4), a potent greenhouse gas. To examine the effects of lowland permafrost thaw over millennial timescales, we measured CO_2 and CH_4 flux from the soil to the atmosphere along a ~1000-y thaw chronosequence of sites at Innoko Flats Wildlife Refuge in western Alaska. Peak CH_4 exchange (+2.52 ± 0.98 mg CH_4-C m^{-2} hr^{-1}) was observed in features that have thawed for 30-590 y, where soils were warmer than at more recently thawed sites (15-34 y), with shallower water tables and a less dense moss structure than at older sites (570-1700 y). In terms of global warming potential, CH_4 flux at intermediate age sites offset 49 ± 21% of site level net ecosystem exchange (NEE). Our results provide evidence that CH_4 emissions following lowland permafrost thaw are enhanced over decadal time scales, but limited over millennia. Over longer timescales (~2000 y), expansion of fen systems may lead to sustained increases in CH_4 flux. Future research should investigate the establishment of thaw features in high-latitude lowland peatlands, which may represent a hot spot and hot moment of methane flux to the atmosphere.

2.2 Introduction

Over half of global belowground C is stored in permafrost soils, largely at high latitudes where rates of climate warming are greatest (Qin *et al.* 2007; Tarnocai *et al.* 2009). Globally, permafrost soils have acted as sinks for atmospheric C since the last interglacial period (MacDonald *et al.* 2006; Froese *et al.* 2008), and are now subject to increased thaw and C release due to climate warming (O'Donnell *et al.* 2010). The area of near-surface permafrost in Arctic and boreal systems has decreased steadily over the past 100 years, releasing stored C as trace gases that can drive positive feedbacks to atmospheric warming (Grosse *et al.* 2011; Lawrence *et al.* 2008; Schuur *et al.* 2008). Yet the outcomes of permafrost thaw depend on landscape context, which determines thaw-induced change in hydrologic processes, plant species assemblages, and thermal regimes (Jorgenson *et al.* submitted). These changes in turn alter the availability of belowground C stores to microbial metabolism, the oxidative state of the belowground environment, and subsequent carbon dioxide (CO_2) and methane (CH_4) emissions. The relative contribution of CH_4 and CO_2 is fundamental for understanding the climate effects of permafrost thaw, as CH_4 has 25 times greater global warming potential (GWP) than CO_2 over a 100-year time horizon (Qin *et al.* 2007).

In thawing peatlands, CH_4 release may be an important pathway of C loss, but controls on the suite of hydrologic and biogeochemical processes controlling CH_4 exchange in these environments are not fully understood (Frolking *et al.* 2011; Jorgenson *et al.* 2010; Turetsky *et al.* 2002). Estimates suggest that northern peatlands contribute ~13% (15-50 Tg y^{-1}) of global CH_4 emissions despite covering less than 3% of the

Earth's surface (Frolking *et al.* 2011; Roulet *et al.* 2007). Soil temperature and soil moisture have a strong influence on CH_4 release, explaining up to 75% of the variance in CH_4 flux in high-latitude wetlands regardless of vegetation type (Torn and Chapin 1993; Olefeldt *et al.* 2012). In a water table manipulation of a boreal peatland site in interior Alaska, CH_4 efflux increased by 80-300% under combined wetter and warmer conditions over five years (Turetsky *et al.* 2002, 2008; Zhuang *et al.* 2007). Understanding the effect of water table and temperature on greenhouse gas exchange and therefore GWP over longer timescales in northern frozen peatland environments is critical for predicting outcomes of climate warming.

To examine the effects of lowland permafrost thaw on C release over decadal to millennial timescales, we quantified CH_4 and CO_2 exchange in a chronosequence of thermokarst bog and fen features developed within a degrading peatland in western Alaska. We seek insight about the long-term effects of thaw by evaluating trace gas exchange in the context of both total C stocks, and the physical collapse, inundation, and plant community succession that accompanies thaw trajectories in lowland settings over millennial timescales.in lowland settings over millennial timescales.

2.3 Methods

2.3.1 Study Area

We conducted our study within the Innoko Flats National Wildlife Refuge (NWR; 63.58˚N, 157.72˚W; Figure 2), in the extensive lowlands developed on eolian and lacustrine silts south of the Innoko River, an area of degrading peatlands with a continental subarctic climate (USDOI 1987, Woodward and Beever 2011). Innoko Flats is the fifth largest NWR in the United States with an area of 15,582 km^2 and no road access. Over half the refuge is wetlands and much of the area is underlain by discontinuous permafrost (USDOI, 1987; Woodward & Beever, 2011). Innoko Flats has a mean daily temperature of -17˚C in January and +14˚C in July (1993-2007; Woodward & Beever, 2011). Mean annual precipitation in this region is 445 mm y^{-1} (1971-2000; Riordan *et al.* 2006). The snow depth in April 2011 was 0.60 ± 0.09 m across 18 locations, consistent with previous observations for the refuge (Woodward and Beever 2011). To our knowledge, this is the first study of trace gas exchange associated with permafrost dynamics in the Innoko Flats NWR.

2.3.2 Study Design

To capture thaw dynamics of lowland permafrost over millennial timescales, we evaluated trace gas fluxes, C stocks, temperature and inundation dynamics, and topographic effects across a thaw chronosequence of thermokarst bogs and in an adjacent fen system (Figure 2). A thaw chronosequence is a series of locations in which factors such as climate, potential vegetation, parent material, and landscape context are similar, but time since thaw varies. Five landscape units differing in thaw stage were identified based on feature size and vegetation: forested plateaus where previous thaw has yet to cause a community shift, ombrotrophic bogs at three stages of thaw (hypothesized to be young, intermediate, and old), and minerotrophic fens. The fen locations are distinct from the bog chronosequence due to active water flow, and represent a possible outcome of thaw depending on regional hydrology. Three field replicates of each landscape unit were identified, for a total of 15 sites. Three field replicates of drying margins surrounding bogs were identified as additional locations representing peat inventories of forested plateaus.

The forested plateaus were characterized by a shallow permafrost table and a black spruce (*Picea mariana*) canopy with an understory of *Ledum decumbens, Rubus chamaemorus Sphagnum fuscum,* and *Cladonia* spp. The young bogs were small pits (2.0 ± 0.6 m^2 in area) within the permafrost plateau that lacked woody vegetation, hosted shallow water tables with acidic pH (4.1-4.6), and were dominated by *S. riparium*, and *S. lindbergii*. Intermediate bogs formed large scars (243.7 ± 82.1 m^2), contained shallow, acidic water tables (pH 3.9-4.3), and hosted vegetation dominated by *Eriophorum scheuchzeri, S. riparium,* and *S. lindbergii*. Old bogs were also acidic (pH 3.9-4.2), and larger (530.4 ± 182.4 m^2), with hummocky microtopography and vegetation dominated by *Andromeda polifolia, Oxycoccus microcarpus, Carex rotundata, S. balticum,* and *S. flexuosum*. The fens were slightly less acidic (pH 4.4-4.8), formed long linear features with surface water movement, and had vegetation dominated by *Carex limosa, C. rotundata, Eriophorum scheuchzeri, S. papillosum,* and *S. majus*.

In September 2009, a SIPRE (Snow, Ice and Permafrost Research Establishment) corer was used to sample the frozen peat and underlying lacustrine and eolian silt for stratigraphy, carbon inventory, ice content and isotopic analysis (Kanevskiy *et al.* in review.). Initial flux measurements were made, porewater profiles of dissolved CH_4 were measured, and frozen peat samples for incubations were collected (see supplemental text). In September 2010, boardwalks were constructed and placed at each site to minimize disturbance to the sample locations, and 37.5 cm diameter PVC collars were placed into the ground at the end of each boardwalk to a depth of ~15 cm. The collars were placed in the plateau and bog locations in September 2010, eight months before initial flux measurements were taken. Collars were placed in the fen locations in May 2011, a few days before initial flux measurements at those locations.

At all plateau and bog sites, soil temperature at 5 and 25 cm depth was continuously logged at one-hour intervals from September 2009 to September 2011 using Hobo V2 loggers (Onset Computer Corp., Bourne, MA). Rainfall was logged from April until October 2011 using a tipping bucket rain gauge (Onset Computer Corp.). In late September 2011, incident and outgoing shortwave and longwave radiation were measured near the PVC collars over eight days using a NR01 four-component net radiometer (Hukseflux Delft, The Netherlands).

2.3.3 Age of Collapse Features

Transitions between permafrost and bog peat were determined using macrofossil indicators, generally *Chamaedaphne* or *Sphagnum riparium*. Forested peat was recognized by char, needles, and bark; aquatic bog peat was recognized by brown mosses. The time of permafrost collapse was estimated by constraining the age of transitional peat as identified by macrofossils.

Two radiogenic isotopes, ^{210}Pb and ^{14}C, were used to estimate age of transitions. ^{210}Pb was generally used for upper and younger strata (<100 y) using the constant rate of supply (CRS) ^{210}Pb method (Appleby and Oldfield 1978) on bulk peat. ^{14}C was generally used for deeper and older strata (>100 y) using samples of *Sphagnum* moss leaves, amorphous peat rich in roots, or peat picked free of roots. We based ^{210}Pb ages on profiles in which inventories of ^{210}Pb were confirmed by the absence of unsupported ^{210}Pb at the base of the profile. We validated our approach by comparing ^{210}Pb and ^{14}C age results from a pair of sites at Koyukuk Flats, Alaska and found close agreement (see supplemental material).

2.3.4 Gas Fluxes

Net ecosystem exchange (NEE), ecosystem respiration (ER), and CH_4 fluxes were measured during three ten-day field campaigns during the early (end of May), middle (end of July) and late (end of September) periods of the 2011 growing season using static chambers (Carroll & Crill, 1997; see supplemental text). During flux measurements air temperatures inside and outside the chamber were manually measured and recorded using thermocouples (Fluke Corporation, Everett, WA), along with photosynthetically active photon flux density (PPFD) within the translucent chamber during NEE measurements.

Our gas flux sampling strategy sought to capture a range of light and temperature conditions over the course of each field campaign. All fluxes were measured in diurnal rounds for each replicate set of sites, with four to six measurements of both CO_2 and CH_4 flux during a 24-hour period. The exception was at the fen locations, where CH_4 was evaluated at all trips throughout the season, but CO_2 measurements were curtailed in September due to difficulty with access (see supplemental material).

Linear regression of CO_2 and CH_4 concentrations in static chambers over time was used to determine a slope (S, ppmv s^{-1}) that could then be converted to a gas flux (F, mg C m^{-2} day^{-1}) for CO_2 or CH_4 using the ideal gas law:

$$F = \frac{P_A}{RT} SHM \quad (1)$$

where F for CO_2 is NEE (light chamber) or ER (dark chamber), P_A is atmospheric pressure (atm), R is the gas constant (0.082057 L atm mol^{-1} K^{-1}), T is temperature (K), H is the height of chamber headspace (m), and M is the molecular weight of the gas (mg mol^{-1}). For slope values, weaker linear regression fits ($R< 0.95$; 8% of measurements), likely due to chamber leakage or soil disturbance, were discarded from subsequent analyses.

Analyses of measured gas fluxes were performed using a one-way ANOVA in R (Team 2012). We used a repeated measures analysis of variance and Tukey's honestly significant difference post hoc comparison of means to determine the effects of soil temperature on gas flux. For assessment of trends with light intensity and temperature (equation 3 below), gas flux results from each site type were pooled across dates in order to have enough measurements for statistical analysis (measurement frequencies shown in supplemental material).

NEE is defined as the sum of ER and gross primary production (GPP):

$$NEE = GPP + ER \quad (2)$$

where negative values of GPP (mg CO_2-C m^{-2} h^{-1}) indicate CO_2 uptake and positive values of ER indicate CO_2 release. The response of NEE to light intensity is expected to follow a non-linear relationship due to the saturating relationship between PPFD and C uptake. This kind of relationship is consistent with limits on physiological responses to light, which dictate that at some light intensity, leaf photosynthesis reaches a maximum

(Talling 1961). The light response of NEE was evaluated as a rectangular hyperbola (Reichstein *et al.* 2012):

$$NEE_{RH} = \frac{\alpha_{RH}\beta_{RH}PPFD}{\alpha_{RH}Q + \beta_{RH}} + \gamma_{RH} \quad (3)$$

where α is the initial slope of the light-response curve (μmol CO_2 μmol photons^{-1}), β is the maximum CO_2 uptake rate of the canopy (μmol m^{-2} s^{-1}), γ represents ER (μmol m^{-2} s^{-1}), and PPFD has units of μmol photons m^{-2} s^{-1}..

The response of ER and CH_4 to soil temperature is expected to follow an exponential function (Cao *et al.* 1996, Wille *et al.* 2008):

$$F = Ae^{bT} \quad (4)$$

where A and b are fitted parameters. Soil respiration and CH_4 production and emission are a function of complex reactions by diverse populations of organisms that vary across sites. These exchanges will differ from one another and across sites in their dependence on substrate availability (A) and the chemical quality of substrate (b); hence we expect that A and b will differ among landscape units for ER and CH_4 flux (Lohila *et al.* 2003).

2.3.5 Water Table Heights

Hourly measurements of water table position were logged in both the fen and two replicates of each bog type using absolute pressure transducers (Onset Computer Corp.) installed in PVC wells. Wells were constructed of screened 3.8 cm PVC placed over a length of rebar inserted into the permafrost with its upper end at ~1m depth. The PVC casing extended from ~20 cm below the height of the rebar to several cm above the vegetation surface, allowing it to move vertically. Pressure transducers were connected by excess cable to the casing lid and placed on top of the rebar so that they remained stationary even if the casing rose and fell during freeze-thaw cycles. Surveys were conducted to establish absolute elevations for water tables, well casings, and bog vegetation surfaces relative to a common benchmark near a frozen plateau site. Based on standard survey techniques and our repeated measurements, we estimate that the uncertainty of these elevations is 5 to 11 cm (Table 1). Logged water table heights were corrected for atmospheric pressure (logged separately) and compared to manual measurements of water table height made during field campaigns. Logged water table records are incomplete after July 28, 2011 due to bear damage of the atmospheric pressure logger.

2.4 Results and Discussion

2.4.1 Thaw Chronosequence

Frozen plateaus and collapse scar bogs show dramatic changes in vegetation and feature size that are related to thaw history (Table 1, Table 2). With increasing time since thaw, our surveyed elevations reveal a dramatic progression of physical collapse, with a maximum collapse of over 2 m in the intermediate bogs (Figure 3). The depth of physical collapse seen in the intermediate bogs is consistent with the ice content in the upper 3-4 m of the frozen plateau sites (>2 m; Kanevskiy *et al.* 2011), suggesting that thaw drove all or most of the lowering (with limited influence from peat decomposition). By the time bogs are old (>600 y), bog peat contributes to increased net C storage (Table 1) and about 20 cm of recovery in elevation relative to the intermediate bogs (Figure 3).

Ages observed in collapse features (Table 1) ranged from 15 y for young bogs (age at base of transition, YB2; Table 5) to 1700 y for old bogs (IFOB3macro115; Table 4), but there was evidence for multiple collapse/refreeze cycles in many cores (see Jorgenson *et al.* submitted). In young bogs, macrofossils indicating the most recent thaw transition (Table 1, Table 5) may be associated with the small collapse features. Old bogs likely encompass deeper, older features (860-1700 y; Table 4), even though younger collapses (<310 y, Table 5) have since occurred. In the intermediate bogs, it is expected that both young (~30 y) and old (~600 y) collapses may influence physical and biogeochemical dynamics (Table 4).

Average C stocks in terrestrial peats at Innoko Flats varied from 28 ± 20 to 69 ± 22 kg C m^{-2} along the chronosequence but were not significantly different among site types (p=0.232; Figure 3; Table 3). Although C loss in young and intermediate bogs did not significantly reduce C stocks, incubation data suggest enhanced potential respiration at young sites (Figure 10). A similar thaw chronosequence at Koyukuk Flats revealed more pronounced losses (57% over 300 y) from larger C stocks (137 ± 37 kg C m^{-2}) as a function of time since thaw (O'Donnell *et al.* 2011c). Preliminary radiocarbon data suggest that the Innoko peat deposit is relatively young (~3700 y; Table 4) compared to the Koyukuk Flats deposit (~7000 y; O'Donnell *et al.* 2011). This difference may explain the smaller C stocks and reduced physical collapse with thaw at Innoko, and hence the reduced effect of thaw on site level C loss at Innoko compared to Koyukuk. Across the

Innoko landscape, however, spatially extensive degradation has occurred (>60% of Figure 2 represents thaw features and fen), and may enhance overall trace gas production with C turnover.

Although the fen system is distinct from the bogs due to groundwater flow and hence potential nutrient supply, it comprises a substantial proportion of the landscape (e.g., 26% of the area in Figure 1). The contribution of fen area to CH_4 fluxes may reflect a dominant outcome of thaw when flow systems expand to include areas where thaw settlement to form bogs has lowered elevations.

2.4.2 Peat Temperature and Water Tables

At all sites, peat temperature at 5 cm depth approached air temperature by late summer (Figure 4a-d). At 25 cm depth, frozen plateaus and young bogs remained 4-6°C colder than the intermediate and old bogs during the growing season, and young bogs thawed to 25 cm about a week later than other bogs (Figure 4e). During fall freeze-up in 2010, forested plateau sites froze about a week earlier than other sites. Intermediate and old bogs consequently had a two-week-longer duration above 0˚C at 25 cm depth, as well as reached a 2.5°C greater average growing season temperature earlier than frozen plateaus and young bogs. The warmer conditions of the intermediate and old bogs suggest that CH_4 production might be enhanced at these locations. Dissolved CH_4 profiles observed in 2009 suggest that increases in subsurface CH_4 production with depth were most pronounced in the intermediate and old bogs (Figure 10a), supporting the idea of increased production at these sites due to warmer temperatures and anoxic conditions.

Water tables were 10-15 cm above the vegetation surface at the intermediate bog and fen sites in May 2011, and fell rapidly with snowmelt between May and June (Figure 5a). In young bogs, with the most limited accumulation area, water levels stayed near the surface of the floating mat. Between June 1 and July 25, water levels in all bogs fell 2 to 6 cm, indicating 10 to 14 cm of total water loss (accounting for 8 cm of rain), and suggesting drawdown by the growing plant community (Figure 5a,b). Subsequently, water levels rose 2 to 6 cm between July 25 and September 25, indicating 6 to 10 cm of total water loss (accounting for 12 cm of rain), and suggesting diminished drawdown by the plant community late in the season (Figure 5a,c).

During the growing season, young and intermediate bogs generally maintained the shallowest water tables and supported a plant community dominated by *S. riparium,* and *S. lindbergii*, with a more open (less dense) structure compared to that of the old bogs, which were dominated by *S. fuscum*. These conditions at young and intermediate bogs suggest enhanced anoxia and atmospheric exchange that promotes CH_4 efflux and/or reduced opportunity for CH_4 consumption. Combined with the temperature data, this suggests that intermediate bogs support the most optimal conditions for CH_4 efflux – warmer subsurface temperatures and shallow, fluctuating water tables within an open plant community structure (Kane *et al.* 2013, Dise *et al.* 1993, Heikkinen *et al.* 2002).

Fen sites experienced similar water table drawdown in early summer compared to young and intermediate bogs (Figure 5b). This followed a more precipitous drop at both intermediate bogs and fens with spring snowmelt (Figure 5a), implying antecedent runoff at these locations. Although water table heights relative to the vegetation surface in fens were generally shallower than those of bogs (Figure 5a), the absolute elevation of the fens was lower than that of the bogs (Figure 3). This is consistent with the idea that the fens focus runoff from the regional flow system with snowmelt and increased rainfall. The small difference in water table heights in fens compared to bogs must be considered in the context of ongoing flow in the fen (discharge rates of 1-10 m^3 min^{-1} observed at the fen outlet), compared to static water tables in the intermediate bogs.

2.4.3 Trace Gas Exchange

The parameters describing the GPP-light response and the ER-temperature response did not differ significantly among landscape units (p=0.841, F-test for a one-way ANOVA; Figure 6; Figure 8a), suggesting a similar carbon metabolism regardless of vegetation composition before and after thaw (Williams *et al.* 2006). The exponential temperature-based model for ER explained about 25% of variance at both frozen and intermediate bog sites, but explained a lower proportion of observed variance at the young bog, old bog, and fen sites. The parameters of the ER model for frozen and intermediate landscape units did not differ significantly with site type (p=0.999; Figure 7a), though warmer temperatures were observed at the intermediate bogs than young and old bogs (p=0.035 and p=0.001 respectively, one-way ANOVA). No significant exponential relationship with peat temperature was found at the old bogs due to increased ER across the range of 25 cm depth soil temperatures (Figure 7a).

Soil temperature at 25 cm depth explained 43% of the variance of CH_4 efflux at intermediate bogs and 36% of the variance of CH_4 efflux at old bogs. Methane fluxes at intermediate bogs were significantly higher than those at other bog sites during the mid and late season campaigns (p=0.019 for a one-way ANOVA), and 100 times higher at the height of the growing season (Figure 8). For the growing season as a whole, CH_4 fluxes ranged from -0.01 ± 0.02 mg CH_4-C m^{-2} hr^{-1} at the frozen plateau to +2.52 ± 0.98 mg CH_4-C m^{-2} hr^{-1} at the intermediate bogs (Table 1; Table 2). Fluxes of CH_4 at the fens were also significantly higher than frozen plateau sites, young bogs and old bogs (p=0.047, one-way ANOVA), producing 0.69 ± 0.12 mg CH_4-C m^{-2} hr^{-1} (Figures 7 and 8). Measured fluxes within trips at the fen were highly variable, which our visual observations suggest was due to ebullition events. All sites displayed net C uptake with 20 to 400 times greater CO_2-C influx than CH_4-C efflux (Table 1). In terms of GWP, CH_4 fluxes offset 49 ± 21% of NEE at the intermediate sites (Table 1). These data are consistent with previous work showing that black spruce forests and *Sphagnum* bogs in the boreal region are a net sink of CO_2 during the growing season (Dunn *et al.* 2007). A similar relationship also has been observed in Siberian lowland peatlands (Smith *et al.* 2004, Heyer *et al.* 2002).

2.4.4 Enhanced CH_4 Efflux at Intermediate Bogs

Peat temperatures at 25 cm depth were generally higher in the intermediate and old bogs, and were the strongest explanatory variable for both ER (25% of variance at intermediates; Figure 7a), and CH_4 flux (43 and 36% of variance, respectively; Figure 7b). When all sites are considered together, there was no significant relationship between CH_4 flux and ER (p=0.409); however at intermediate bogs alone, there was a linear relationship, with 22% of variance in CH_4 explained by ER. The response of ER to temperature at 25 cm depth was stronger (p=0.001) in the intermediate bogs (Figure 7a), and the response of CH_4 flux to temperature was significantly higher ($p=0.038$) in the intermediate bogs compared to the old sites (Figure 7), with a growing season average of $+2.52 \pm 0.98$ mg CH_4-C m^{-2} hr^{-1} at the intermediate sites compared to $+0.69 \pm 0.12$ mg CH_4-C m^{-2} hr^{-1} at the older sites (Table 1).

Across all sites, 11-44% of CH_4 flux was explained by both soil temperature and water table height relative to the vegetation surface, suggesting that other variables are at play, such as CH_4 consumption or decreases in atmospheric pressure that may cause ebullition (Dise *et al.* 1993). At old bogs, the small lowering of water tables relative to the moss surface and damping of water table fluctuation (Figure 5) may support enhanced methanotrophy, which would diminish observed diffusive fluxes (Zhuang *et al.* 2007, Turetsky *et al.* 2008). In addition, CH_4 ebullition may be physically limited by the solidified peat mat in the old bogs. At the fen sites, moderate CH_4 fluxes ($+0.69 \pm 0.12$ mg CH_4-C m^{-2} hr^{-1}) suggest that prolonged peat degradation may be facilitated by evolution of regional flow systems with thaw.

2.4.5 Century and Millennial Scale Ecosystem Response to Permafrost Thaw

Our results suggest that thaw feature size and age, as well as plant structure and composition, influence both water table height and soil thermal regimes, leading to a prolonged, decadal-to-century scale "pulse" in CH_4 fluxes in the intermediate bogs, here estimated as representing 30-590 years of thaw. Permafrost thaw and shifts in vegetation contribute to the altered hydrological and thermal conditions that predispose intermediate thaw features to large CH_4 emissions. In addition, the presence of light colored *Cladonia* spp. on the frozen plateau may provide a negative feedback to the soil thermal regime by reflecting radiation and limiting ground heat flux and hence thaw susceptibility (Stoy *et al.* 2012). Once young bogs are initiated, inundation supports *Sphagnum riparium* communities at the expense of *Cladonia* spp., while continued shading by trees and the higher heat capacity of the water in the wet young bogs reduces incident radiation (Tables 1, 2), providing a positive feedback to lateral thaw and collapse. Young bogs remain cold as they are small depressions within the surrounding permafrost, but even their limited physical collapse promotes absorption of additional radiation, enhanced decomposition (Figure 10b) and accumulation of runoff (Figure 5) that further promotes thaw and maintains a shallow water table. Expanded collapse to form intermediate bogs eliminates shading through tree-kill, decreases albedo (Table 1) and continues to promote accumulation of liquid water both from thawing ice rich permafrost and from rainfall accumulation (Figure 5).

The combination of warmer soil temperatures and shallower water tables leads to dramatically enhanced CH_4 production mid-summer and over the course of the growing season in the intermediate age bogs (Figure 8). A positive C balance persists, as indicated by bog peat accumulation (Figure 3) and CO_2 uptake outweighing CO_2 equivalent CH_4 release by a factor of two to 400 during the growing season (Table 1). At the same time, the succession of vegetation and accumulation of peat over hundreds of years in old bogs physically elevates the land surface (Figure 3). The transformation to dwarf evergreen shrub and *S. fuscum* vegetation physically insulates subsurface liquid water, which may in turn limit lateral thaw propagation, increase CH_4 consumption, and enhance absorption of solar radiation as indicated by reduced albedo (Figure 10; Table 1; (Bonan *et al.* 1992). Under constant climate conditions, this vegetation succession could lead to re-aggradation of permafrost and re-establishment of black spruce communities, but this outcome may already be unlikely with a continued warming climate. An important contributor to regional trace gas response will be evolution of the flow system represented here by the fen locations, which exhibit high water tables, reduced albedo, and higher CH_4 fluxes when compared to frozen plateaus (Table 1). In some situations, fen locations can facilitate more rapid permafrost loss through thermal effects of enhanced flows (Jorgenson *et al.* 2001).

2.5 Conclusions

Thawing of ice-rich peat leads to water impoundment, soil saturation, and both vertical and lateral thaw propagation. This progression in turn leads to soil warming and increasing CH_4 emissions. In peat deposits in western Alaska, these CH_4 emissions may reflect a loss of older forest peat that has accumulated during the mid- to late Holocene, even as CO_2 uptake results in accumulation of new bog peat. After ~600 y post-thaw, peat accumulation, water table lowering, and subsurface cooling reduce CH_4 emissions. At Innoko Flats, as is common in other boreal permafrost lowlands, permafrost collapse has created a complex mosaic of small thermokarst bogs of varying ages and states of bog and fen succession, each with differing rates of trace gas emissions. While further warming is likely to accelerate thawing of permafrost plateaus, the areal extent of bogs relative to forest plateaus at this site (Figure 2) suggest that >60% the permafrost plateau has already thawed, and hence that peak CH_4 production may have occurred or is occurring now. The limited thickness of the Innoko peat deposit is likely related to its relatively young age and advanced thaw progression, such that extensive degradation over the past few decades has resulted in enhanced CH_4 production in this area, at this time. If thaw progression increases hydrologic connection with flow systems (bog transformation to fen) sustained CH_4 production may result.

2.6 Acknowledgements

This research was made possible by funding from the National Science Foundation (EAR #0630319 and DBI #1021095), the United States Geological Survey, the Montana State University College of Agriculture, and the MSU VP of Research, with assistance from the North and West Alaska Cooperative Ecosystems Studies Unit, and crucial logistical support by the US Fish and Wildlife Service. Thank you to Jon O'Donnell and Mikhail Kanevskiy for soil sampling and instrumentation, as well as ongoing discussion of permafrost landscape evolution, and to Kristen Manies for soil analyses and insight. Thanks also to Rob Striegl for discussion of field strategy, Miriam Jones for assistance with age estimates, Aiden Johnson for assistance with albedo observations, and to Christine Miller, Chris Dorich, Claire Treat, and Chris Welch for insightful participation in fieldwork. Additional thanks to Karin Bodony of USFWS and Jim Webster of Webster Flying Service for superb logistical support.

Table 1. Estimated ages, total carbon stocks, and average seasonal CO_2 and CH_4 fluxes during the 2011 growing season at the Innoko, AK thaw chronosequence. Uncertainties are in parentheses. For total C stocks uncertainties are presented as one standard deviation, while uncertainty for elevation and fluxes are one standard error of the mean (n=3 sites except at frozen plateau where n=6). See Table 4 for age estimate details. Fluxes of CO_2 and CH_4 are averages of measured values for three field campaigns. No flux value is reported for fen net CO_2 flux as insufficient numbers of measurements were recorded. For CO_2 equivalent-CH_4 flux calculation see supplemental text. Negative flux values represent uptake to land.

Site	Estimated time since thaw (y)[a]	Absolute elevation relative to BM (m)	Total C stock (kg C m^{-2})	Average September albedo under diffuse sky conditions[c]	Net CO_2 flux (mg CO_2-C m^{-2} hr^{-1})	CH_4 flux (mg CH_4-C m^{-2} hr^{-1})
Frozen Plateau	0	0	55 (20)[a]	0.14 (<0.01)	-40.88 (7.93)	-0.01 (0.02)
Young Bog	15 to 34	-1.20 (0.11)	28 (20)	0.18 (0.01)	-38.30 (11.33)	0.04 (0.03)
Intermediate Bog	28 to 592	-2.53 (0.05)	41 (23)	0.13 (<0.01)	-47.06 (8.34)	2.52 (0.98)
Old Bog	569 to 1688	-2.10 (0.06)	69 (22)	0.15 (0.01)	-14.40 (5.48)	0.16 (0.07)
Fen	2211 to 2338	-2.84 (0.05)	49[b]	0.14 (<0.01)	-	0.69 (0.12)

[a] Mean and one standard deviation for three frozen, forested plateau sites is 48 ± 2 kg C m^{-2}. Value shown includes three drying margin locations at bog edges representing ice free carbon inventory of forested plateaus.
[b] N=1 for the fen site ; n=2 for the young bog, intermediate bog, and old bog
[c] Presented albedo estimates for the frozen plateau and young bog sites refer to the forest floor and exclude any overlying trees.

Table 1. Estimated ages, total carbon stocks, and average seasonal CO_2 and CH_4 fluxes during the 2011 growing season at the Innoko, AK thaw chronosequence. Uncertainties are in parentheses. For total C stocks uncertainties are presented as one standard deviation, while uncertainty for elevation and fluxes are one standard error of the mean (n=3 sites except at frozen plateau where n=6). See Table 3 for age estimate details. Fluxes of CO_2 and CH_4 are averages of measured values for three field campaigns. No flux value is reported for fen net CO_2 flux as insufficient numbers of measurements were recorded. For CO_2 equivalent-CH_4 flux calculation see supplemental text. Negative flux values represent uptake to land - continued.

CO_2 equivalent- CH_4 flux (mg CO_2-C m^{-2} hr^{-1})	Net CO_2 flux: CO_2 equivalent- CH_4 flux ratio	Percent CO_2 equivalent- CH_4 flux offset of NEE
-0.09 (0.17)	442 (815)	0.2 (0.4)
0.38 (0.26)	101 (75)	1.0 (0.7)
23.00 (8.92)	2 (1)	48.9 (20.9)
1.45 (0.60)	10 (5)	10.1 (5.7)
6.27 (1.14)	-	-

[a] Mean and one standard deviation for three frozen, forested plateau sites is 48 ± 2 kg C m^{-2}. Value shown includes three drying margin locations at bog edges representing ice free carbon inventory of forested plateaus.

[b] N=1 for the fen site ; n=2 for the young bog, intermediate bog, and old bog

[c] Presented albedo estimates for the frozen plateau and young bog sites refer to the forest floor and exclude any overlying trees.

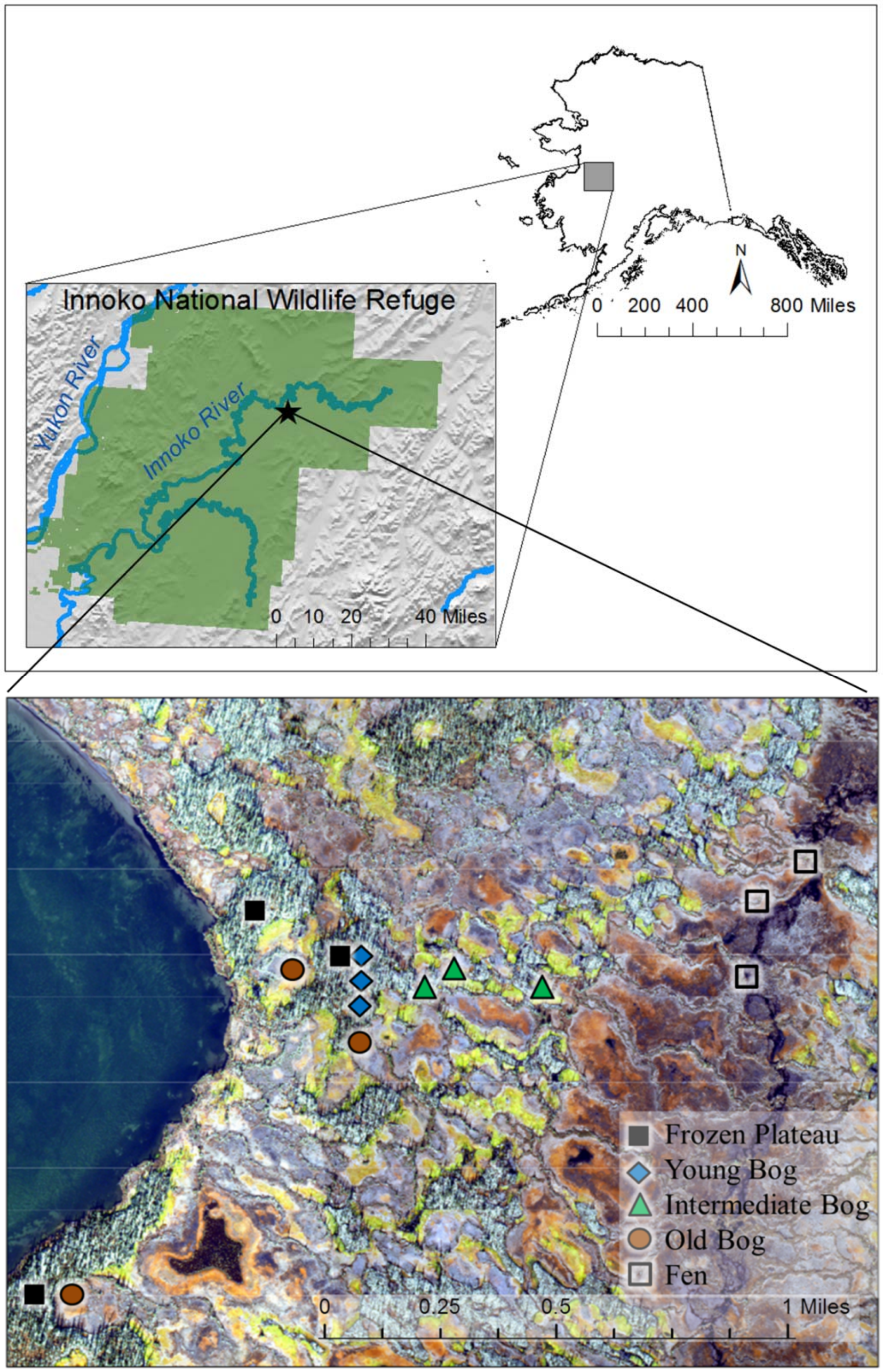

Figure 2. Map of the Innoko National Wildlife Refuge (63.58˚N, 157.72˚W) denoting the position of 2011 field season sampling site located within the refuge (top). Aerial photograph of Innoko study area with locations of each site denoted by symbols. This study area is approximately 24% frozen, 39% bog, 26% fen, and 11% open water, determined by aerial photograph interpretation using a grid overlay.

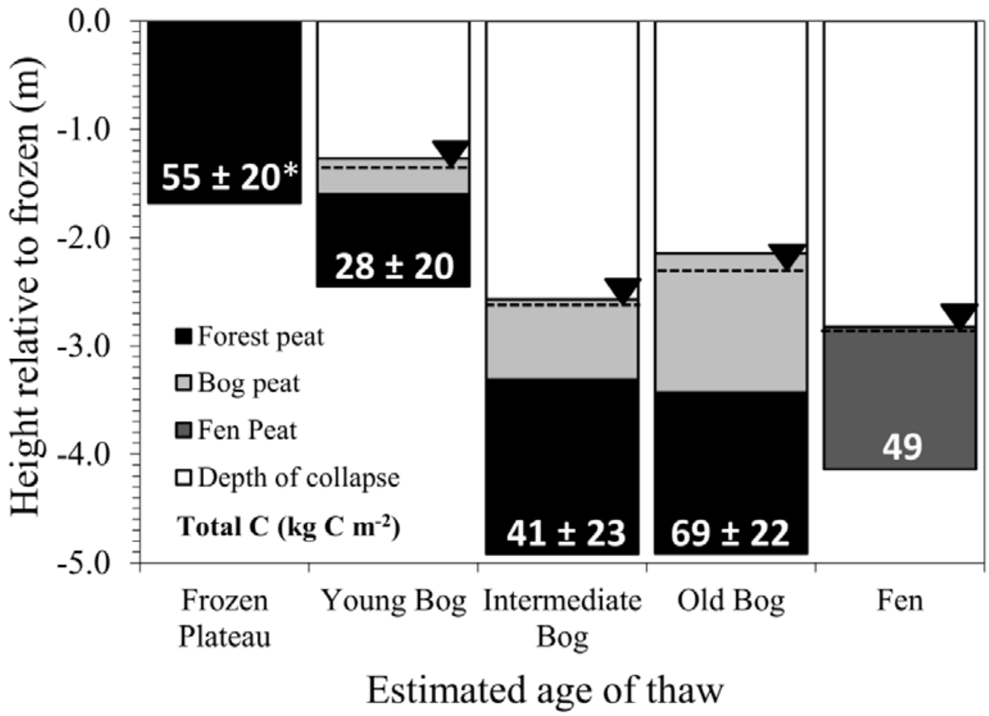

Figure 3. Depth of collapse for frozen (0 y), young (15-34 y), intermediate (28-592 y), old (569-1688 y), thermokarst bogs and fen (1800 y) resulting from permafrost thaw at the Innoko study site (n=3 replicates per landscape unit). Depth of bog peat is measured to the forest peat-silt layer at frozen and bog sites and to the limnic silt layer at the fen. Numbers inside bars indicate total carbon stocks (kg C m^{-2}, ±1 standard deviation; n=1 fen site; n=2 for the young bog, intermediate bog, and old bog; n=6 for frozen plateau and includes three drying margin sites). Total C stocks include all peat types. Each elevation is averaged across three field replicates with uncertainties ≤ 0.11 m (Table 1). Note that the absolute elevation of the fens is lower than all other sites. The relative elevation of the average water table position to vegetated surface is denoted with dashed line and inverted triangles (n=9, 3 sites x 3 dates).

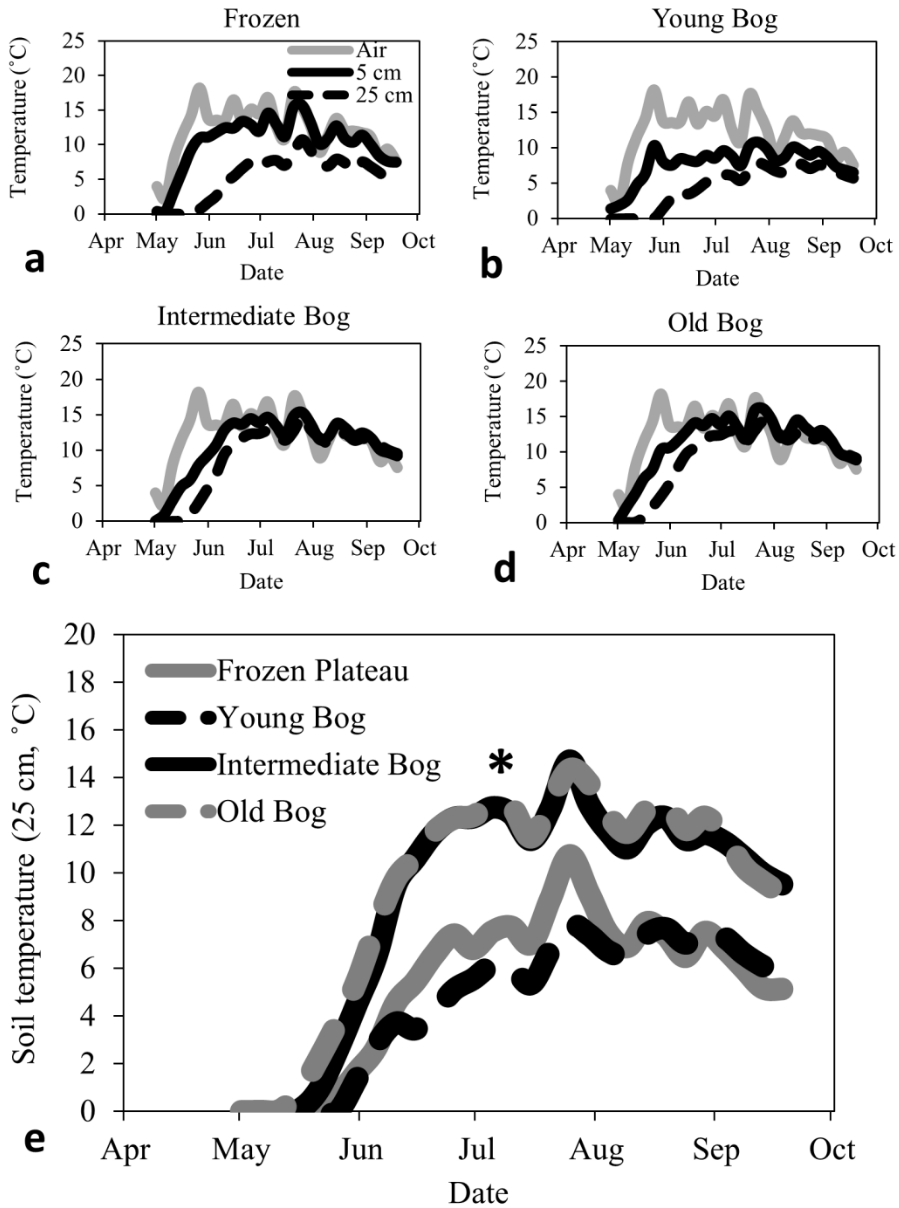

Figure 4. (a-d) Five day running averages of continuously recorded temperature of air, peat at 5 cm depth, and peat at 25 cm depth for chronosequence sites during the 2011 growing season. Values at each time step are averaged across sites with complete temperature records as follows: (a) frozen 1 & 2; (b) young bog 1,2, & 3; (c) intermediate bog 1,2 & 3; and (d) old bog 1 & 3. Panel (e) compares peat temperature records at 25 cm depth. The asterisk denotes significant statistical differences (intermediate and old warmer than frozen and young) based on a post hoc comparison of means test.

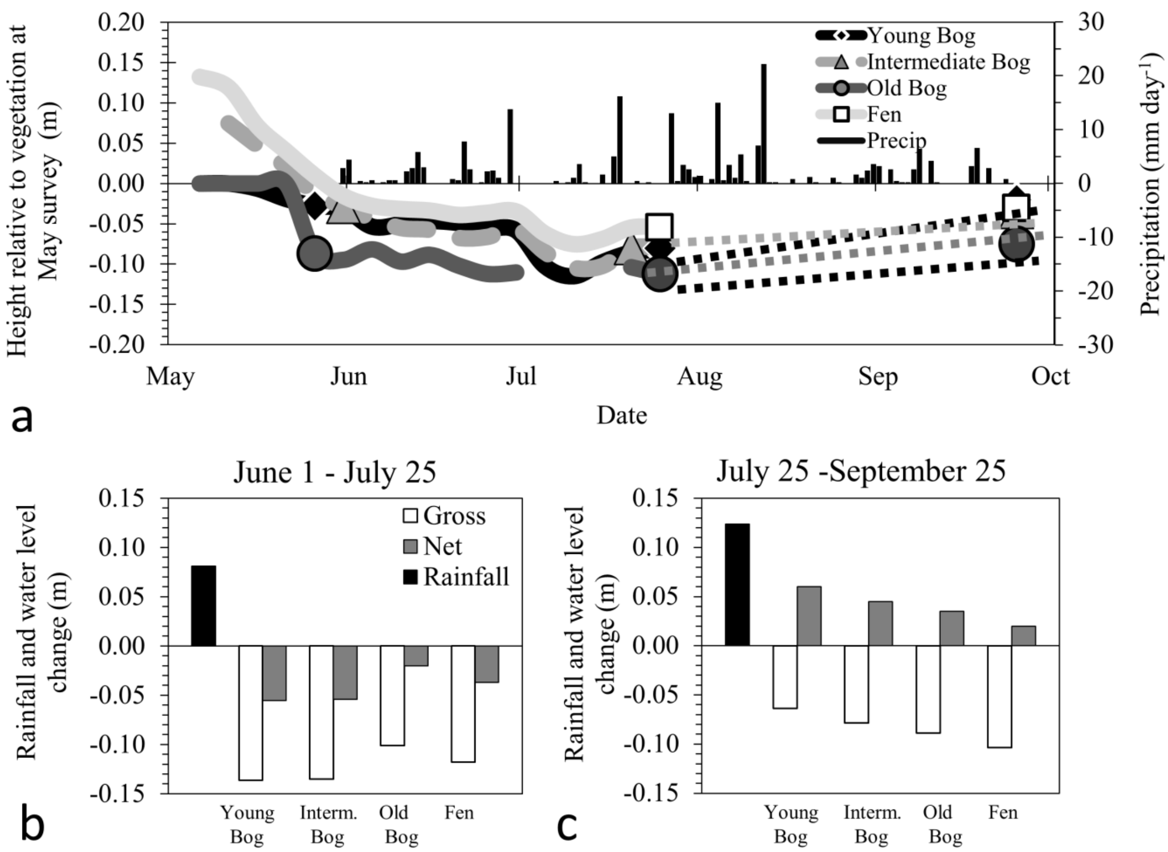

Figure 5. (a) Rainfall during the study period and five-day running average of continuously recorded water table height relative to height at thaw for seven sites with complete temperature records: young bog 1 and 3, intermediate bog 2, old bog 2 and 3, and fen 1 and 3 during the 2011 growing season (numbers indicate replicates; Table 6). Symbols represent surveyed water table levels at the three field campaigns. Bold lines represent water table data as measured with a pressure transducer and are corrected to elevations measured during the May survey. Narrow dotted lines connect the July 25 and September 25 survey heights, as pressure transducer data are not available for this time period. (b-c) Rainfall and the gross and net changes in water level for each site type (young, intermediate (interm.), old, and fen) during (b) June 1 – July 25 and (c) July 25 to September 25, 2011. Net change accounts for the amount of rainfall measured during each time interval.

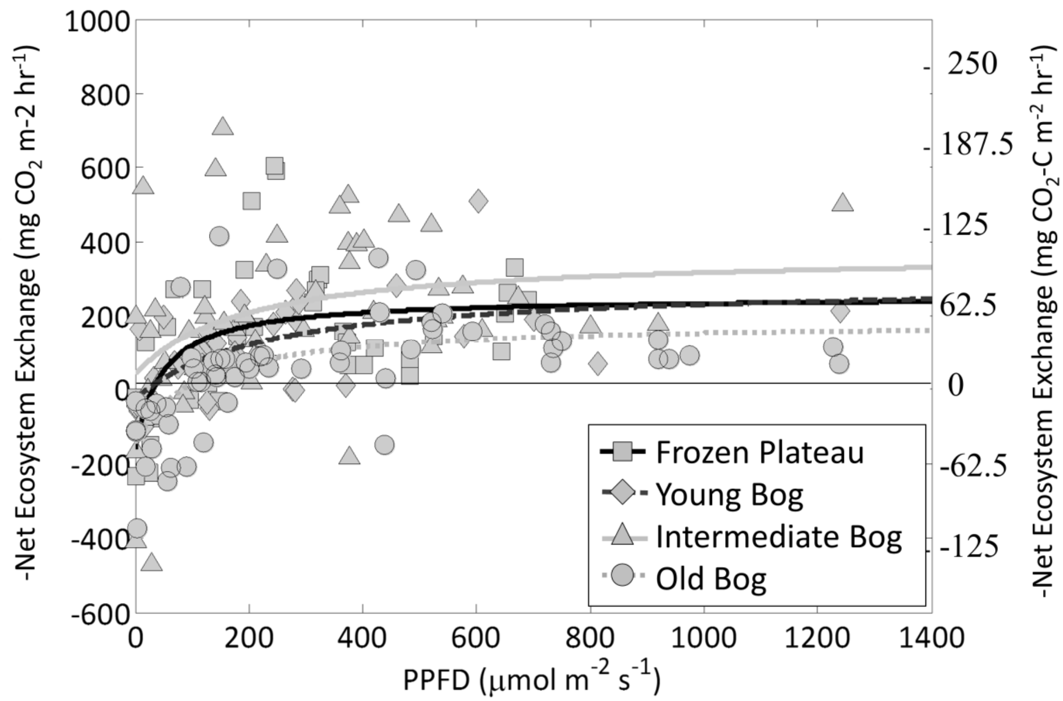

Figure 6. Response of net ecosystem exchange (mg CO_2 m^{-2} hr^{-1}, left; mg CO_2-C m^{-2} hr^{-1},right) to light intensity (PPFD; µmol m^{-2} s^{-1}) at all sites during the 2011 measurements. The fit lines are rectangular hyperbolic fit for all data points of each site. Fits reflect point measurements at three replicates of each site type. Rectangular hyperbolic fits for each site were not significantly different from one another (p=0.841). Positive values as displayed indicate CO_2 uptake. Results of model fits (equation 3) are shown in Table 5.

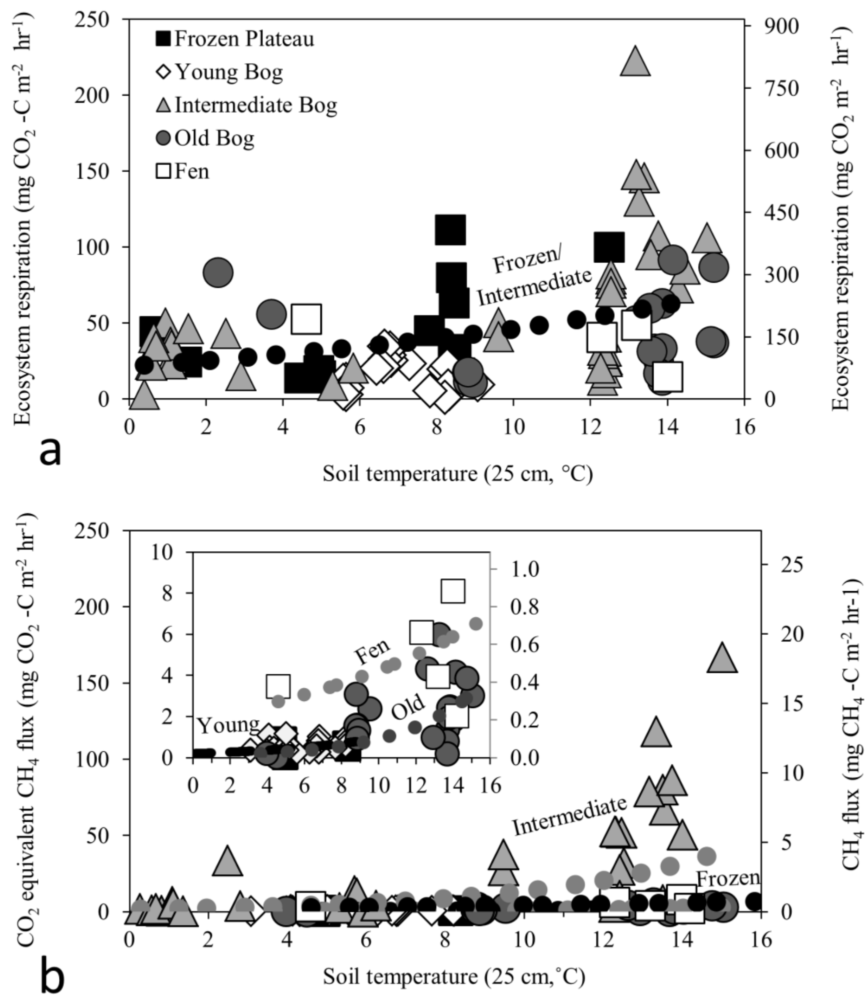

Figure 7. The relationship between (a) ecosystem respiration (ER) and (b) CH_4 flux and peat temperature at 25 cm depth in 2011 at the Innoko Flats study sites. Values for each site type include results for three replicates of each landscape unit (Table 3). Methane fluxes are reported on the left vertical axis as the CO_2-C equivalent of CH_4 for ease of comparison against CO_2 fluxes. Sites for which the relationship between efflux and temperature was significant are presented as dotted lines. The inset in (b) shows a narrower range of values on the y-axis (units same as primary y-axis) to illustrate effect at old bog and fen sites, where fluxes were significantly lower ($p=0.019$; F-test for a one-way ANOVA) than intermediate sites. Best-fit equations are based on equation 4 and parameter values are presented in Table S3.

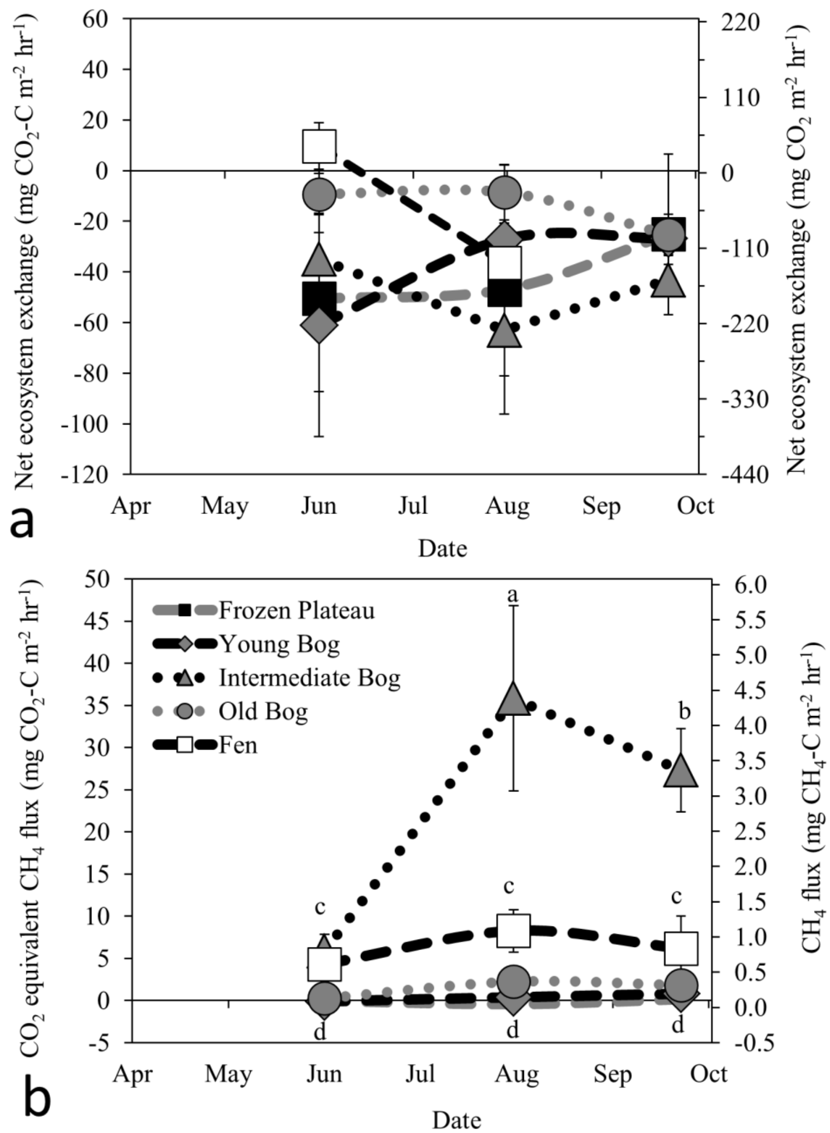

Figure 8. Average NEE (a) and CO_2 equivalent CH_4 flux (b) at the five site types over the course of the 2011 growing season (n=3 for each site type). Methane fluxes are reported as the 100-year GWP equivalent of CO_2 (left vertical axis) for ease of comparison to CO_2 fluxes (see supplement). Error bars are ± one standard error of the mean for three sites from each landscape unit. Lines are connectors between point measurements, not modeled values. Lower case letters distinguish significant differences based on a post hoc comparison of means test (p=0.003). Please note the different scale of the axes.

2.7 Supplemental Material

2.7.1 Detailed Methods

2.7.1.1 Peat Ages. For ^{14}C analysis, materials were submitted to the USGS extraction laboratory for complete combustion and trapping of CO_2. Targets were prepared and submitted for accelerator mass spectrometry at Lawrence Livermore National Laboratory. Resulting ^{14}C data were corrected to post-bomb deposit ages ($F^{14}C$ >1; Reimer *et al.*., 2004) and were calibrated according to Hua & Barbetti (2004).

The efficacy of using ^{210}Pb for dating of peats was tested by comparing CRS ages to post-bomb deposit ages (Tables 4 and 5) for picked moss leaves from near-surface samples derived from the uppermost 25 cm of bog peat from Koyukuk Flats (Hua and Barbetti 2004, O'Donnell *et al.* 2011c). For old bog profiles, the depth of bog/forest peat transition was >80 cm and beyond the utility of ^{210}Pb; therefore, ^{14}C was used for dating thaw transitions.

2.7.1.2 Gas Fluxes. Cylindrical chambers with a height (H) of 20 cm, and inner diameter of 19.5 cm were constructed of clear polycarbonate Lexan (to measure NEE) and opaque polyvinyl chloride (to measure ER and CH_4 fluxes) having five sample ports and a pressure equilibration port (Wickland *et al.* 2006). Two ports on the chamber were used to circulate the sample air through a small external pump at approximately 3 L min^{-1}. For NEE and ER, chamber air was circulated through two separate ports connected to a LI-840A (LI-COR) or EGM-4 CO_2/H_2O analyzer (PP Systems, Amesbury MA, USA), and CO_2 concentrations were automatically recorded every three seconds over a six minute period for each chamber type. For CH_4 fluxes, six 60 mL chamber air samples were manually collected from a dedicated port over 30 minutes in a syringe, followed by immediate transfer of each gas sample into a pre-evacuated 40 mL glass vial. Sample vials were shipped to the University of New Hampshire where they were analyzed for CH_4 concentrations using a Shimadzu GC-8A gas chromatograph system with flame ionization detector (for analytical methodologies, see Treat *et al.* 2007).

2.7.1.3 Albedo Measurement. The solar zenith angle (θ) was consistently large, not less than 62.5 degrees, during the September 2011 measurement campaign, and diffuse light conditions dominated due to prevailing cloudy conditions. We therefore highlight observations made under diffuse light with (θ) between 62.5 degrees and 80 degrees, and present observations made during sunny periods for reference. Albedo measured under conditions of direct solar radiation (α_{dir}) can be expressed as a function of albedo measured under diffuse light conditions (α_{diff}) and (θ) following for example Briegleb and Ramanathan (1982) as discussed in Coakley (2003):

$$\alpha_{dir} = \alpha_{diff} \frac{1+d}{1+2d\cos(\theta)} \qquad \text{(S1)}$$

where d is an adjustable parameter that varies by surface type. The paucity of α_{dir} observations make d difficult to calculate for different cover types here, so instead we present average α_{dir} and α_{diff} for each site for reference in Table 2.

Global warming potential are calculated on the basis of molecular mass (Qin *et al.* 2007) and therefore must be applied to CH_4-C fluxes with a correction:

$$F_{CO_2\text{-}CH_4} = F_{CH_4} \, GWP \frac{M_{CH_4}}{M_{CO_2}} \qquad (S2)$$

where $F_{CO2\text{-}CH4}$ is the global warming potential equivalent CO_2 flux (mg CO_2 m^{-2} hr^{-1}), F_{CH4} is methane flux (mg CH_4-C m^{-2} hr^{-1}), GWP is the 100 year GWP of CH_4 (25), and M is the molecular weight of the gas (mg mol^{-1}).

2.7.1.4 Total C Respiration Incubations. Field-moist peat samples of known volume were placed in 473 mL mason jars and incubated at 10^{o}C for 112 days. Soil respiration was measured weekly to bi-weekly by capping the jars and analyzing the change in headspace CO_2 concentration over 24 hours on a LI-6252 infrared gas analyzer (Li-COR, Lincoln, NE, USA). Headspace gases were sampled through a rubber septa installed in the container lids immediately upon closing the containers, and again 24 hours later. Soil respiration rates were calculated as the change in headspace CO_2 concentration (adjusted for headspace volume and ambient temperature) plus the change in dissolved CO_2 concentration in soil pore water (calculated from headspace concentrations, soil water contents, and known CO_2 equilibrium constants adjusted for temperature and pressure) over time. The jars were kept slightly open between measurements to avoid anoxia, and any evaporative water loss was determined by weight and replaced with DI if necessary on a weekly basis. Cumulative soil respiration (mg C as CO_2) during the entire 112-day incubation period was determined by linear interpolation between measurements. Percent of total soil C respired is calculated as cumulative soil respiration (mg C-CO_2) divided by the initial g soil C in each sample (g soil dry weight x soil C content).

Table 2. Summary of collapse-scar bogs and characteristics of each feature during the 2011 field season. Albedo observations were taken during times when the solar zenith angle, θ, was between 62.5 and 80 degrees and uncertainty is on the order of 1%.

Site	GPS positions (lat; long)	Thaw depth (most recent collapse; cm)	Years since most recent thaw	Absolute elevation	Albedo under diffuse solar radiation (α_{diff})	Albedo under direct solar radiation (α_{diff})	Dominant vegetation
Frozen Plateau 1	63.5738 ; -157.7289	-	0	-	0.14		*Picea mariana, Ledum decumbens,Rubus*
Frozen Plateau 2	63.5709; -157.7333	-	0	-			*chamaemorus Cladonia arbuscula*, *Sphagnum*
Frozen Plateau 3	63.5740; -157.7304	-	0	-			*fuscum*
Young Bog 1	63.5736; -157.7286	28	34	-1.337	0.18	0.15	*Sphagnum riparium, S. lindbergii*
Young Bog 2	63.5735; -157.7286	25	15	-1.7785	0.21		
Young Bog 3	63.5738; -157.7286	16	ND	-1.022	0.16	0.14	
Intermediate Bog 1	63.5738; -157.7272	21 (and 97)	ND	-2.7065			*Eriophorum scheuchzeri, Sphagnum*
Intermediate Bog 2	63.5738; -157.7272	32 (and 119)	498 to 592	-2.5715			*riparium, S. lindbergii*
Intermediate Bog 3	63.5737; -157.7256	60	28 to 54	-2.7415	0.14	0.19	
Old Bog 1	63.5736; -157.7297	80 and 100	569 to 933	-2.2265	0.13	0.23	*Andromeda polifolia, Oxycoccus microcarpus,*
Old Bog 2	63.5709; -157.7326	180	ND	2.024			*Carex rotundata, Sphagnum balticum, S.*
Old Bog 3	63.5731; -157.7284	115	1586 to 1688	-2.4215	0.17	0.16	*flexuosum*

Table 2. Summary of collapse-scar bogs and characteristics of each feature during the 2011 field season. Albedo observations were taken during times when the solar zenith angle, θ, was between 62.5 and 80 degrees and uncertainty is on the order of 1% - continued.

Site	GPS positions (lat; long)	Thaw depth (most recent collapse; cm)	Years since most recent thaw	Absolute elevation	Albedo under diffuse solar radiation (α_{diff})	Albedo under direct solar radiation (α_{diff})	Dominant vegetation
Fen 1	63.5741; -157.7223			-2.94			*Carex limosa, C. rotundata, Eriophorum scheuchzeri, Sphagnum papillosum, S. majus, S. fallax, Menyanthes trifoliata,*
Fen 3	63.5750; -157.7217			-2.982			
Fen 4	63.5734; -157.7216			-2.845	0.14	0.12	

Table 3. Summary of carbon stocks and gas fluxes from each feature during the 2011 field season.

Site	Total C stock ($kg\ m^{-2}$)	Net CO_2 –C flux ($mg\ m^{-2}\ hr^{-1}$)	Net CH_4 –C flux ($mg\ m^{-2}\ hr^{-1}$)	CO_2 –C equivalent CH_4 flux ($mg\ m^{-2}\ hr^{-1}$)
Frozen Plateau 1	47.0	-59.59 ± 17.29	-0.03 ± 0.28	-0.25 ± 2.48
Frozen Plateau 2	45.7	-21.97 ± 8.97	-0.01 ± 0.03	-0.07 ± 0.25
Frozen Plateau 3	33.1	-31.87 ± 11.14	-0.02 ± 0.02	-0.18 ± 0.27
Young Bog 1	18.8	-37.80 ± 5.85	0.08 ± 0.03	0.66 ± 0.19
Young Bog 2	14.1	-4.79 ± 11.07	0.05 ± 0.03	0.39 ± 0.20
Young Bog 3	51.7	-21.06 ± 5.71	0.04 ± 0.02	0.32 ± 0.18
Intermediate Bog 1	63.6	-42.43 ± 14.53	4.38 ± 1.14	39.87 ± 0.11
Intermediate Bog 2	16.9	-50.57 ± 14.67	2.04 ± 1.46	18.51 ± 0.11
Intermediate Bog 3	42.8	-58.77 ± 11.07	1.04 ± 0.18	9.40 ± 0.12
Old Bog 1	50.1	-29.44 ± 6.28	0.17 ± 0.03	1.52 ± 0.12
Old Bog 2	63.4	-4.47 ± 5.10	0.20 ± 0.08	1.80 ± 0.15
Old Bog 3	92.1	-10.02 ± 9.35	0.18 ± 0.06	1.57 ± 0.14
Fen 1	49.1	-1.09 ± 12.42	1.04 ± 0.62	9.42 ± 0.12
Fen 3	-	-10.29 ± 25.38	0.68 ± 0.19	6.17 ± 0.10
Fen 4	-	-10.70 ± 3.82	0.46 ± 0.07	4.11 ± 0.09

Table 4. Radiocarbon data in support of age-dating transitional peat. See http://calib.qub.ac.uk/CALIBomb/frameset.html using Levin post-bomb data set. Sample name reflects peat core and type of sample dated (bulk = bulk peat, pbulk = bulk sample picked free of roots, macro = macrofossil). Bold indicates transitional peat.

SampleID	**Depth**	**$\Delta^{13}C$**	**$\Delta^{14}C$**	**SD $\Delta^{14}C$**	**Uncorrected Age**	**SD age**	**Calibrated $\Delta^{14}C$ Min Age, in CalBP1950**
KFUI 3.008	8	-24.04	53.81	2.67			
KFUI 3.010	10	-25.50	57.95	3.72			
KFUI 3.012	12	-25.12	116.66	3.16			
KFUI 3.014	14	-24.81	115.27	3.08			
KFUI 3.016	16	-25.00	150.65	4.56			
KFUI 3.019	19	-25.48	19.29	2.78			
KFUI 3.020	20	-25.10	-17.25	2.86			
KFUY 2.002	2	-24.26	52.25	4.25			
KFUY 2.004	4	-23.99	44.46	2.83			
KFUY 2.006	6	-24.13	47.40	3.15			
KFUY 2.008	8	-25.35	61.67	3.19			
KFUY 2.010	10	-25.52	66.70	3.76			
KFUY 2.012	12	-23.89	82.91	4.69			
KFUY 2.014	14	-24.15	109.12	3.33			
KFUY 2.016	16	-23.98	118.86	3.36			
KFUY 2.018	18	-24.94	162.29	3.45			
KFUY 2.020	20	-24.52	173.70	3.25			
KFUY 2.022	22	-24.39	185.46	3.37			
IFOB1pbulk68	68	-24.97	45.47	3.72			
IFOB1pbulk80	**80**	**-25.30**	**-21.78**	**3.87**			
IFOB1bulk100	**100**	**-26.10**	**-118.10**	**2.59**	**950**	**25**	**796**
IFOB3macro95	95	-24.78	-67.44	2.25	500	20	510
IFOB3macro115	**115**	**-23.71**	**-194.65**	**2.67**	**1680**	**30**	**1527**
IFOB3macro116	116	-26.29	-200.01	2.09	1735	25	1591
IFIB2pbulk139	**139**	**-25.95**	**-59.45**	**3.80**	**435**	**35**	**439**
IFIB3pbulk60	**60**	**-24.16**	**386.17**	**3.89**	**40.5**	**13**	
IFIB3bulkS75	75	-25.41	331.65	4.58	37.5	17	
IFIB3pbulk133	133	-25.90	-350.10	2.24	3400	30	3569
IFIF1pbulk98	98	-26.11	-247.1	2.51	2220	30	2216

Table 4. Radiocarbon data in support of age-dating transitional peat. See http://calib.qub.ac.uk/CALIBomb/frameset.html using Levin post-bomb data set. Sample name reflects peat core and type of sample dated (bulk = bulk peat, pbulk = bulk sample picked free of roots, macro = macrofossil). Bold indicates transitional peat, continued.

SampleID	**CalBPmax**	**Prob (%)**	**Min ^{14}Cage in 2009**	**Max ^{14}CAge in 2009**	**Notes**
KFUI 3.008			4	55	Sphagnum moss leaves
KFUI 3.010			4	55	Sphagnum moss leaves
KFUI 3.012			11	53	Sphagnum moss leaves
KFUI 3.014			11	53	Sphagnum moss leaves
KFUI 3.016			16	52	Sphagnum moss leaves
KFUI 3.019			57	57	Sphagnum moss leaves
KFUI 3.020			59	316	Sphagnum moss leaves
KFUY 2.002			4	56	Sphagnum moss leaves
KFUY 2.004			3	56	Sphagnum moss leaves
KFUY 2.006			4	56	Sphagnum moss leaves
KFUY 2.008			4	56	Sphagnum moss leaves
KFUY 2.010			10	55	Sphagnum moss leaves
KFUY 2.012			9	56	Sphagnum moss leaves
KFUY 2.014			12	56	Sphagnum moss leaves
KFUY 2.016			14	51	Sphagnum moss leaves
KFUY 2.018			19	51	Sphagnum moss leaves
KFUY 2.020			24	51	Sphagnum moss leaves
KFUY 2.022			22	51	Sphagnum moss leaves
IFOB1pbulk68			56	57	Bulk fibrous peat picked free of roots
IFOB1pbulk80			**59**	**311**	Chamadaphne and moss peat picked free of roots
IFOB1bulk100	**874**	**64.2**	**855**	**933**	Bulk amorphous peat over limnic peat; no roots noted
IFOB3macro95	540	95	569	599	Moss leaves
IFOB3macro115	**1629**	**80.7**	**1586**	**1688**	Moss leaves from terrestrial boundary; sedge leaves 1470 +/- 20 y uncalibrated age (lab no. WW7759)
IFOB3macro116	1707	86.7	1650	1766	Charred terrestrial peat from top of terrestrial Boundary at 116 cm. Limnic below 154 cm.
IFIB2pbulk139	**533**	**90**	**498**	**592**	Bulk fibrous peat picked free of roots; additional sample also ran and was dated as 255 yrs +/- 30 y uncalibrated age (lab no. WW8372).
IFIB3pbulk60			**28**	**54**	Bulk sedge peat picked free of roots

Table 4. Radiocarbon data in support of age-dating transitional peat. See http://calib.qub.ac.uk/CALIBomb/frameset.html using Levin post-bomb data set. Sample name reflects peat core and type of sample dated (bulk = bulk peat, pbulk = bulk sample picked free of roots, macro = macrofossil). Bold indicates transitional peat-continued.

SampleID	**CalBPmax**	**Prob (%)**	**Min ^{14}CAge in 2009**	**Max ^{14}Cage in 2009**	**Notes**
IFIB3bulkS75			30	47	Bulk sedge peat
IFIB3pbulk133	3717	95	3628	3776	Moss and sedge leaves from lake/forest peat boundary
IFIF1pbulk98	2279	74	2211	2338	Sedge, Sphagnum sp. peat , roots picked

Table 5. ^{210}Pb CRS dating of peat layers at Koyukuk Flats (KF) and Innoko Flats Young Bogs (IFYB). Bold values indicates transitional layer between frozen forest and thawed bog peats. Regression fits between ^{210}Pb (x) and ^{14}C (y) were y = 0.99x - 3.0; R^2 = 0.95 for KFUY2 (2-22 cm depth); y = 1.6x + 2.7, R^2 = 0.86 for KFUI3 (8-20 cm depth).

Sample	Depth	+/-s1	^{210}Pb (dpm/g)	+/-	^{226}Ra (dpm/g)	+/-	Drymass (g/cm^2)	CRS date at bottom of interval	CRS date at middle of interval
KFUI 3.002	2	0.29	6.10	1.60	2.25	0.43	0.02	2008	2008
KFUI 3.006	6	0.41	15.45	2.37	1.98	0.46	0.04	2005	2006
KFUI 3.008	8	0.17	18.36	2.36	3.85	0.45	0.04	2002	2004
KFUI 3.010	10	0.12	21.04	2.13	2.80	0.39	0.04	1998	2000
KFUI 3.012	12	0.10	19.71	1.84	-0.57	0.32	0.06	1989	1994
KFUI 3.014	14	0.10	14.99	1.43	0.79	0.25	0.08	1978	1984
KFUI 3.016	16	0.09	9.63	1.21	0.39	0.21	0.14	1958	1969
KFUI 3.019	19	0.06	6.02	0.71	0.76	0.13	0.21	1917	1941
KFUI 3.020	20	0.06	7.23	0.99	0.78	0.19	0.05	1853	1887
KFUY 2.002	2	0.08	6.68	1.07	0.56	0.21	0.02	2008	2008
KFUY 2.004	4	0.46	8.70	1.50	1.83	0.31	0.02	2007	2007
KFUY 2.006	6	0.37	8.78	1.98	0.94	0.39	0.02	2007	2007
KFUY 2.008	8	0.27	4.73	0.92	1.01	0.19	0.04	2006	2006
KFUY 2.010	10	0.16	9.07	1.27	1.53	0.25	0.06	2004	2005
KFUY 2.012	12	0.16	13.92	2.39	1.19	0.46	0.08	2000	2002
KFUY 2.014	14	0.10	13.99	1.52	-0.29	0.28	0.06	1996	1998
KFUY 2.016	16	0.10	11.60	1.47	1.47	0.29	0.06	1993	1995
KFUY 2.018	18	0.09	10.79	1.36	2.13	0.27	0.06	1990	1992
KFUY 2.020	20	0.09	6.45	1.41	2.35	0.30	0.06	1989	1989
KFUY 2.022	22	0.10	9.40	1.31	2.26	0.27	0.04	1987	1988
KFUY 2.024	24	0.09	6.70	0.90	0.15	0.23	0.04	1985	1986
KFUY 2.026	26	0.07	4.85	0.70	0.45	0.18	0.06	1983	1984
KFUY 2.028	28	0.08	3.83	0.81	1.00	0.21	0.08	1981	1982
KFUY 2.030	30	0.08	3.57	0.78	0.10	0.20	0.06	1980	1981
KFUY 2.035	35	0.06	4.70	0.58	0.12	0.14	0.20	1971	1976
KFUY 2.040	40	0.06	3.25	0.56	0.17	0.14	0.25	1962	1967
KFUY 2.050	50	0.05	2.75	0.47	0.15	0.12	0.40	1942	1953
KFUY 2.053	53	0.04	2.16	0.37	0.11	0.09	0.18	1930	1935
KFUY 2.060	60	0.05	1.42	0.48	-0.19	0.13	0.56	1865	1906

Table 5. ^{210}Pb CRS dating of peat layers at Koyukuk Flats (KF) and Innoko Flats Young Bogs (IFYB). Bold values indicates transitional layer between frozen forest and thawed bog peats. Regression fits between ^{210}Pb (x) and ^{14}C (y) were y = 0.99x - 3.0; R^2 = 0.95 for KFUY2 (2-22 cm depth); y = 1.6x + 2.7, R^2 = 0.86 for KFUI3 (8-20 cm depth), continued.

Sample	Depth	+/-s1	^{210}Pb (dpm/g)	+/-	^{226}Ra (dpm/g)	+/-	Drymass (g/cm^2)	CRS date at bottom of interval	CRS date at middle of interval
IFYB 1.004	4	0.11	4.72	0.96	1.56	0.25	0.04	2008	2009
IFYB 1.010	10	0.07	5.64	0.63	0.12	0.15	0.06	2006	2007
IFYB 1.013	13	0.05	4.91	0.52	0.59	0.12	0.12	2001	2004
IFYB 1.019	19	0.06	4.94	0.59	0.90	0.14	0.24	1991	1997
IFYB 1.028	**28**	**0.04**	**3.42**	**0.35**	**0.43**	**0.08**	**0.36**	**1975**	**1984**
IFYB 1.040	40	0.03	0.84	0.35	0.47	0.09	0.60	1970	1972
IFYB 1.051	51	0.02	0.79	0.23	0.12	0.06	1.10	1945	1959
IFYB 1.065	65	0.02	0.89	0.26	0.50	0.07	1.54	1881	1921
IFYB 1.082	82	-	-	-	-	-			
IFYB 2.007	7	0.10	2.79	0.99	-0.31	0.26	0.06	2008	2009
IFYB 2.014	14	0.07	4.06	0.64	0.10	0.16	0.06	2007	2008
IFYB 2.018	18	0.09	6.91	0.96	0.71	0.25	0.04	2006	2006
IFYB 2.022	22	0.06	8.87	0.78	-0.11	0.18	0.08	2002	2004
IFYB 2.025	**25**	**0.05**	**12.45**	**0.67**	**0.02**	**0.12**	**0.09**	**1994**	**1998**
IFYB 2.030	30	0.13	6.44	0.52	0.45	0.11	0.45	1963	1981
IFYB 2.041	41	0.03	2.07	0.27	0.17	0.07	0.66	1913	1942
IFYB 2.048	48	0.02	1.19	0.22	0.90	0.06	0.63	1849	1872
IFYB 2.053	53	0.02	0.99	0.22	1.25	0.06	1.45	-	-

.

Table 6. Parameter values for the rectangular hyperbolic light response curves (eq. 3) and exponential response of ER and CH_4 to soil temperature at 25 cm depth (eq. 4). Bold values indicate correlation between explanatory and response variables.

Parameter	Units	Frozen	Young	Intermediate	Old	Fen
Rectangular hyperbola: NEE~PPFD						
α_{RH}	mg C μmol photons $^{-1}$	211	34	101	102	-
β_{RH}	mg C m^{-2} hr^{-1}	9940	7586	10342	8729	-
γ_{RH}	mg C m^{-2} hr^{-1}	3895	662	1828	4380	-
Exponential relationship: ER~ 25 cm soil temp						
A	mg CO_2-C m^{-2} hr^{-1}	14.7	17.5	21.8	29.5	65.0
b	mg CO_2-C m^{-2} hr^{-1}	0.115	-0.063	0.007	0.010	-0.052
r^2		**0.24**	0.01	**0.25**	0.00	**0.28**
Exponential relationship: CH_4~ 25 cm soil temp						
A	mg CH_4-C m^{-2} hr^{-1}	3.9	8.4	68.8	3.5	82.7
b	mg CH_4-C m^{-2} hr^{-1}	0.217	0.160	0.215	0.245	0.082
r^2		0.10	**0.29**	**0.43**	**0.36**	**0.24**

Table 7. Number of samples per measurement for each site throughout the growing season 2011. NEE: net ecosystem CO_2 exchange, ER: ecosystem respiration, CH_4: methane efflux.

Measurement	NEE			ER			CH_4		
Site	6/1/2011	7/25/2011	9/25/2011	6/1/2011	7/25/2011	9/25/2011	6/1/2011	7/25/2011	9/25/2011
Frozen Plateau 1	2	8	4	2	8	0	2	8	5
Frozen Plateau 2	2	6	4	2	7	5	2	6	4
Frozen Plateau 3	2	8	5	2	9	5	2	7	4
Young Bog 1	1	9	5	1	10	5	3	7	5
Young Bog 2	1	5	4	0	6	5	2	7	5
Young Bog 3	1	9	5	1	8	5	3	7	5
Intermediate Bog 1	12	9	5	13	9	5	10	7	4
Intermediate Bog 2	2	6	7	3	5	6	3	7	6
Intermediate Bog 3	2	8	5	2	8	5	3	8	5
Old Bog 1	2	7	5	2	7	4	3	8	5
Old Bog 2	2	6	5	2	7	5	3	5	5
Old Bog 3	17	8	6	15	8	6	6	7	5
Fen 1	3	1	0	3	1	0	3	6	6
Fen 3	2	2	0	2	2	0	3	6	4
Fen 4	2	1	0	2	1	0	3	4	6

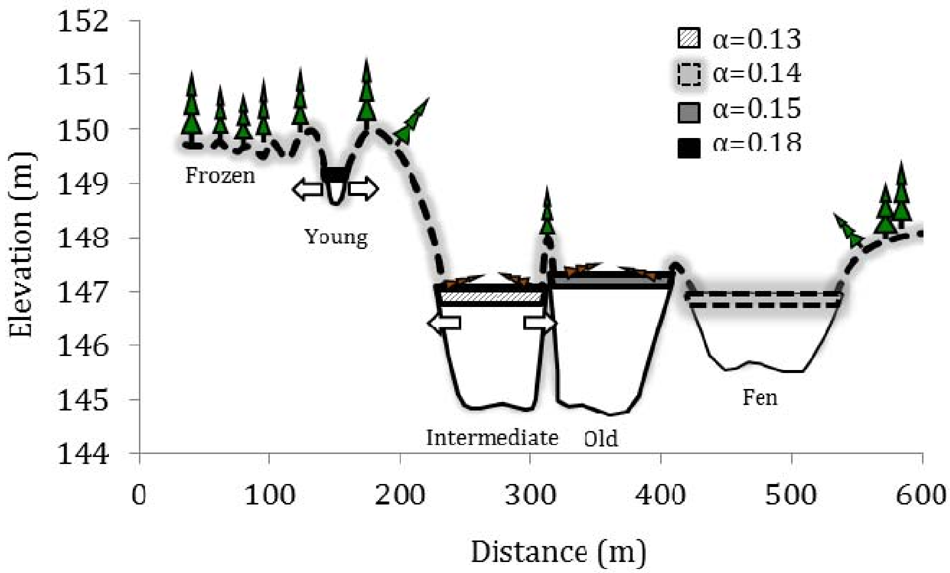

Figure 9. Conceptual model illustrating the transformation of frozen plateau to bog and fen features. The black dashed line represents the vegetated ground surface of the frozen plateau. White arrows indicate degree of lateral expansion of thaw features. The color of the surface of each feature is related to the albedo (α), here measured under diffuse radiation conditions (Table 1) with the forest floor (excluding young bog sites) being characterized by α=0.14 (see Table 1, Table 2), shown with medium grey shadow surrounding the dashed line. The depth of each feature represents the distance from the feature surface to the contact with silt.

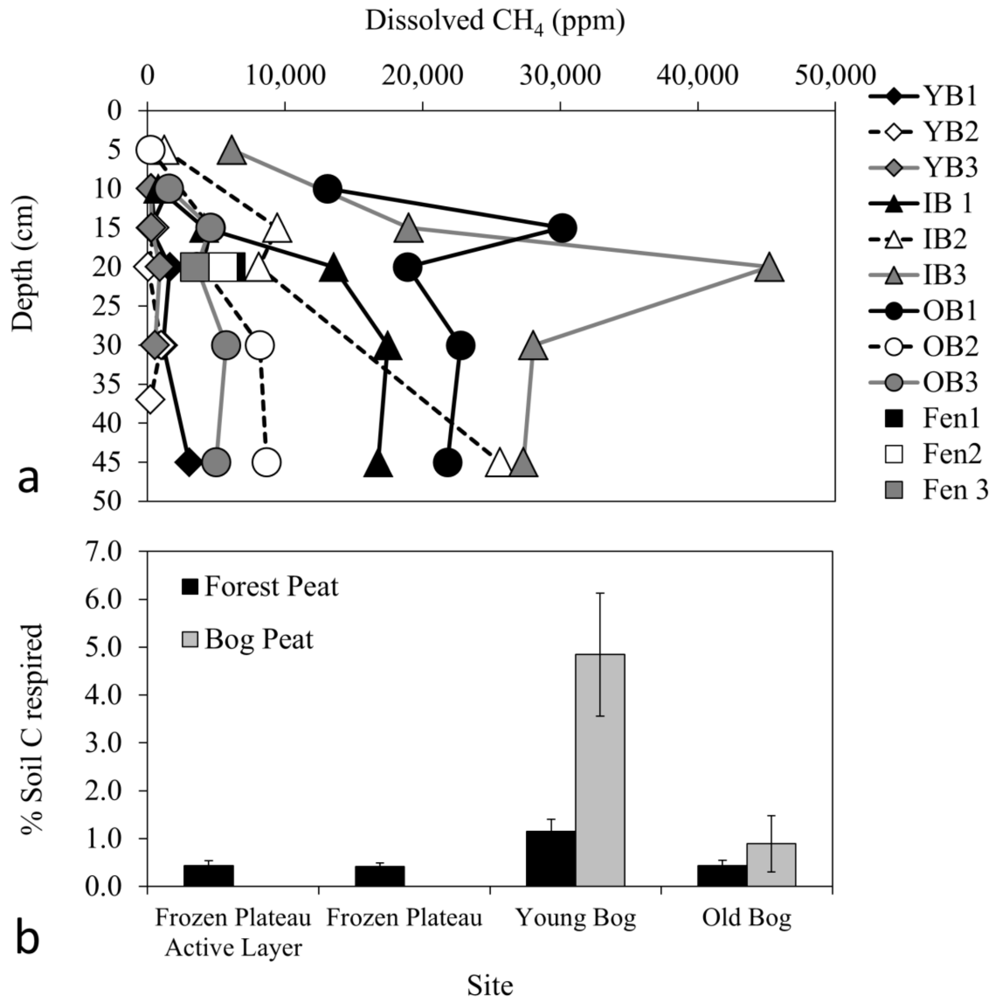

Figure 10. (a) Dissolved CH_4 (ppm) with depth for each site type, collected during the 2009 growing season. For dissolved CH_4 methodologies, see Wickland *et al.*. (2006). Site types are abbreviated in the legend: young bogs (YB), intermediate bogs (IB), and old bogs (OB). (b) Percent of total soil C respired during 112-day incubations of peat material collected during the 2009 growing season. Percent respired was significantly higher for young bog peat than forest peat s or old bog peat ($p<0.001$).

2.8 References

Appleby P G and Oldfield F 1978 The calculation of lead-210 dates assuming a constant rate of supply of unsupported ^{210}Pb to the sediment *Catena* **5** 1–8

Bonan G B, Pollard D and Thompson S L 1992 Effect of boreal forest vegetation on global climate *Nature* **359** 719–718

Briegleb B and Ramanathan V 1982 Spectral and Diurnal Variations in Clear Sky Planetary Albedo *Journal of Applied Meteorology* **21** 1160–71

Cao M, Marshall S and Gregson K 1996 Global carbon exchange and methane emissions from natural wetlands: Application of a process-based model *Journal of Geophysical Research* **101** 14,399–14,414

Carroll P and Crill P M 1997 Carbon balance of a temperate poor fen period *Global Biogeochemical Cycles* **11** 349–56

Coakley J A 2003 Reflectance and albedo, surface *Encyclopedia of the Atmosphere* 1914–23

Dise N B, Gorham E and Verry E S 1993 Environmental factors controlling methane emissions from peatlands in northern Minnesota *Journal of Geophysical Research* **98** 10583

Dunn A L, Barford C C, Wofsy S C, Goulden M L and Daube B C 2007 A long-term record of carbon exchange in a boreal black spruce forest: means, responses to interannual variability, and decadal trends *Global Change Biology* **13** 577–90

Froese D G, Westgate J A, Reyes A V., Enkin R J and Preece S J 2008 Ancient permafrost and a future, warmer Arctic. *Science* **321** 1648

Frolking S, Talbot J, Jones M C, Treat C C, Kauffman J B, Tuittila E and Roulet N 2011 Peatlands in the Earth's 21st century climate system *Environmental Review* **19** 371–96

Grosse G, Harden J, Turetsky M, McGuire A D, Camill P, Tarnocai C, Frolking S, Schuur E A G, Jorgenson T, Marchenko S, Romanovsky V, Wickland K P, French N, Waldrop M, Bourgeau-Chavez L L and Striegl R G 2011 Vulnerability of high-latitude soil organic carbon in North America to disturbance *Journal of Geophysical Research* **116** 1–23

Heikkinen J E P, Maljanen M, Aurela M, Hargreaves K J and Martikainen P J 2002 Carbon dioxide and methane dynamics in a sub-Arctic peatland in northern Finland *Polar Research* **21** 49–62

Heyer J, Berger U, Kuzin I L and Yakovlev O N 2002 Methane emissions from different ecosystem structures of the subarctic tundra in Western Siberia during midsummer and during the thawing period *Tellus* **54** 231–49

Hua Q and Barbetti M 2004 Review of tropospheric bomb ^{14}C data for carbon cycle modeling and age calibration purposes *Radiocarbon* **46** 1273–98

Jorgenson M T, Racine C H, Walters J C and Osterkamp T E 2001 Permafrost degradation and ecological changes associated with a warming climate in central alaska *Climate Change* **48** 551–79

Jorgenson M T, Romanovsky V, Harden J, Shur Y, O'Donnell J A, Schuur E A G, Kanevskiy M and Marchenko S 2010 Resilience and vulnerability of permafrost to climate change *Canadian Journal of Forestry Research* **40** 1219–36

Jorgenson M T, Harden J, Kanevskiy M, Donnell J O, Wickland K, Ewing S, Manies K, Zhuang Q, Shur Y, Striegl R and Koch J 2013 Reorganization of vegetation , hydrology and soil carbon after permafrost degradation across heterogeneous boreal landscapes *Environmental Research Letters* **8** 1–13

Kane E S, Chivers M R, Turetsky M R, Treat C C, Petersen D G, Waldrop M P, Harden J W and McGuire A D 2013 Response of anaerobic carbon cycling to water table maniplation in an Alaskan rich fen *Soil Biology and Biochemistry* **58** 50–60

Kanevskiy M, Jorgenson T, Shur Y, O'Donnell J, Harden J, Zhuang Q and Fortier D Cryostratigraphy and Permafrost Evolution in Lacustrine Lowlands of West-Central Alaska *Permafrost and Pariglacial Processes* in review

Kanevskiy M, Shur Y, Fortier D, Jorgenson M T and Stephani E 2011 Cryostratigraphy of late Pleistocene syngenetic permafrost (yedoma) in northern Alaska, Itkillik River exposure *Quaternary Research* **75** 584–96

Lawrence D M, Slater A G, Romanovsky V E and Nicolsky D J 2008 Sensitivity of a model projection of near-surface permafrost degradation to soil column depth and representation of soil organic matter *Journal of Geophysical Research* **113** 1–14

Lohila A, Aurela M, Regina K and Laurila T 2003 Soil and total ecosystem respiration in agricultural fields : effect of soil and crop type *Plant and Soil* **251** 303–17

MacDonald G M, Beilman D W, Kremenetski K V, Sheng Y, Smith L C and Velichko A A 2006 Rapid early development of circumarctic peatlands and atmospheric CH_4 and CO_2 variations. *Science (New York, N.Y.)* **314** 285–8

O'Donnell J A, Aiken G R, Kane E S and Jones J B 2010 Source water controls on the character and origin of dissolved organic matter in streams of the Yukon River basin, Alaska *Journal of Geophysical Research* **115** 1–12

O'Donnell J A, Jorgenson M T, Harden J W, McGuire a. D, Kanevskiy M Z and Wickland K P 2011 The Effects of Permafrost Thaw on Soil Hydrologic, Thermal, and Carbon Dynamics in an Alaskan Peatland *Ecosystems* **15** 213–29

Olefeldt D, Turetsky M R, Crill P M and McGuire a D 2012 Environmental and physical controls on northern terrestrial methane emissions across permafrost zones *Global Change Biology* **19** 589–603

Qin D, Manning M, Marquis M and Averyt K 2007 *Climate Change 2007: The Physical Science Basis* (Cambridge University Press)

Reichstein M, Stoy P C, Desai A R, Lasslop G and Richardson A D 2012 Chapter 9 Partitioning of Net Fluxes *Eddy Covariance: A Practical Guide to Measurement and Data Analysis* ed M Aubinet, T Vesala and D Papale (Dordrecht: Springer Netherlands) pp 263–89

Reimer P J, Brown T A and Reimer R W 2004 Discussion : Reporting and calibration of post-bomb 14C data *Lawrence Livermore National Labs*

Riordan B, Verbyla D and McGuire A. D 2006 Shrinking ponds in subarctic Alaska based on 1950–2002 remotely sensed images *Journal of Geophysical Research* **111** 1–11

Roulet N T, Lafleur P M, Richard P J H, Moore T R, Humphreys E R and Bubier J L 2007 Contemporary carbon balance and late Holocene carbon accumulation in a northern peatland *Global Change Biology* **13** 397–411

Schuur E A G, Bockheim J G, Canadell J G, Euskirchen E, Field C B, Goryachkin S V., Hagemann S, Kuhry P, Lafleur P M, Lee H, Mazhitova G, Nelson F E, Rinke A, Vladimir E, Shiklomanov N, Tarnocai C, Venevsky S, Vogel J G and Zimov S A 2008 Vulnerability of permafrost carbon to climate change : implications for the global carbon cycle *Bioscience* **58** 701–14

Smith L C, MacDonald G M, Velichko A A, Beilman D W, Borisova O K, Frey K E, Kremenetski K V and Sheng Y 2004 Siberian peatlands a net carbon sink and global methane source since the early Holocene. *Science (New York, N.Y.)* **303** 353–6

Stoy P C, Street L E, Johnson A V., Prieto-Blanco A and Ewing S A 2012 Temperature, heat flux, and reflectance of common subarctic mosses and lichens under field conditions: might changes to community composition impact climate-relevent surface fluxes? *Arctic, Antarctic, and Alpine Research* **44** 500–8

Talling F 1961 Photosynthesis under natural conditions *Annual Review Plant Physiology* **12** 133–54

Tarnocai C, Canadell J G, Schuur E A G, Kuhry P, Mazhitova G and Zimov S A 2009 Soil organic carbon pools in the northern circumpolar permafrost region *Global Biogeochemical Cycles* **23** 1–11

Torn M and Chapin III F S 1993 Environmental and biotic controls over methane flux from arctic tundra *Chemosphere* **26** 357–68

Treat C C, Bubier J L, Varner R K and Crill P M 2007 Timescale dependence of environmental and plant-mediated controls on CH_4 flux in a temperate fen *Journal of Geophysical Research* **112** 1–9

Turetsky M R, Treat C C, Waldrop M P, Waddington J M, Harden J W and McGuire A D 2008 Short-term response of methane fluxes and methanogen activity to water table and soil warming manipulations in an Alaskan peatland *Journal of Geophysical Research* **113** 1–15

Turetsky M R, Wieder R K and Vitt D H 2002 Boreal peatland C fuxes under varying permafrost regimes *Soil Biology and Biochemistry* **34** 907–12

United States Department of Interior 1987 *Innoko National Wildlife Refuge Comprehensive Consrevaation Plan, Environmental Impact Statement, Wilderness Review*

Wickland K P, Striegl R G, Neff J C and Sachs T 2006 Effects of permafrost melting on CO2 and CH4 exchange of a poorly drained black spruce lowland *Journal of Geophysical Research* **111** 1–13

Wille C, Kutzbach L, Sachs T, Wagner D and Pfeiffer E-M 2008 Methane emission from Siberian arctic polygonal tundra: eddy covariance measurements and modeling *Global Change Biology* **14** 1395–408

Williams M, Street L E, Wijk M T and Shaver G R 2006 Identifying differences in carbon exchange among arctic ecosystem types *Ecosystems* **9** 288–304

Woodward A and Beever E A 2011 Conceptual Ecological Models to Support Detection of Ecological Change on Alaska National Wildlife Refuges *United States Geological Survey*

Zhuang Q, Melillo J M, McGuire A D, Kicklighter D W, Prinn R G, Steudler P A, Felzer B S and Hu S 2007 Net emissions of CH_4 and CO_2 in Alaska: implications for the region's greenhouse gas budget *Ecological Applications* **17** 203–12

CHAPTER 3

3.0 EFFECT OF RECENT PERMAFROST THAW ON THE SPATIAL DISTRIBUTION OF CO_2 AND CH_4 EXCHANGE IN A WESTERN ALASKA PEATLAND

Contribution of Authors and Co-Authors

Manuscript in Chapter 3

Author: Type Carmel Eliise Johnston

Contributions: Carmel Johnston contributed to project design, and led data collection, data analysis, and original manuscript composition.

Co-Author: Dr. Stephanie A. Ewing

Contributions: Dr. Stephanie Ewing was responsible for project design, securing funding, data collection methodologies, data analysis, and original composition and editing of manuscript.

Co-Author: Dr. Merritt R. Turetsky

Contributions: Dr. Merritt Turetsky was responsible for project design, contributed methodologies for data collection and analysis, and critiqued the manuscript.

Co-Author: Dr. Jennifer W. Harden

Contributions: Dr. Jennifer W. Harden was responsible for project design, securing funding, radiocarbon data analysis, and manuscript editing.

Co-Author: Dr. A. David McGuire

Contributions: Dr. A. David McGuire contributed to project design.

Co-Author: Dr. Miriam C. Jones

Contributions: Dr. Miriam C. Jones contributed radiocarbon data analysis and manuscript editing.

Manuscript Information Page

Carmel E. Johnston, Stephanie A. Ewing, Merritt R. Turetsky, Jennifer W. Harden, A. David McGuire, Miriam Jones

Status of Manuscript:

_X__ Prepared for submission to a peer-reviewed journal
____ Officially submitted to a peer-review journal
____ Accepted by a peer-reviewed journal
____ Published in a peer-reviewed journal

IOP Publishing: Environmental Research Letters
Focus on the Impact of Climate Change on Wetland Ecosystem Carbon Dynamics

3.1 Abstract

Thawing of permafrost soils in northern ecosystems can enhance production of the greenhouse gas methane (CH_4), releasing it through diffusion, ebullition, and advection pathways. Recent work has shown that peak CH_4 exchange may occur in features that had thawed decades to centuries, but spatial variation in the rate and mode of CH_4 release has not been extensively tested. Here we test the idea that spatial variation is an important aspect of flux rates and pathways. To address this aspect of flux variability, we quantified temporal and spatial aspects of CH_4 and CO_2 emissions during summer 2012, at sites along lateral transects in three young to intermediate aged (30-500 y since most recent thaw) collapse-scar features at the Alaska Peatland Experiment (APEX) site near Fairbanks. At APEX, spatial variability within and among thaw features was substantial, with average surface CH_4 fluxes of 5.42 ± 1.16 mg CH_4-C m^{-2} hr^{-1} and average CH_4 fluxes in subsurface bubbles of 0.83 ± 0.34 mg CH_4-C m^{-2} hr^{-1}. The highest surface flux (130.53 ± 67.34 mg CH_4-C m^{-2} hr^{-1}), volumetric subsurface bubble production (13 ± 5 mL m^{-2} hr^{-1}) and CH_4 fluxes in subsurface bubbles (2.78 ± 1.71 mg CH_4-C m^{-2} hr^{-1}) were observed at locations characterized by both warmer and wetter soil conditions compared to other positions. Methane production in subsurface bubbles at APEX equaled an average of 20.5 ± 11% of surface flux. At APEX bogs CO_2-C equivalent CH_4 efflux was 113 ± 21% of CO_2-C influx when considered as 100-y global warming potential. We propose that the APEX sites represent a trend of increased net warming potential as the frequency – if not the duration – of thaw feature development increases during the coming century.

3.2 Introduction

The area of northern hemisphere permafrost has been decreasing steadily in the last several decades and is predicted to reach a minimum by the end of this century (Lawrence *et al.* 2012). Carbon dynamics in thawing peatlands are of increasing concern, as CH_4 and CO_2 release may be an important positive feedback to a warming atmosphere. However, the controls on the suite of hydrologic and biogeochemical processes controlling trace gas exchange in these environments are not fully understood (Frolking *et al.* 2011, Jorgenson *et al.* 2010, Turetsky *et al.* 2002).

A particular challenge in peatland CH_4 flux assessment is spatial and temporal variability. One source of this variability is CH_4 release by the process of ebullition. Ebullition refers to episodic release of bubbles and is the topic of increased research interest in wetlands and northern peatlands (Walter *et al.* 2006, 2007, Baird 2004). In these carbon-rich, anoxic environments, 18-50% of CH_4 release may occur as ebullition (Christensen and Panikov 2003, Goodrich *et al.* 2011, Whalen 2005). Ebullition events can be difficult to quantify because their magnitude and frequency reflect both biotic and physical controls, resulting in highly stochastic and episodic fluxes (Strack *et al.* 2005, Strack and Waddington 2007, Tokida *et al.* 2007a, Cronk and Fennessy 2001, Goodrich *et al.* 2011). In northern frozen peatland environments, understanding the pathways of greenhouse gas exchange in general – and methane flux in particular - is critical for understanding the effect of climate change on C cycling and thus global warming potential (GWP) over longer timescales.

Previous work at Innoko National Wildlife Refuge in western Alaska (Johnston *et al.* in review) evaluated trace gas fluxes across a ~1000-y thaw chronosequence (Figure 11) and concluded that CH_4 emissions following lowland permafrost thaw are enhanced over centuries, but limited over millennia. Peak CH_4 exchange (+2.52 ± 0.98 mg CH_4-C m^{-2} hr^{-1}) occurred in features that thawed 100-590 ya, where soils were warmer than those sites that thawed more recently (10-30 y), which have shallower water tables and a less dense moss structure than older sites (570-1700 y). In terms of global warming potential, CH_4 flux at these intermediate age sites offset 49 ± 21% of site level net ecosystem exchange (NEE), compared to 1.0 ± 0.7% and 10.1 ± 5.7% at young and old sites, respectively.

In this work, we draw upon previously unpublished results at Innoko, suggesting that although observed ebullition fluxes were small relative to surface CH_4 fluxes, their spatial variation could be significant. At the Alaska Peatland Experiment near Fairbanks (APEX), initial ebullition sensor deployment (Klapstein 2012) showed the greatest shallow and deep subsurface bubble production at the youngest of thawed sites (most recent tree mortality 27 y ago based on aerial photo interpretation), but observations were limited to the edges of thaw features. To further investigate temporal and spatial variation in surface and ebullitive flux across similar thaw features, we identified lateral transects across three collapse-scar features at APEX (30-500 y), and monitored surface fluxes and subsurface bubble production during the 2012 growing season.

3.3 Methods

3.3.1 Study Areas

The APEX site is located adjacent to the Bonanza Creek Long Term Ecological Research site (64.69˚N, 148.32˚W; Figure 11). We conducted our study at APEX in order to investigate spatial dynamics for comparison to results from previous work at the Innoko Flats National Wildlife Refuge (NWR; 63.58˚N, 157.72˚W) (Johnston *et al..,* in review). Although the two sites are not identical, the APEX site provides opportunity for an accessible comparison to the Innoko intermediate aged sites. The APEX site represents the transition from rolling uplands southwest of Fairbanks, AK, to the floodplain north of the Tanana River, whereas the Innoko Flats site is located in extensive collapse-scar bog and fen lowlands, developed on the eolian and lacustrine silts south of the Innoko River (Kanevskiy *et al.*., in review; Jorgenson *et al.*., 2013). The APEX site is characterized by a subarctic continental climate with a mean daily temperature of -24˚C in January and +16˚C in July, and mean annual precipitation of 287 mm y^{-1} (1971-2000; Hinzman *et al.* 2006). At APEX, 30% of precipitation (269 mm y^{-1}) comes in the form of snow (Hinzman *et al.* 2006). The Innoko site is also in the subarctic continental boreal region but is somewhat colder and wetter, with a mean daily temperature of -17 ˚C in January and +14 ˚C in July, and mean annual precipitation of 445 mm y^{-1} (1993-2007; Woodward & Beever, 2011). The snow depth in April 2011 at Innoko was 0.60 ± 0.09 m across 18 locations, consistent with previous observations for the refuge (Johnston *et al.* in review, Woodward and Beever 2011)

3.3.2 Study Design

Following work by Johnston *et al.* (in review), we focused this effort on a series of previously identified thaw features at the APEX site (Klapstein 2012; Tables 8-9), including four landscape units: a zone of frozen forested peat underlain by permafrost and three collapse scar bogs interpreted as forming after the most recent episode of permafrost thaw occurred 30-500 years ago based on a combination of radiocarbon dates from the transition of forest peat to collapse-scar bog peat and observation of tree loss in aerial photographs (see results section). These features are referred to in order of their interpreted time intervals since most recent possible thaw (as of 2012): 'Bog 1', 'Bog 2', and 'Bog 3', respectively. These bogs are similar in size (2000-5000 m^2), but Bog 3 has a thicker acrotelm and woodier vegetation, suggesting greater time since thaw. To determine the timing of thaw in the older sites, Russian peat cores were collected by Brian Benscoter in 2009 and stored frozen at the University of Alaska Fairbanks (UAF). Cores were subsampled and analyzed for plant macrofossils to determine the transition from forest peat to collapse-scar bog peat. Terrestrial plant macrofossils were picked and cleaned with deionized water before being sent to the U.S. Geological Survey Eastern Geology and Paleoclimate Science Center ^{14}C laboratory for graphitization and to the Center for Accelerator Mass Spectrometry (CAMS), Lawrence Livermore National Laboratory for accelerator mass spectrometry (AMS) radiocarbon dating.

Landscape units comprising the thaw chronosequence at Innoko included a forested permafrost plateau and collapse scar bogs at three stages of thaw (young (15-34y), intermediate (100-590), and old (570-1700)) (Johnston *et al.* in review). The thaw features of APEX were selected in order to examine spatial patterns in features at approximately the same stage of development as the Innoko intermediate bogs. The size, morphology, and vegetation at the APEX bogs are most similar to the intermediate bogs at Innoko (Table 9).

A detailed drawing of the site layout and location of deployments is presented in Figure 19. Boardwalks were constructed between 2008 and 2012, and each bog feature was sampled at three positions: 'edge' (0-2 m from edge of bog), 'middle' (2-8 m from edge of bog), and 'center' (8-16 m from edge of bog).

A static flux chamber collar was placed at each location, and one set of two bubble traps was installed next to each static flux collar within each section at Bog 2 and Bog 3. Two sets of installations were located in each section of Bog 1(Figure 19).

Vegetation surveys were conducted in 2012 using standard methods (Viereck 2007) and more detail can be found in Wickland *et al.* (2006). The forested permafrost zones are characterized by a shallow permafrost table and a black spruce (*Picea mariana*) canopy with an understory dominated by ericaceous evergreen and deciduous dwarf-shrubs, tussock-forming cotton grass (*Eriophorum vaginatum)*, lichens, and feather mosses. Bog 1 and Bog 2 are large, well-developed collapse scar bogs (5000 and 4000 m^2, respectively), and are dominated by *Sphagnum. obtusum, Carex. aquatilis, E. palustris, C. calyculata, Andromeda. polifolia and E. chamissonis.* Bog 3 is smaller (2000 m^2) with a floating mat of peat over approximately 50 cm of standing water and hummock-hollow microtopography. Deciduous woody plants include dwarf and bog birch (*Betula. nana* and *Betula. glandulosa*), and larch (*Larix. laricinia*). Black spruce saplings are present in the larger, drier hummocks, while hollows remain saturated and close to the water table with more hydrophilic vegetation *S. platyphyllum, S. warnstorfii,* and *Drepanocladus. aduncus*

Surface CO_2 emissions, surface CH_4 emissions, ebullient CH_4 emissions, vegetation, temperature, and hydrologic conditions were monitored at APEX from June to October of 2012. Water table position was measured at the time of each flux measurement using a blow tube technique, measuring the position of the water table against the height of the vegetation. Soil temperature at 20 cm depth was measured using a handheld soil temperature thermistor during each flux measurement. Soil moisture was measured using a ThetaProbe soil moisture sensor for volumetric moisture content (%VMC; accurate to ± 1%; Delta-T Devices).

Surface fluxes were measured at Innoko Flats using static chambers (Carroll and Crill 1997), with specifics described in Johnston *et al.* (in review). At APEX, net ecosystem exchange (NEE), ecosystem respiration (ER), and CH_4 fluxes were measured every week during the 2012 growing season using static chambers (Carroll and Crill 1997). Cubic chambers with a height (H) of 61 cm were constructed of 1/8” aluminum angle and clear 1/8” polycarbonate Lexan with two sample ports and two internal fans powered by an external battery. For NEE and ER, chamber air was circulated through the two ports connected to a PP Systems EGM-4 CO_2/H_2O analyzer, and CO_2 concentrations were automatically recorded every three seconds over a three minute period for each chamber type (840-500 PC Communication Software). For CH_4 fluxes, six 20 mL chamber air samples were manually collected from a dedicated port over 30 minutes in a syringe. If samples could not be analyzed within 24 hours, they were immediately transferred into a pre-evacuated 40 mL glass vial. Sample vials were transferred back to the University of Alaska, Fairbanks where they were analyzed for CH_4 concentrations using a Varian 3900 gas chromatograph (GC) system equipped with flame ionization detector. The chromatograph was equipped with a Haysep Q column and flame ionization detector, and signal was converted to concentration using a seven point calibration curve (0-501,000 ppm CH_4; see Treat *et al.*. 2007). During flux measurements air temperature inside and outside the chamber was manually recorded, along with photosynthetically active photon flux density (PPFD) within the chamber during NEE measurements.

Our gas flux sampling strategy sought to capture a range of light and temperature conditions over the course of each field campaign. Most fluxes were measured during the daylight hours, with one diurnal round for each replicate set of sites. Seven to eight rounds of measurements of surface CO_2 and CH_4 flux were taken at each site throughout the growing season with diurnal measurements during one round.

<u>3.3.3 APEX- Subsurface Sensors</u>

Shallow bubble traps (Figure 21; footprint area = 0.0314 m^2) were installed using methods described in Klapstein (2012). Bubble traps were constructed using inverted plastic funnels connected to polyvinyl chloride (PVC) piping attached to Tygon tubing and a 10 mL syringe (plunger removed). A set of funnels was positioned 20 cm below the peat surface to capture bubbles traveling up through peat at depths greater than 20 cm. Deep bubble traps (footprint area = 0.00865 m^2) were installed 60 cm below the peat surface, capturing bubbles from depths deeper than 60 cm. A three-way stopcock on the top allowed for each apparatus to be manually backfilled with groundwater, so that any bubble accumulation would displace the water and be isolated at the top of the syringe. Upon installation, funnels were backfilled, allowed to settle for one day, and then all were backfilled again within 30 minutes of each other.

Bubble traps were installed June 1, 2012, and samples were collected through September 25, 2012. When the gas volume in the syringe was greater than 5 mL (approximately once every two weeks), the gas was extracted with a 10 mL syringe, acting to capture the sample and backfill the trap. The sample syringes were transported to the lab where their contents were analyzed for CH_4 concentration at the University of Alaska, Fairbanks within 24 hours of collection, as described above.

3.3.4 Diffusive Flux Calculations

Linear regression of CO_2 and CH_4 concentrations in static chambers over time was used to determine a slope (S, ppmv s^{-1}) that could then be converted to a gas flux (F, mg C m^{-2} day^{-1}) for CO_2 or CH_4 using the ideal gas law:

$$F = \frac{P_A}{RT} SHM \quad (1)$$

where F for CO_2 is NEE (light chamber) or ER (dark chamber), P_A is atmospheric pressure (atm), R is the gas constant (0.082057 L atm mol^{-1} K^{-1}), T is temperature (K), H is the height of chamber headspace (m), and M is the molecular weight of the gas (mg mol^{-1}). For slope values, weaker linear regression fits ($R < 0.95$; 2% of measurements), likely due to chamber leakage or soil disturbance, were discarded from subsequent analyses.

Analyses of measured gas fluxes were performed using a one-way ANOVA in R (Team 2012). We used a repeated measures analysis of variance and Tukey's honestly significant difference post hoc comparison of means to determine the effects of soil temperature on gas flux. For assessment of trends with light intensity and temperature (equation 3 below), gas flux results from each site and position were pooled across dates in order to have enough measurements for statistical analysis (measurement frequencies shown in Table 12).

NEE is defined as the sum of ER and gross primary production (GPP):

$$NEE = GPP + ER \tag{2}$$

where negative values of GPP and ER (mg CO_2-C m^{-2} h^{-1}) indicate CO_2 uptake. The response of NEE to light intensity is expected to follow a non-linear relationship due to the saturating relationship between PPFD and C uptake. This kind of relationship is consistent with limits on physiological responses to light, which dictate that at some light intensity, leaf photosynthesis reaches a maximum (Talling 1961). The light response of NEE was evaluated as a rectangular hyperbola (Reichstein *et al.* 2012):

$$NEE_{RH} \frac{\alpha_{RH}\beta_{RH}PPFD}{\alpha_{RH}Q + \beta_{RH}} + \gamma_{RH} \tag{3}$$

where α is the initial slope of the light-response curve (μmol CO_2 μmol photons^{-1}), β is the maximum CO_2 uptake rate of the canopy (μmol m^{-2} s^{-1}), γ represents ER (μmol m^{-2} s^{-1}), and PPFD has units of μmol photons m^{-2} s^{-1}..

The response of ER and CH_4 to soil temperature is expected to follow an exponential relationship (Cao *et al.* 1996, Wille *et al.* 2008):

$$F = Ae^{bT} \tag{4}$$

where A and b are fitted parameters. Soil respiration and CH_4 production and emission are a function of complex reactions by diverse populations of organisms that vary across sites. These exchanges will differ from one another and across sites in their dependence on substrate availability (A) and the chemical quality of substrate (b); hence we hypothesize that A and b will differ among landscape units for ER and CH_4 flux (Lohila *et al.* 2003).

One hundred year global warming potentials are calculated on the basis of molecular mass (Qin *et al.* 2007) and therefore must be applied to CH_4-C fluxes with a correction:

$$F_{CO_2-CH_4} = F_{CH_4} GWP \frac{M_{CH_4}}{M_{CO_2}} \tag{5}$$

where $F_{CO2\text{-}CH4}$ is the global warming potential equivalent CO_2 flux (mg CO_2 m^{-2} hr^{-1}), F_{CH4} is methane flux (mg CH_4-C m^{-2} hr^{-1}), GWP is the 100 year GWP of CH_4 (25), and M is the molecular weight of the gas (mg mol^{-1}).

3.4 Results and Discussion

3.4.1 Physical Lowering of Thaw Features

At Innoko Flats we observed a dramatic progression of physical collapse that was consistent with the ice content in the upper 3-4 m of the frozen plateau sites (>2 m; Kanevskiy *et al.* in review), suggesting that physical collapse with thaw drove all or most of the lowering (limited influence from peat decomposition (Johnston *et al.* in review)).

The physical collapse at APEX is much less dramatic (1 m) when compared to Innoko (Figure 20), likely as a function of different permafrost origin, mineral substrate, ice content, and local climate.

3.4.2 Peat Age

Minimum thaw ages in the APEX collapse features (i.e., time since most recent thaw episode) ranged from 27-42 y based on aerial photograph interpretation for Bogs 1-3, to 500 y based on radiocarbon results for charred wood and shrub parts in Bogs 2 and 3 (at base of transition; Table 10; cores collected by B. Benscoter). These thaw ages are considered estimates, as difficulty in sampling the soft peat and the presence of a water pocket at ~50 cm made peat-core extraction difficult. Consequently, peat depths may not be precise and minimal sampling material made obtaining dates from certain depths difficult. For example, the basal sample age from BetaSW.146 is likely too young, which is attributable to the very small sample size and should be rejected. However, the other radiocarbon ages reported in Table 10 are generally consistent with accumulation rates observed at a nearby site (Jones *et al.* 2013). All of the ages from the transition to thaw were taken from the peat horizons that are characterized as forest peat, just below the *Sphagnum* peat that comprises the collapse-scar bog. Therefore, these ages are likely somewhat older than the initiation of thaw. Generally, our combined metrics of thaw age, as well as macrofossil evidence (Jones, *unpublished data*), suggest multiple collapse/refreeze cycles have occurred in these sites (Table 10).

3.4.3 Peat Thaw, Temperature,
Water Table, and Vegetation Structure

APEX temperatures at 20 cm depth were most similar to Innoko temperatures at 25 cm depth within intermediate and old sites (30-1700 y), which were consistently warmer than younger sites (Figure 12; Johnston *et al.,* in review). At APEX, the 20 cm depth temperature for frozen plateaus remained 4-6°C colder than the bogs during the growing season, consistent with results at Innoko, where frozen plateaus were 2.5°C colder than intermediate and old bogs during the 2011 growing season. APEX bogs also thawed earlier to 20 cm depth than the frozen plateau (Figure 12). The warmer conditions of these sites suggest that CH_4 production might be enhanced at these locations. When positions were considered together, the mean temperature at 20 cm depth for Bog 1 was 12.2 ± 0.4°C, significantly greater than the 20 cm depth temperature at Bog 2 or Bog 3 (10.6 ± 0.4°C and 10.3 ± 0.4°C, respectively; p=0.002, Tukey multiple comparison of means), but there was no significant difference in temperature among edge, middle, and center positions when features were considered together (p=0.5133; Tukey multiple comparison of means).

Water table fluctuations in APEX bogs were similar to those observed at Innoko throughout the growing season. At Innoko Flats, water tables were 10-15 cm above the vegetation surface at the intermediate bog and fen sites in May 2011, and fell rapidly with snowmelt between May and June (Johnston *et al.* in review). Similarly, at APEX bogs, water tables were 10-12 cm above the vegetation surface in early June 2012 and persisted through the middle of June, when they began to draw down to the level of the vegetation. At APEX, the edge of Bog 1 and Bog 2 features maintained a water table at the surface of the vegetation throughout the entire growing season, whereas the center of these features had a water table 5-10 cm below the surface throughout the growing season. Thus, although the edges were not significantly warmer, they were wetter at the bog surface.

Innoko intermediate and old bogs and APEX bogs all lost seasonal frost beyond 1.5 m depth at the beginning of the growing season (Table 9). By August 1, 2012, Bog 1 and Bog 3 had no remaining seasonal frost detectable within 1.5 m of the vegetation surface at any point along the transects (Table 8; Table 9). At three meters from the edge of Bog 2 (middle position), seasonal frost remained within 1 m of the ground surface throughout the growing season. All other positions along this transect did not maintain seasonal frost within 1.5 meters any time after August 1, 2012.

The dominant vegetation at APEX bogs was most similar to Innoko intermediate and old bogs. APEX Bog 1 and Bog 2, which maintained the shallowest water tables, supported a plant community dominated by *C. aquatilis* and *E. palustris*, with a relatively open (less dense) structure. These conditions were similar to the intermediate bogs of Innoko Flats (100-590 y), where Johnston *et al.* (in review) suggested that enhanced anoxia and atmospheric exchange promoted CH_4 efflux and/or reduced opportunity for CH_4 consumption. Conditions were somewhat different at Bog 3, which was dominated by *S. fuscum* and *Betula* spp., indicating a drier bog surface that may enhance CH_4 oxidation. The plant community also suggests a more advanced successional stage, similar to the old bogs at Innoko (570-1700 y).

3.4.4 Trace Gas Exchange

The response of NEE and ER to light intensity and 20 cm soil temperature was similar at both the Innoko and APEX sites (Figure 13). The relationship of NEE to light intensity at each Innoko or APEX site was not significantly different from other sites at those locations (p=0.999 amongst APEX sites; Johnston *et al.*., in review) and did not differ significantly between the Innoko and APEX sites (p=0.876). Similarly, the response of ER to temperature did not differ significantly among individual APEX bogs (p=0.141), among APEX bog positions (p=0.239), or between the Innoko and APEX study sites (p=0.857, F-test for a one-way ANOVA; Figure 14). The exponential temperature-based model for ER explained 25% of variance at Innoko frozen and intermediate bog sites, whereas the model explained only 12% of variance at APEX Bog 3, and a lower proportion of observed variance at the other sites (Figure 14). Although these relationships are relatively weak, we suspect that a similar carbon metabolism exists at both locations due to similar vegetation composition (Williams *et al.* 2006).

At APEX, soil temperature at 20 cm depth was the best-observed predictor of CH_4 efflux. The strongest relationship between temperature and CH_4 efflux occurred at Bog 3, explaining 38% of variance. For all APEX sites combined, 21% of variance in CH_4 efflux could be attributed to 20 cm depth soil temperature. Johnston *et al.*. (in review) observed a similar relationship at Innoko, where soil temperature at 25 cm depth explained 43% of the variance of CH_4 efflux at intermediate bogs (30-590 y since thaw), and 36% at old bogs (570-1700 y). Across all Innoko and APEX sites, 11-44% of CH_4 flux was explained by both soil temperature and water table height relative to the vegetation surface, indicating that additional drivers may be influencing CH_4 efflux.

Methane fluxes at APEX bogs exhibited greater variability on a given measurement date than Innoko sites (Figure 17). Several factors are at play in this difference. First, fewer measurements were taken at APEX (18-33 seasonal measurements Table 12) compared to Innoko (44-53 seasonal measurements; Johnston *et al..,* in review), and measurements were spread throughout the growing season instead of being clustered around one date. Moreover, samples were taken at three positions in each bog, potentially increasing variation in the substrate and time since thaw (assuming bogs expand from center outward). When averaged across the transect positions, CH_4 fluxes at APEX Bog 2 were significantly greater than all Innoko frozen, young and old sites and APEX frozen, Bog 1 and Bog 3 (p=0.031; F-test for a one-way ANOVA). The CH_4 flux at APEX Bog 2 was not significantly different from the flux at each of the three Innoko intermediate sites (p=0.944, 0.187, and 0.104 for intermediate replicates 1, 2, and 3, respectively; Tukey multiple comparison of means; Figure 15). When considered together, CH_4 fluxes at the APEX sites (all positions) were not significantly greater than those at the Innoko intermediates (p=0.791).

When fluxes were considered as global warming potential, APEX Bog 1 and Bog 2 showed a tendency toward greater CO_2-equivalent CH_4 efflux than CO_2 influx, with 121 ± 25% to 137 ± 77% offset of NEE (Figure 15). In contrast, APEX Bog 3 exhibited somewhat less CO_2-equivalent CH_4 efflux than CO_2 influx, offsetting 82 ± 8% of NEE, though not significantly less than Bog 1 and Bog 2 (p=0.280). At Innoko, all locations displayed net C uptake with 2 to 400 times greater CO_2-C influx than CH_4-C efflux; in terms of GWP, CH_4 fluxes offset 49 ± 21% of NEE at the Innoko intermediate sites (Johnston *et al.* in review). The Innoko data are consistent with previous work showing that black spruce forests and *Sphagnum* bogs in the boreal region are a net sink of C during the growing season (Dunn *et al.* 2007, Smith *et al.* 2004, Heyer *et al.* 2002). However, less often, peatlands can become a net source of C, specifically under changes that promote drying conditions or different vegetation (Strack and Zuback 2013, Heikkinen *et al.* 2002). The APEX sites have demonstrated pronounced CH_4 production (Turetsky *et al.* 2002, 2008, Treat *et al.* 2007) in locations where thermokarst bog vegetation has established, in addition to a generally warmer mean annual air temperature (16°C) compared to Innoko (14°C).

3.4.5 Subsurface Bubble Production

Spatial variability of subsurface bubble production was prominent at the APEX sites. Subsurface bubble production was greatest at the edge of the Bog 1 (13 ± 5.5 mL gas m^{-2} hr^{-1}) followed by the center and edge of the Bog 2 (8.6 ± 3.4 mL gas m^{-2} hr^{-1} and 5.0 ± 2.2 mL gas m^{-2} hr^{-1}, respectively; Table 9). The center and the edge of Bog 1 also produced the greatest ebullitive CH_4-C flux (2.78 ± 1.71 mg CH_4-C m^{-2} hr^{-1} and 2.16 ± 1.45 mg CH_4-C m^{-2} hr^{-1}, respectively). Despite high subsurface bubble production at Bog 2 edge, it had low CH_4-C flux (+0.32 ± 0.13 mg CH_4-C m^{-2} hr^{-1}) due to low concentrations in bubbles. The center of Bog 3 had a minimal amount of bubbles produced (+1.6 ± 0.8 mL gas m^{-2} hr^{-1}) but had one of the highest CH_4-C efflux rates (+1.35 ± 0.43 mg CH_4-C m^{-2} hr^{-1}) due to high CH_4 concentrations in bubbles. This lack of correlation between bubble production and CH_4 emission could be caused by variation in the lability of the peat with thaw; or changes in vegetation type and thus CH_4 production due to resulting changes in hydrologic conditions (Grosse *et al.* 2011, Lai 2009).

APEX fluxes showed variability both among sites and among positions within each site, yet there was no systematic position or age effect among APEX sites (Figure 15; Figure 16; Table 9). The average ratio of subsurface bubble CH_4 flux to surface CH_4 flux across the transects ranged from 2 ±1% at Bog 2 to 40 ± 20% at Bog 1 (24 ± 10% for all sites combined; Figure 16; Table 8). The Innoko intermediate bogs had fewer measures of subsurface bubble production but these amounted to 4 ±2% of surface CH_4 flux. Each APEX site reached a peak average flux around August 20th, 2012, dropping off steadily through the middle of September to a growing season low flux. Innoko followed a similar pattern, though with limited seasonal time points evaluated; peak flux was measured on August 2nd, 2011 (Figure 17). The variability along the transects and among bog features suggests that the hot spots and hot moments of CH_4 efflux (Shea 2010, Klapstein 2012), do not correspond strongly to thaw age or transect position at APEX sites of similar age. This similarity of thaw age, lack of finer-scale age replication, and feedbacks among physical and biological processes, may obscure age- and transect-related trends. At Innoko, for example, old bogs exhibited a slight lowering of water tables relative to the moss surface as well as changes in vegetation community, which seemed to dampen the fluctuation of water tables. This change could enhance methanotrophy near the surface in the acrotelm, and thus diminish diffusive fluxes (Zhuang *et al.* 2007, Turetsky *et al.* 2008). Additionally, CH_4 ebullition may be physically limited by the dense peat mat in the Innoko old bogs, which increase in density as succession changes the plant community. Bog 3 at APEX shows signs of a drier and denser peat mat, with vegetation similar to that of the Innoko old bogs than that of the Innoko intermediate bogs or the APEX Bog 1 and Bog 2, though it maintained a similar CH_4 flux to the Innoko intermediate sites. With replication of landscape units at Innoko, age-related differences became more apparent; at APEX, elevated CH_4 fluxes were similar among sites and consistent with Innoko intermediates, though they did not vary systematically across position transects. Generally, all sites at APEX approximated replicates of intermediate age at Innoko.

3.5 Conclusions

Permafrost thaw in these lowland settings causes a shift from forested frozen peatlands to saturated unfrozen wetlands. As thaw progresses over decades, vertical and lateral thaw yields larger thaw features characterized by warmer soil temperatures, shallower water tables, and increased CH_4 efflux. In this work at APEX sites, we investigated the effect of position (edge vs. center) on surface flux and subsurface bubble production within three intermediate aged bog features (30-500 y) over a growing season. We found no significant effect of temperature or position within thaw features on chamber methane flux or subsurface bubble production, although wetter positions did produce the highest methane fluxes. We observed variable surface CH_4 efflux and active subsurface production of CH_4 that comprised $24 \pm 10\%$ (ranging from $1 \pm 1\%$ to $80 \pm 53\%$) of surface flux. However, in contrast to earlier work at Innoko Flats (Johnston *et al.*

in review), effluxes of CO_2-equivalent CH_4 approached or exceeded the uptake of CO_2 by a factor of 0.8 to 1.5 when considered as global warming potential, tending toward overall net warming potential from these features (Figure 18). This potential for net warming suggests that other factors such as ice legacy and overall warmer air conditions of the APEX site compared to the Innoko Flats chronosequence (14ºC vs. 16ºC MAAT, respectively), coupled with a distinct landscape position, result in a positive feedback to warming and chronic increase in warming potential from thaw within the APEX northern peatland environment.

3.6 Acknowledgements

This research was made possible by funding from the National Science Foundation (EAR #0630319), the United States Geological Survey, the Montana State University College of Agriculture, and the MSU VP of Research. Thank you to Sara Klapstein for instrument design and initial deployment, and to Chris Dorich, Rebecca Finger, Lillian Aoki, Anna Lello-Smith, and Lily Cohen, and Carme Estruch for insightful participation in fieldwork

3.7. Hydrophone Methodology

Hydrophone devices developed by Varner and Palace (R.K. Varner personal communication) were installed to 20 cm below the peat surface to avoid the water table dropping below the bottom of the device (Klapstein 2012, Goodrich *et al.* 2011). Within a “periscope” shaped PVC casing (figure 21), a lower funnel trapped bubbles at the base of the instrument and funneled the bubbles past a microphone wired to a continuously logging recorder. An upper funnel trapped bubbles within a length of Tygon tubing secured by a three-way stopcock, allowing each apparatus to be manually backfilled with groundwater. Similarly to the bubble traps, any bubble accumulation would displace the water and be isolated at the top of the syringe or in the tubing. Recorders were downloaded once every 14 days, and sound files were converted to bubble counts using an algorithm executed in Matlab (Mathworks Inc, Natick, MA).

Table 8. Average seasonal CO_2 and CH_4 fluxes during the 2012 growing season at the APEX thaw sites. Uncertainties are in parentheses. For total C stocks uncertainties are presented as one standard deviation, while uncertainty for elevation and fluxes are one standard error of the mean (n=3 sites except at frozen plateau where n=6). Fluxes of CO_2 and CH_4 are averages of measured values throughout the growing season. For CO_2 equivalent-CH_4 flux calculation see supplemental text. Negative flux values represent uptake to land.

Site	Years since most recent thaw[1]	Average growing season temperature	Net CO_2 flux (mg CO_2-C m^{-2} hr^{-1})	CH_4 flux (mg CH_4-C m^{-2} hr^{-1})	CO_2 equivalent- CH_4 flux (mg CO_2-C m^{-2} hr^{-1})	Net CO_2 flux: CO_2 equivalent- CH_4 flux ratio
Frozen Plateau	0	3.6 (0.7)	-29.07 (19.00)	-0.02 (0.02)	-0.14 (0.22)	203.7 (339.1)
Bog 1	≥27	12.2 (0.4)	-34.90 (4.80)	4.64 (0.69)	42.30 (6.33)	0.8 (0.2)
Bog 2	32-500	10.6 (0.4)	-51.51 (17.56)	7.72 (3.45)	70.32 (31.43)	0.7 (0.4)
Bog 3	42-500	10.3 (0.4)	-43.61 (3.71)	3.91 (0.18)	35.65 (1.64)	1.2 (0.1)

Site	Percent CO_2 equivalent- CH_4 flux offset of NEE	Average subsurface bubble production (mL gas m^{-2} hr^{-1})	Subsurface CH_4 –C flux (mg m^{-2} hr^{-1})	Subsurface CO_2 –C equivalent CH_4 flux (mg m^{-2} hr^{-1})	Average percent of surface that is subsurface bubble production
Frozen Plateau	0.5 (0.8)		-	-	-
Bog 1	121.2 (24.6)	5.13 (1.98)	1.72 (0.77)	15.70 (7.00)	0.40 (0.19)
Bog 2	136.5 (76.7)	9.43 (3.93)	0.18 (0.08)	1.60 (0.71)	0.02 (0.01)
Bog 3	81.8 (7.9)	2.00 (0.37)	0.58 (0.38)	5.32 (3.50)	0.20 (0.16)

[1]Based on a combination of radiocarbon results and aerial photograph interpretation; see Table 9.

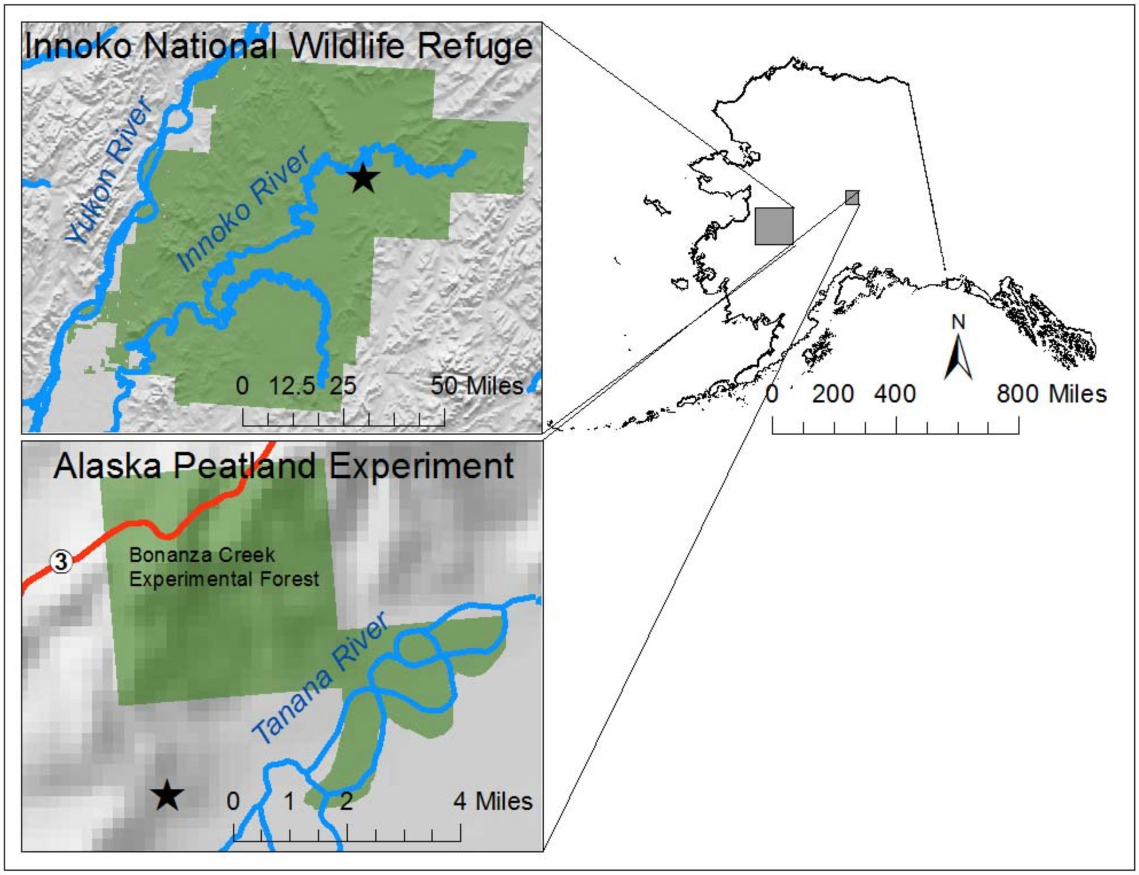

Figure 11 Map of the Innoko National Wildlife Refuge (63.58˚N, 157.72˚W) and the Alaska Peatland Experiment (64.69˚N, 148.32˚W), denoting the position of 2011 (Innoko) and 2012 (APEX) field season sampling site locations.

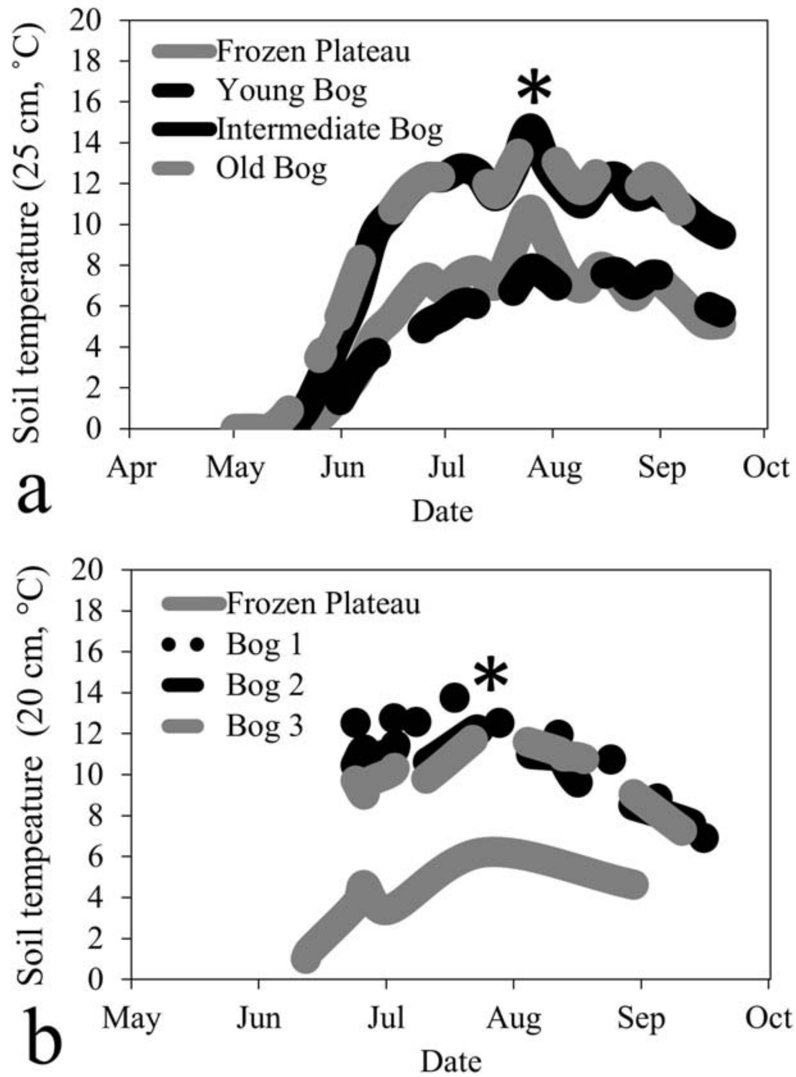

Figure 12. Peat temperature records at Innoko (a; 25 cm depth; Johnston *et al..,* in review) and APEX (b; 20 cm depth) during the 2011(a) and 2012 (b) growing seasons. The asterisk denotes significant statistical differences (intermediate and old warmer than frozen and young at Innoko; Bog 1, Bog 2, and Bog 3 warmer han frozen at APEX) based on a post hoc comparison of means test.

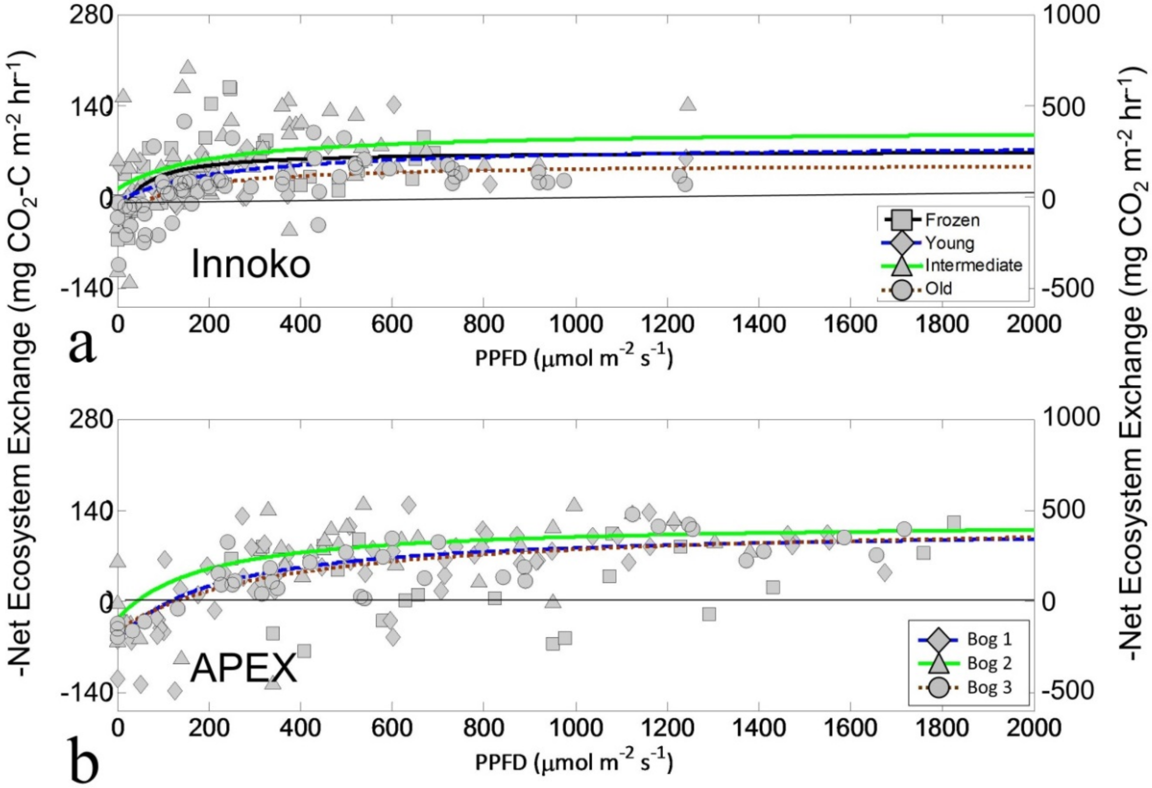

Figure 13. Response of net ecosystem exchange (mg CO_2 m^{-2} hr^{-1}, left; mg CO_2-C m^{-2} hr^{-1},right) to light intensity (PPFD; µmol m^{-2} s^{-1}) at all sites during the 2011 (a; Johnston *et al..,* in review) and 2012 (b) measurements. Positive values indicate CO_2 uptake. The fit lines are rectangular hyperbolic fit for all data points of each site. Fits reflect point measurements at three points along the transect of each site type. Rectangular hyperbolic fits for each landscape unit (Innoko) or individual site (APEX) were not significantly different from one another (p=0.999 amongst APEX sites and p=0.876 for comparison to Innoko sites). Results of model fits (equation 3) are shown in Table S3. No fit is shown for the frozen sites in 2012 as there was no relationship detected between light intensity and net ecosystem exchange, possibly due to a smaller number of measurements at the frozen plateau than the bog features (1/3-2/3 fewer measurements than at bog sites) or to the contribution of trees to NEE, which was not measured.

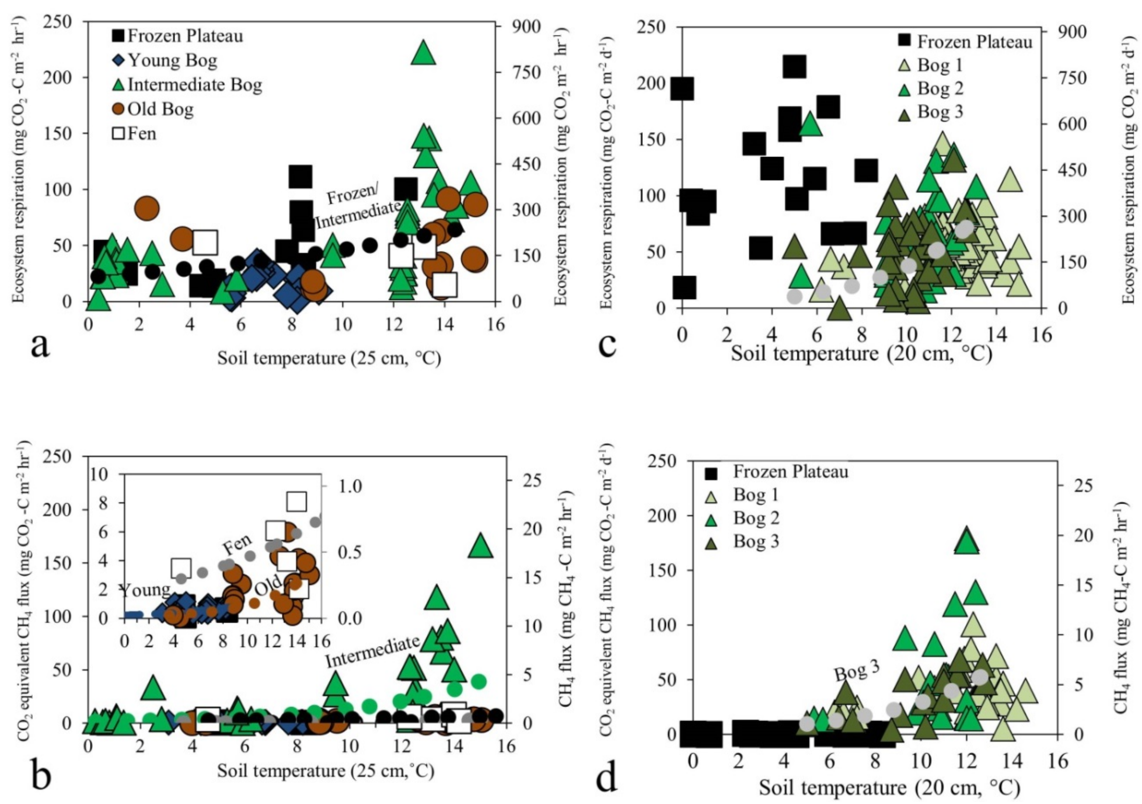

Figure 14. The relationship of (a,c) ecosystem respiration (ER) and (b,d) CH_4 to peat temperature at 20 cm depth in 2012 at the Innoko (a,b) and APEX (c,d) study sites. Values for each site type at Innoko include results for three replicates of each landscape unit (Table 11). Methane fluxes are reported on the left vertical axis as the global warming potential in terms of CO_2-C equivalent of CH_4, for ease of comparison against CO_2 fluxes. Sites for which the relationship between efflux and temperature was significant are presented as grey dotted lines. For Innoko, a significant relationship was found for the frozen and intermediate sites for ER, and young, intermediate, old, and fen sites for CH_4. For APEX, a significant relationship was found for Bog 3 for ER and CH_4. Best-fit equations are based on equation 4 and parameter values are presented in Table S3.

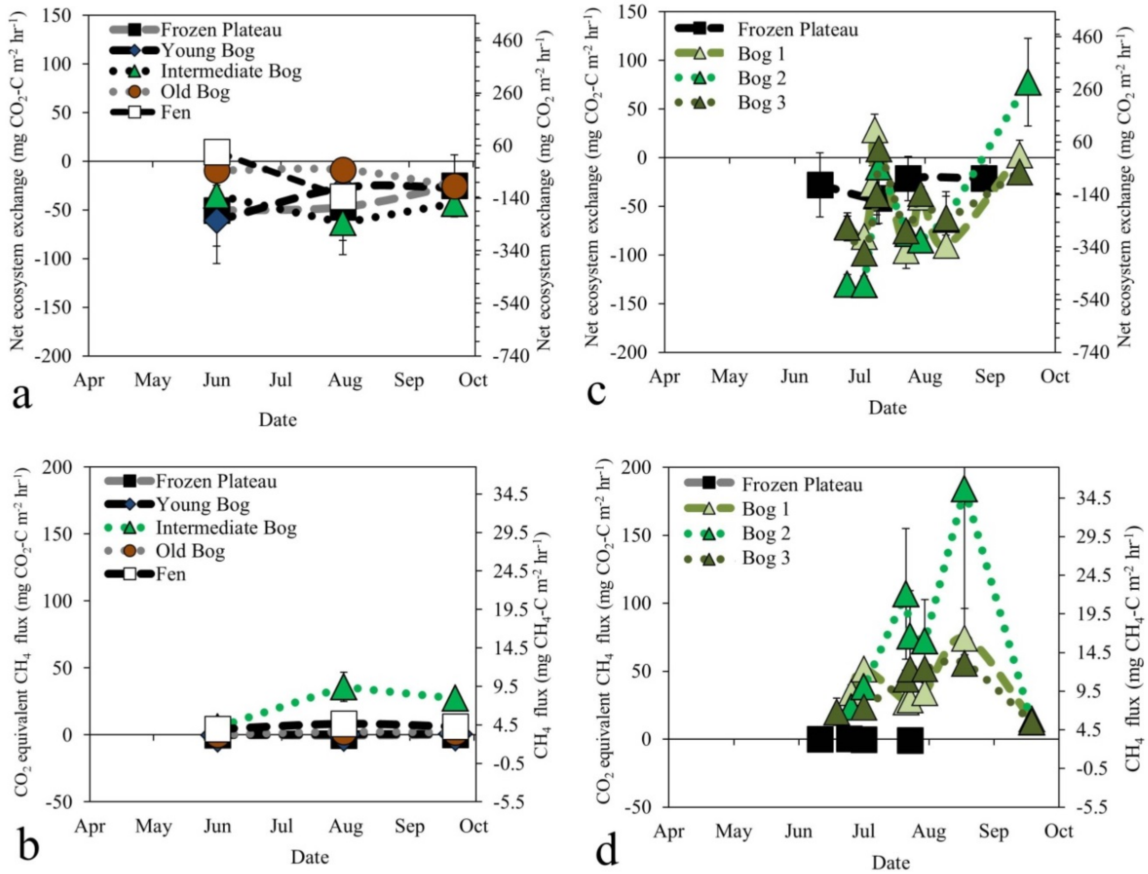

Figure 15. Average NEE (a,c) and CO_2 equivalent CH_4 flux (b,d) at the Innoko sites over the course of the 2011 (a,b) and APEX bogs during 2012 (c,d) growing season (n=3). Innoko replicates are three sites of approximately the same age sites, with error bars representing error in repeated measurements across sites. APEX replicates are three locations within an individual aged site, where error represents the variation across the three transect positions at each aged site. Methane fluxes are reported as the CO_2-C equivalent of CH_4 (9.1 times greater than observed methane flux as CH_4) for ease of comparison to CO_2 fluxes. Error bars are ± one standard error. Lines are connectors between point measurements, not modeled values.

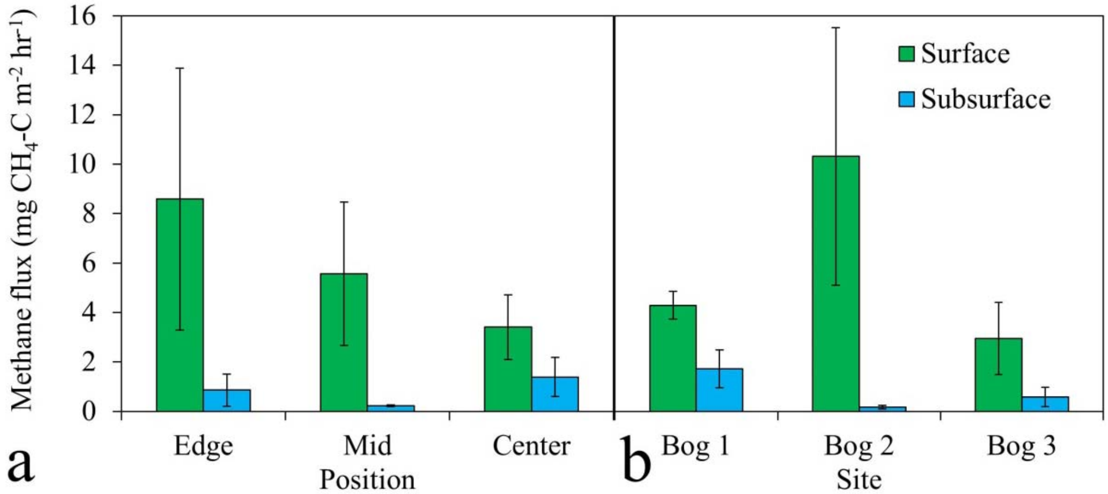

Figure 16. Average surface and subsurface CH_4 flux for edge, middle, and center positions along the transects at Bog 1, Bog 2, and Bog 3 of APEX bogs during the 2012 growing season. Error bars represent average throughout the growing season, n=6). There was no statistical difference across positions on the transect (p=0.285) or across sites (p=0.6124).

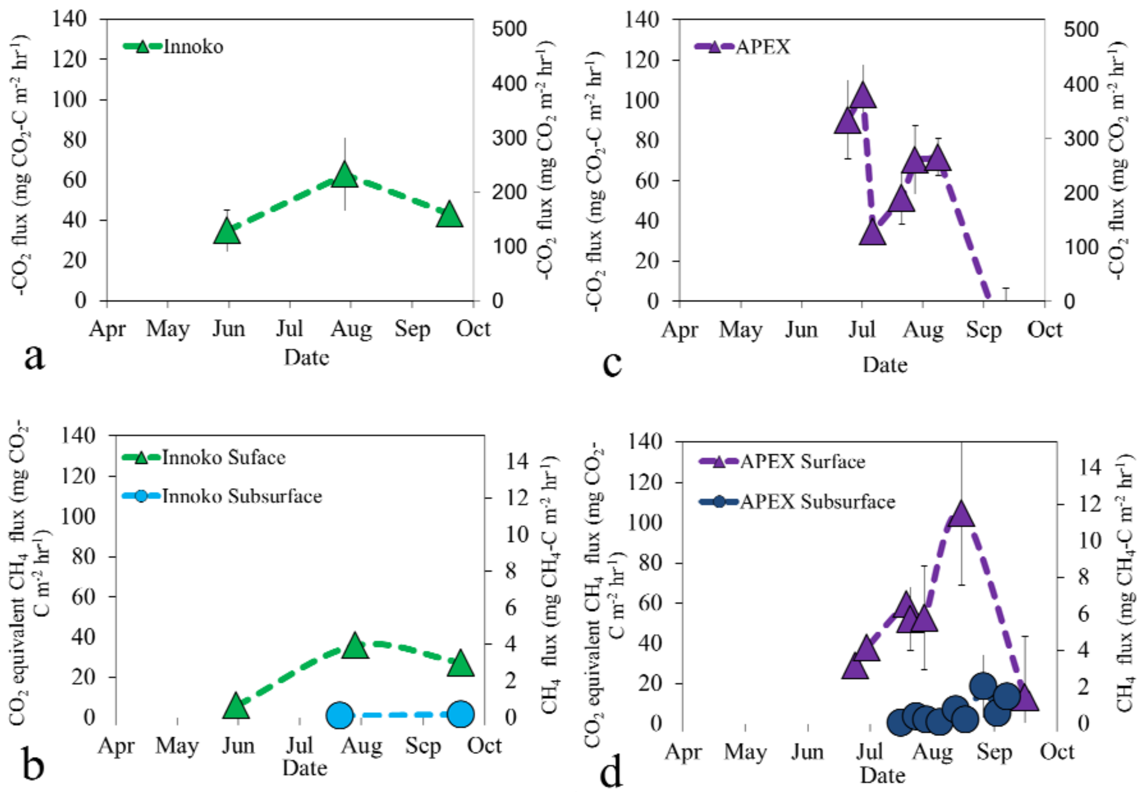

Figure 17. Comparison of surface CO_2 (a,c; NEE) and CH_4 (b,d) flux and subsurface bubble production flux at during the growing season at Innoko (a,b; 2011) and APEX (c,d; 2012). Innoko surface is the surface flux at intermediate (30 to 590y) sites. Innoko subsurface bubble fluxes were calculated using equation 1 and the average CH_4 concentration at APEX. Negative CO_2 flux represents uptake of CO_2. Positive CH_4 efflux represents release of CH_4 to the atmosphere. For both sites, only a small proportion (<25%) of the surface flux is accounted for by subsurface bubble production. For Innoko in 2011, CO_2 uptake outweighed CO_2 equivalent CH_4 flux by 200%. At APEX in 2012, CH_4 efflux outweighed CO_2 uptake by 100-150%

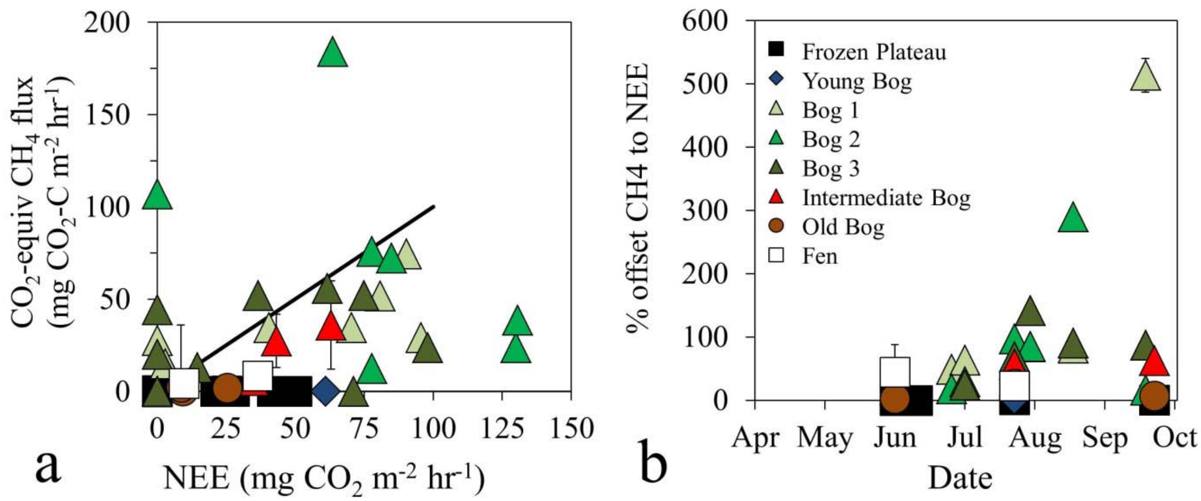

Figure 18. Average percent offset of CH_4 to NEE (a) and comparison of NEE to CO_2 equivalent CH_4 flux (b) at Innoko and APEX. Methane fluxes are reported as the CO_2-C equivalent of CH_4 (9.1 times greater than observed methane flux as CH_4) for ease of comparison to CO_2 fluxes. Innoko points represent individual site observations throughout the 2011 growing season. APEX points represent aggregated transect position observations at each thaw feature throughout the 2012 growing season. Error bars are ± one standard error. Lines on plots b and d represent a 1:1 line where NEE and CH_4 would be equivalent.

3.8 Supplemental Material

Table 9. Summary of collapse-scar bogs and characteristics of each feature during the 2012 field season

Site	Rep	GPS positions (lat; long)	August 1, 2012 thaw depth (cm)	Dominant vegetation	Surface Net CO_2 –C flux (mg m^{-2} hr^{-1})	Surface Net CH_4 –C flux (mg m^{-2} hr^{-1})
Frozen Plateau	1	63.5738; -157.7289	-29.0	*Picea mariana, Ledum decumbens,Rubus chamaemorus Cladonia arbuscula, Sphagnum fuscum*	-6.05 (23.33)	-0.09 (0.09)
Frozen Plateau	2	63.5709; -157.7333	-40.0		10.04 (23.90)	-0.05 (0.04)
Frozen Plateau	3	63.5740; -157.7304	-32.0		13.50 (12.07)	0.05 (0.04)
Frozen Plateau	4	63.5738; -157.7289	-29.0		-17.67 (8.75)	-0.07 (0.06)
Frozen Plateau	5	63.5709; -157.7333	-41.0		-82.37 (7.11)	0.03 (0.02)
Frozen Plateau	6	63.5740; -157.7304	-54.0		-91.89 (3.33)	0.02 (0.01)
Bog 1	Edge	63.5736; -157.7286	>150	*Sphagnum riparium, S. lindbergii*	-44.43 (3.16)	3.89 (0.51)
Bog 1	Middle	63.5735; -157.7286	>150		-29.14 (3.10)	5.78 (1.54)
Bog 1	Center	63.5738; -157.7286	>150		-31.13 (3.07)	4.26 (1.05)
Bog 2	Edge	63.5738; -157.7272	>150	*Eriophorum scheuchzeri, Sphagnum riparium, S. lindbergii*	-76.19 (5.12)	14.33 (7.39)
Bog 2	Middle	63.5738; -157.7272	>150		-60.81 (5.29)	8.00 (2.11)
Bog 2	Center	63.5737; -157.7256	-76.0		-17.55 (8.09)	0.83 (0.90)
Bog 3	Edge	63.5736; -157.7297	>150	*Andromeda polifolia, Oxycoccus microcarpus, Carex rotundata, Sphagnum balticum, S. flexuosum*	-38.63 (4.66)	3.53 (0.78)
Bog 3	Middle	63.5709; -157.7326	>150		-50.87 (4.35)	3.86 (0.95)
Bog 3	Center	63.5731; -157.7284	>150		-41.32 (3.96)	4.34 (1.14)

Table 9. Summary of collapse-scar bogs and characteristics of each feature during the 2012 field season-continued.

Site	Surface Net CH_4 –C flux (mg m^{-2} hr^{-1})	Surface CO_2 –C equivalent CH_4 flux (mg m^{-2} hr^{-1})	Average subsurface bubble production (mL gas m^{-2} hr^{-1})	Subsurface CH_4 –C flux (mg m^{-2} hr^{-1})	Subsurface CO_2 –C equivalent CH_4 flux (mg m^{-2} hr^{-1})	Average percent of surface that is subsurface bubble production
Frozen Plateau	-0.09 (0.09)	-0.79 (0.78)	-	-	-	-
Frozen Plateau	-0.05 (0.04)	-0.43 (0.34)	-	-	-	-
Frozen Plateau	0.05 (0.04)	0.49 (0.36)	-	-	-	-
Frozen Plateau	-0.07 (0.06)	-0.61 (0.51)	-	-	-	-
Frozen Plateau	0.03 (0.02)	0.27 (0.17)	-	-	-	-
Frozen Plateau	0.02 (0.01)	0.23 (0.14)	-	-	-	-
Bog 1	3.89 (0.51)	35.45 (4.64)	8.63 (3.40)	2.16 (1.45)	19.72 (13.22)	0.54 (0.37)
Bog 1	5.78 (1.54)	52.68 (13.99)	1.77 (0.33)	0.23 (0.06)	2.08 (0.52)	0.04 (0.02)
Bog 1	4.26 (1.05)	38.78 (9.54)	4.98 (2.23)	2.78 (1.71)	25.31 (15.62)	0.80 (0.53)
Bog 2	14.33 (7.39)	130.53 (67.34)	13.37 (5.55)	0.32 (0.13)	2.90 (1.15)	0.02 (0.01)
Bog 2	8.00 (2.11)	72.86 (19.25)	0.00 (0.00)	0.16 (0.07)	1.45 (0.64)	0.01 (0.01)
Bog 2	0.83 (0.90)	7.58 (8.23)	5.50 (1.87)	0.05 (0.01)	0.44 (0.07)	0.04 (0.04)
Bog 3	3.53 (0.78)	32.20 (7.10)	0.00 (0.00)	0.12 (0.05)	1.10 (0.45)	0.05 (0.03)
Bog 3	3.86 (0.95)	35.20 (8.65)	2.37 (1.16)	0.29 (0.19)	2.60 (1.69)	0.45 (0.92)
Bog 3	4.34 (1.14)	39.56 (10.37)	1.62 (0.80)	1.35 (0.43)	12.26 (3.94)	0.24 (0.10)

Table 10. Minimum ages of most recent thaw are based on changes observed on repeat aerial photography. Radiocarbon ages are taken from peat cores in each bog and indicate dates of previous thaws. Ages were comparable to adjacent sites, based on accumulation rates in Jones *et al.* 2013. The age listed in italics was rejected on the basis of it being too young, a consequence of the small sample size. Bog 3 results are reported from two cores, and are denoted Bog 3^A for the first core, and Bog 3^B for the second core.

Site	Minimum age of most recent thaw (aerial photograph year)*	LabID	Sample Depth (cm)	Stratigraphic Significance	Materials
Bog 1	27 y (1985)				
Bog 2	32 y (1980)	WW9313	50-52	above transition	betula seed, Ericaceous leaf frag, Sphagnum stemps
Bog 2	32 y (1980)	WW9264	128-130	below transition (forest)	charred wood
Bog 2	32 y (1980)	WW9315	*146-148*	*basal*	*charred wood*
Bog 3^A	42 y (1970)	WW9312	100-102	transition	charred wood
Bog 3^B	42 y (1970)	WW9268	108-110	below transition (forest)	charred needle, woody shrub stem
Bog 3^B	42 y (1970)	WW9267	144-146	basal	charred wood

Site	$\delta^{13}C$	^{14}C Age	±	2 sig cal age -	2 sig cal age +	2 sig probability
Bog 1						
Bog 2	-25	1.4111	0.0065	>modern		
Bog 2	-25.9	2030	25	1921	2059	0.9752
Bog 2	*-25*	*390*	*30*	*427*	*509*	*72.85*
Bog 3^A	-25	2620	40	2706	2813	94.04
Bog 3^B	-25	470	30	493	540	1.0000
Bog 3^B	-25	2020	30	1892	2055	1.0000

Table 11. Parameter values for the rectangular hyperbolic light response curves (eq. 3) and exponential response of ER and CH_4 to soil temperature at 25 cm depth (eq. 4). Bold values indicate correlation between explanatory and response variable.

		Innoko					APEX			
Parameter	Units	Frozen Plateau	Young	Intermediate	Old	Fen	Frozen Plateau	Bog 1	Bog 2	Bog 3
Rectangular hyperbola: NEE~PPFD										
α_{RH}	mg C μmol photons $^{-1}$	8.7817	1.4126	1.7128	3.1245	-	5.95E+10	2.9331	2.9197	1.7464
β_{RH}	mg C m^{-2} hr^{-1}	414.16	316.07	329.28	329	-	1433	622	541.81	604.17
γ_{RH}	mg C m^{-2} hr^{-1}	162.28	27.586	-40.388	144.96	-	1325.7	218.86	101.97	162.9
Exponential relationship: ER~ 25 cm soil temp										
A	mg CO_2-C m^{-2} hr^{-1}	**14.7**	17.5	**21.8**	29.5	**65.0**	103.23	26.055	29.385	**2.9918**
b	mg CO_2-C m^{-2} hr^{-1}	**0.115**	-0.063	**0.007**	0.010	**-0.052**	0.0371	0.0541	0.0585	**0.2516**
r^2		**0.24**	0.01	**0.25**	0.00	**0.28**	0.023	0.0467	0.027	**0.1219**
Exponential relationship: CH_4~ 25 cm soil temp										
A	mg CH_4-C m^{-2} hr^{-1}	3.9	**8.4**	**68.8**	**3.5**	**82.7**	0.0118	1.5115	**0.893**	**0.3452**
b	mg CH_4-C m^{-2} hr^{-1}	0.217	**0.160**	**0.215**	**0.245**	**0.082**	0.1747	0.0848	**0.1615**	**0.2238**
r^2		0.10	**0.29**	**0.43**	**0.36**	**0.24**	0.0752	0.0826	**0.1259**	**0.3799**

Table 12. Number of samples per measurement for each site throughout the growing season 2012. NEE: net ecosystem CO_2 exchange, ER: ecosystem respiration, CH_4: methane efflux

Site	NEE	ER	CH_4
Frozen 1	3	3	4
Frozen 2	3	3	4
Frozen 3	4	4	4
Frozen 4	4	4	4
Frozen 5	4	4	4
Frozen 6	3	2	4
Bog 1 edge	21	21	21
Bog 1 middle	21	21	21
Bog 1 center	22	22	22
Bog 2 edge	10	10	6
Bog 2 middle	11	11	6
Bog 2 center	11	11	6
Bog 3 edge	11	11	6
Bog 3 middle	12	12	6
Bog 3 center	12	12	6

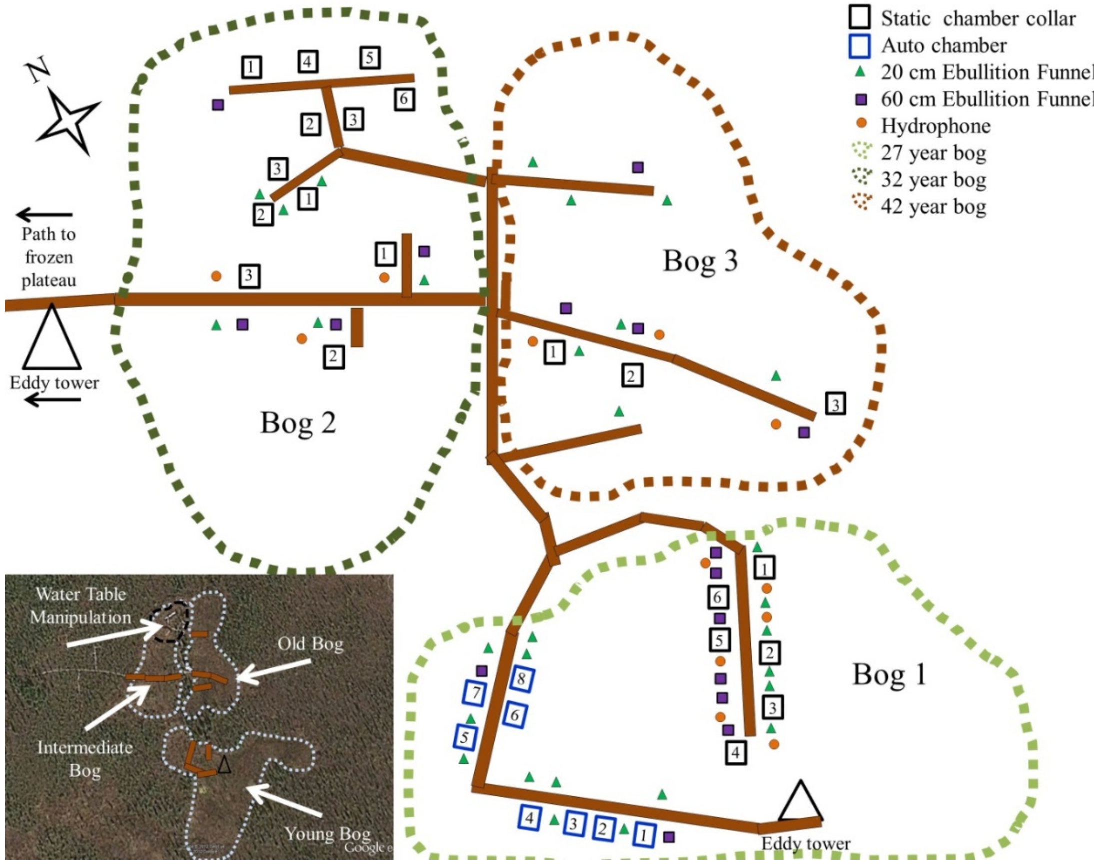

Figure 19. Location of sensors deployed in each bog feature. Note the nested placement of each static chamber collar, ebullition funnels, and hydrophones.

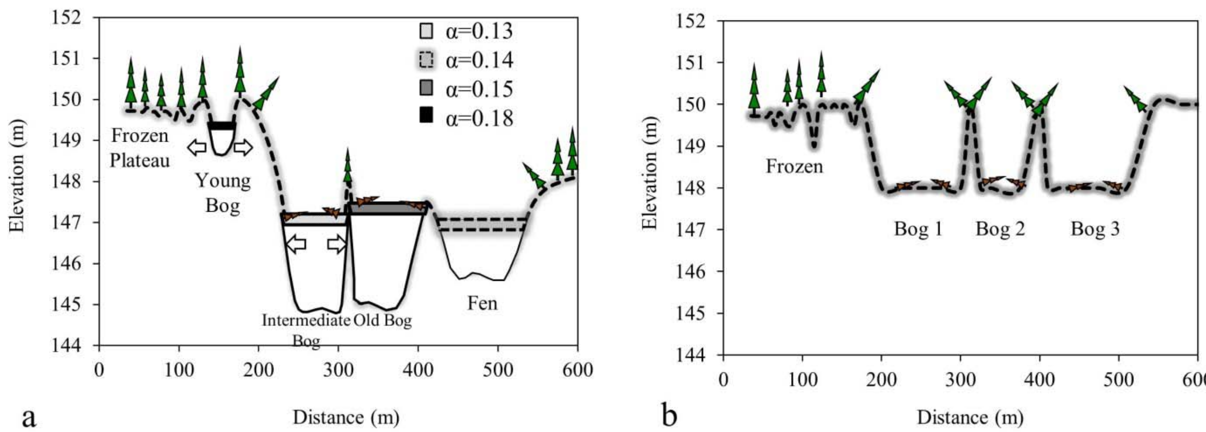

Figure 20**.** Elevation comparison of sites along a transect of frozen plateau to bog and fen features at Innoko (a) and APEX (b). Features and processes indicated in black dashed line represents the vegetated ground surface of the frozen plateau. White arrows indicate degree of lateral expansion of thaw features. The color of the surface of each feature (in a) is related to the albedo (α), here measured under diffuse radiation conditions (Table 10) with the forest floor (excluding young bog sites) being characterized by α=0.14 (see Table 10, Table 11), shown with medium grey shadow surrounding the dashed line. The depth of each feature represents the distance from the feature surface to the contact with silt.

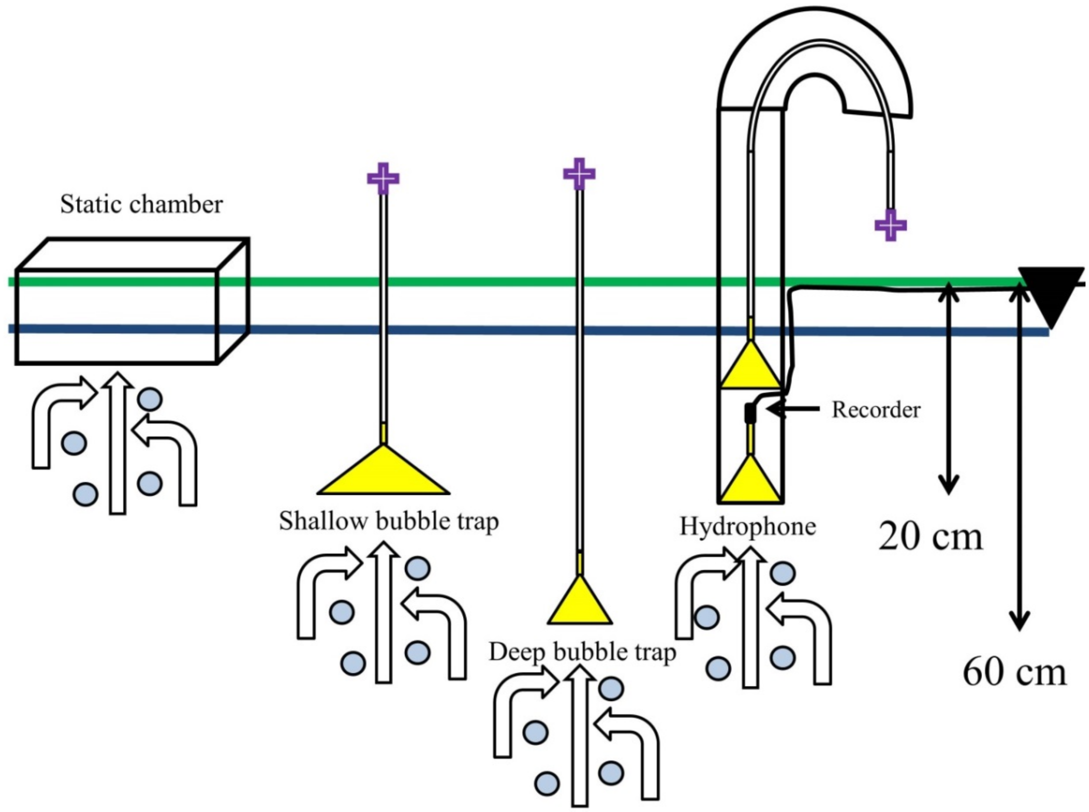

Figure 21. Design of shallow bubble trap, deep bubble trap, and hydrophone installation below the peat surface. Shallow and hydrophone traps capture bubble below 20 cm and deep traps collect bubble below 60 cm below the peat surface. Peat surface is denoted by the green line while the water table is denoted with the blue line.

4.0 CONCLUSIONS

In northern lowland settings, thaw of permafrost plateaus leads to vertical and lateral expansion with time since thaw, creating wetland environments conducive to methane efflux. Inundation and warmer soil temperatures occur as a function of physical lowering with thaw, coupling with tree kill opening the canopy, and thermal properties of water to enhance thaw trajectories. We did not observe changes in net ecosystem exchange across thaw features at either Innoko Flats or APEX, despite changing topography and plant communities as a function of thaw progression. Yet with warmer soil temperatures and shallower water tables surface CH_4 efflux reached a maximum rate in thaw features 30-590 years post thaw at Innoko Flats, counteracting 49% ± 21 % of carbon uptake when considered as global warming potential. Thaw sites of comparable age at APEX exhibited surface and ebullitive flux that did not vary systematically with position, but revealed potential net warming effect, with CH_4 efflux offsetting 82 ± 8% to 137 ± 77% of NEE when considered as 100-y global warming potential. Across features, subsurface bubble production was equal to 24 ± 10% of surface CH_4 flux, contributing to a variable but potentially significant degree to net warming potential. The role of ebullition flux in this balance merits further investigation, as does the role of landscape position. Future work should explore the use of remote sensing techniques to expand the scale of these observations for regional evaluation of methane release with permafrost thaw.

4.1 References

Anderson K, Bennie J J, Milton E J, Hughes P D M, Lindsay R and Meade R 2010 Combining LiDAR and IKONOS data for eco-hydrological classification of an ombrotrophic peatland. *Journal of environmental quality* **39** 260–73

Anisimov O a 2007 Potential feedback of thawing permafrost to the global climate system through methane emission *Environmental Research Letters* **2** 045016

Becker, D.A., 1990, Homogeneity and evaluation of the new NIST leaf certified reference materials, in Nuclear analytical methods in the life sciences, Gaithersburg, MD, National Institute of Standards, p. 571-577.

Bremond L, Alexandre A, Peyron O and Guiot J 2005 Grass water stress estimated from phytoliths in West Africa *Journal of Biogeography* **32** 311–27

Bubier J L, Moore T, Savage K and Crill P 2005 A comparison of methane flux in a boreal landscape between a dry and a wet year *Global Biogeochemical Cycles* **19** 1–11

Becker, D.A., 1990, Homogeneity and evaluation of the new NIST leaf certified reference materials, in Nuclear analytical methods in the life sciences, Gaithersburg, MD, National Institute of Standards, p. 571-577.

Campbell J B and Wynne R H 2011 *Introduction to Remote Sensing*

Chander G, Markham B L and Helder D L 2009 Summary of Current Radiometric Calibration Coefficients for Landsat MSS, TM, ETM+, and EO-1 ALI sensors *Remote Sensing of Environment* **1** 1–24

Committee, C.A.S.C. The Canadian system of soil classification. Ontario (Canada): NRC Canada Research Press. p. 1-187.

Cutler D R, Edwards T C, Beard K H, Cutler A, Hess K T, Gibson J and Lawler J J 2007 Random forests for classification in ecology. *Ecology* **88** 2783–92

Fox J 2002 Bootstrapping Regression Models *An R and S-PLUS Companion to Applied Regression* pp 1–14

Govindaraju, K., 1989, Compliation of working value and sample description for 272 geostandards: Geostandards Newsletter, v. 13, p. 1-113.

Harden, J. W., Trumbore, S. E., Stocks, B. J., Hirsch, A., Gower, S. T., O'Neill, K. P., & Kasischke, E. S. (2000). The role of fire in the boreal carbon budget. *Global Biogeochemical Cycles*, *6*, 174–184.

Harris A and Bryant R G 2009 Northern Peatland Vegetation and the Carbon Cycle : A Remote Sensing Approach *Geophysical Monography Series* **184** 79–98

Heginbottom, J. A., Brown, J., Humlum, O., & Svensson, H. (2013). *State of the Earth's Cryosphere at the Beginning of the 21st Centry: Glaciers, Global Snow Cover, Floating Ice, and Permafrost and Periglacial Environments- Permafrost and Periglacial Environments* (pp. 1–78).

Hugelius, G., Tarnocai, C., Bockheim, J., Camill, P., Elberling, B., Grosse, G., … Yu, Z. (in review). Short communication: A new dataset for estimating organic carbon storage to 3 m depth in soils of the northern circumpolar permafrost region. *Earth System Science Data Discussions*, *6*. doi:doi:10.5194/essdd-6-73-2013

Johnston C E, Ewing S A, Harden J W, Stoy P C, Ruth R K, Wickland K P, Koch J C, Fuller C C and Jorgenson M T Effect of permafrost thaw on CO_2 and CH_4 exchange in a western Alaska peatland chronosequence *Environmental Research Letters*

Jorgenson M T, Harden J, Kanevskiy M, O'Donnell J, Wickland K, Ewing S, Maines K, Zhuang Q, Shur Y, Striegl R and Koch J 2013 Hydrologic reorganization and soil carbon changes after permafrost degradation across heterogeneous boreal landscapes *Environmental Research Letters*

Jorgenson, M. T., Harden, J., Kanevskiy, M., Donnell, J. O., Wickland, K., Ewing S, Maines K, Zhuang Q, Shur Y, Striegl R and Koch J (2013). Reorganization of vegetation , hydrology and soil carbon after permafrost degradation across heterogeneous boreal landscapes. *Environmental Research Letters*, *8*(035017), 1–13. doi:10.1088/1748-9326/8/3/035017

Jorgenson M T, Racine C H, Walters J C and Osterkamp T E 2001 Permafrost degradation and ecological changes associated with a warming climate in central alaska *Climate Change* **48** 551–79

Juang J-Y, Katul G, Siqueira M, Stoy P and Novick K 2007 Separating the effects of albedo from eco-physiological changes on surface temperature along a successional chronosequence in the southeastern United States *Geophysical Research Letters* **34** 1–5

Lawrence D M, Slater A G, Romanovsky V E and Nicolsky D J 2008 Sensitivity of a model projection of near-surface permafrost degradation to soil column depth and representation of soil organic matter *Journal of Geophysical Research* **113** 1–14

Lawrence, D. M., Slater, A. G., Romanovsky, V. E., & Nicolsky, D. J. (2008). Sensitivity of a model projection of near-surface permafrost degradation to soil column depth and representation of soil organic matter. *Journal of Geophysical Research*, *113*(F2), 1–14. doi:10.1029/2007JF000883

Lawrence R L, Wood S D and Sheley R L 2006 Mapping invasive plants using hyperspectral imagery and Breiman Cutler classifications (randomForest) *Remote Sensing of Environment* **100** 356–62

Li F 2004 Deriving land surface temperature from Landsat 5 and 7 during SMEX02/SMACEX *Remote Sensing of Environment* **92** 521–34

Lund M, Lafleur P M, Roulet N T, Lindroth A, Christensen T R, Aurela M, Chojnicki B H, Flanagan L B, Humphreys E R, Laurila T, Oechel W C, Olejnik J, Rinne J, Schubert P and Nilsson M B 2009 Variability in exchange of CO2 across 12 northern peatland and tundra sites *Global Change Biology* **16** 2436–48

Nadler, I.A., and Wein, R.W., 1998, A new forest floor corer for rapid sampling, minimal disturbance and adequate precision: Silva Fennica, v. 32, no. 4, p. 373-381.

Payette, S., Delwaide, A., Caccianiga, M., Beauchemin, M. 2004. Accelerated thawing of subarctic peatland permafrost over the last 50 years. Geophysical Research Letters 31: doi:10.1029/2004GL020358.

Pella, E., 1990a, Elemental organic analysis. Part 1: Historical developments: American Laboratory, v. 22, no. 2, p. 116-125.

Pella, E., 1990b, Elemental organic analyzer. Part 2: State of the art: American Laboratory, v. 22, no. 12, p. 28-32.

Riordan, B., Verbyla, D., & McGuire, a. D. (2006). Shrinking ponds in subarctic Alaska based on 1950–2002 remotely sensed images. *Journal of Geophysical Research*, *111*(G4), 1–11. doi:10.1029/2005JG000150

Savage S L, Lawrence R L, Custer S G, Jewett J T, Powell S L and Shaw J a. 2010 Review of Alternative Methods for Estimating Terrestrial Emittance and Geothermal Heat Flux for Yellowstone National Park Using Landsat Imagery *GIScience & Remote Sensing* **47** 460–79

Shauai Y, Masek J G, Gao F and Schaaf C B 2011 An algorithm for the retrieval of 30-m snow-free albedo from Landsat surface reflectance and MODIS BRDF *Remote Sensing of Environment* **115** 2204–16

Staff, S.S. 1998. Keys to Soil Taxonomy. Blacksburg (VA): Pocahontas Press, Inc. 599 p.

Stow D a, Hope A, McGuire D, Verbyla D, Gamon J, Huemmrich F, Houston S, Racine C, Sturm M, Tape K, Hinzman L, Yoshikawa K, Tweedie C, Noyle B, Silapaswan C, Douglas D, Griffith B, Jia G, Epstein H E, Walker D, Daeschner S, Petersen A, Zhou L and Myneni R 2004 Remote sensing of vegetation and land-cover change in Arctic Tundra Ecosystems *Remote Sensing of Environment* **89** 281–308

Stuvier, M., and Polach, H.A., 1977, Discussion: reporting of ^{14}C data: Radiocarbon, v. 19, p. 355-363.

Tarnocai, C., Canadell, J. G., Schuur, E. A. G., Kuhry, P., Mazhitova, G., & Zimov, S. A. (2009). Soil organic carbon pools in the northern circumpolar permafrost region. *Global Biogeochemical Cycles*, *23*(2), 1–11. doi:10.1029/2008GB003327

Treat C C, Bubier J L, Varner R K and Crill P M 2007 Timescale dependence of environmental and plant-mediated controls on CH_4 flux in a temperate fen *Journal of Geophysical Research* **112** 1–9

Turetsky M R, Treat C C, Waldrop M P, Waddington J M, Harden J W and McGuire A D 2008 Short-term response of methane fluxes and methanogen activity to water table and soil warming manipulations in an Alaskan peatland *Journal of Geophysical Research* **113** 1–15

Turetsky M R, Wieder R K and Vitt D H 2002 Boreal peatland C fuxes under varying permafrost regimes *Soil Biology and Biochemistry* **34** 907–12

United States Department of Interior 1987 Innoko National Wildlife Refuge Comprehensive Consrevaation Plan, Environmental Impact Statement, Wilderness Review *Fish and Wildlife Service*

Viereck, L.A., Dyrness, C.T., Batten, A.R., and Wenzlick, K.J., 1992, The Alaska Vegetation Classification: General Technical Report PNW-GTR-286, U.S. Department of Agriculture, Forest Service, Pacific Northwest Research Station.

Watts J D, Powell S L, Lawrence R L and Hilker T 2011 Improved classification of conservation tillage adoption using high temporal and synthetic satellite imagery *Remote Sensing of Environment* **115** 66–75

Woodward A and Beever E A 2011 Conceptual Ecological Models to Support Detection of Ecological Change on Alaska National Wildlife Refuges *United States Geological Survey*

Yang J and Wang Y Q 1995 Estimation of land surface temperature using Landsat-7 ETM+ thermal infared and weather station data

APPENDICES

APPENDIX A

SITE DESCRIPTIONS

This appendix describes the locations of each site sampled along the collapse-scar bog chronosequence at Innoko Flats National Wildlife Refuge. All study sites were accessed via floatplane from the village of Galena, Alaska.

- **IFUW 1**- The plot is located at coordinates N63.5738º, W157.7289º (NAD83). The study plot is located in a poorly-drained mature black spruce stand with *Ledum spp*. and *Sphagnum spp*. The soil profile was sampled on August 22, 2009, by Jennifer Harden.
- **IFUW 2 –** The plot is located at coordinates N63.5709º, W157.7333º (NAD83). The study plot is located in a poorly-drained mature black spruce stand with *Ledum spp*. and *Sphagnum spp*. The soil profile was sampled on August 25, 2009, by Jonathan O'Donnell and Misha Kanevskiy.
- **IFUW 3 –** The plot is located at coordinates N63.5739º, W157.7302º (NAD83). The study plot is located in a poorly-drained mature black spruce stand with *Ledum spp*. and *Sphagnum spp*. The soil profile was sampled on August 22, 2009, by Jennifer Harden, Jonathan O'Donnell, and Torre Jorgenson.
- **IFOB 1 -** The plot is located at coordinates N63.5736º, W157.7296º (NAD83). The study plot is an old collapse-scar bog with *Sphagnum* spp. and the shrubs *Andromeda polifolia* and *Oxycoccus microcarpus*. The soil profile was sampled on August 24, 2009, by Torre Jorgenson and Jennifer Harden.
- **IFOB 2 –** The plot is located at coordinates N63.5709º, W157.7326º (NAD83). The study plot is an old collapse-scar bog with *Sphagnum* spp. and the shrub

Andromeda polifolia and some sedges. The soil profile was sampled on August 25, 2009, by Torre Jorgenson and Jennifer Harden.

- **IFOB 3 –** The plot is located at coordinates N63.57314º, W157.7284º (NAD83). The study plot is an old collapse-scar bog with *Sphagnum* spp. and the shrubs *Andromeda polifolia* and *Oxycoccus microcarpus*. The soil profile was sampled on August 23, 2009, by Torre Jorgenson and Jennifer Harden
- **IFIB 1 -** The plot is located at coordinates N63.5736º, W157.7276º (NAD83). The study plot is an intermediate-aged collapse-scar bog with *Sphagnum* spp. and *Eriophorum scheuchzeri*. The soil profile was sampled on August 24, 2009, by Jennifer Harden and Torre Jorgenson
- **IFIB 2 -** The plot is located at coordinates N63.5738º, W157.7274º (NAD83). The study plot is an intermediate-aged collapse-scar bog with *Sphagnum* spp. and *Eriophorum scheuchzeri*. The soil profile was sampled on August 23, 2009, by Jennifer Harden and Torre Jorgenson
- **IFIB 3 -** The plot is located at coordinates N63.5737º, W157.7256º (NAD83). The study plot is an intermediate-aged collapse-scar bog with *Sphagnum* spp. and *Eriophorum scheuchzeri.* The soil profile was sampled on August 25, 2009, by Jennifer Harden and Torre Jorgenson
- **IFYB 1 -** The plot is located at coordinates N63.5736º, W157.7286º (NAD83). The study plot is a young collapse-scar bog with *Sphagnum* spp. The soil profile was sampled on August 24, 2009, by Jennifer Harden and Torre Jorgenson

- **IFYB 2 -** The plot is located at coordinates N63.5735º, W157.7286º (NAD83). The study plot is a young collapse-scar bog with *Sphagnum* spp. and *Eriophorum scheuchzeri*.. The soil profile was sampled on August 24, 2009, by Jennifer Harden and Torre Jorgenson
- **IFYB 3 -** The plot is located at coordinates N63.5738º, W157.7286º (NAD83). The study plot is a young collapse-scar bog with *Sphagnum* spp. and *Eriophorum scheuchzeri*.. The soil profile was sampled on August 23, 2009, by Jennifer Harden and Torre Jorgenson
- **IFUD 1 –** The plot is located at coordinates N63.5737º, W157.7280º (NAD83). The study plot is drying margin of a collapse-scar bog with *Cladina* spp. and *Ledum decumbens*. The soil profile was sampled on August 23, 2009, by Jennifer Harden and Torre Jorgenson
- **IFUD 2 -** The plot is located at coordinates N63.5738º, W157.7260º (NAD83). The study plot is drying margin of a collapse-scar bog with *Cladina arbuscula*. The soil profile was sampled on August 25, 2009, by Jennifer Harden and Torre Jorgenson
- **IFUD 3-** The plot is located at coordinates N63.5738º, W157.7275º (NAD83). The study plot is drying margin of a collapse-scar bog with *Cladina arbuscula*. The soil profile was sampled on August 24, 2009, by Jennifer Harden and Torre Jorgenson
- **IFEX 2 -** The plot is located at coordinates N63.5752º, W157.7204º (NAD83). The study plot is a young collapse-scar bog with *Sphagnum* spp. and *Eriophorum*

scheuchzeri.. The soil profile was sampled on August 23, 2009, by Jonathan O'Donnell and Misha Kanevskiy.

- **IFIF 1 -** The plot is located at coordinates N63.5742º, W157.7223º (NAD83) and is a collapse-scar fen with *Sphagnum* spp., *Carex* spp., and *Eriphorum scheuchzeri*. The soil profile was sampled on August 26, 2009, by Torre Jorgenson.
- **IFOF 1 -** The plot is located at coordinates N63.5741º, W157.7231º (NAD83) and is a collapse-scar fen with *Sphagnum* spp., *Carex* spp., and *Eriphorum scheuchzeri*. The soil profile was sampled on August 29, 2008, by Torre Jorgenson.

APPENDIX B

DATA FILE DESCRIPTIONS

This appendix details what information is found within each of the columns of the three data files that accompany this report.

InnokoFlats_Field

This file contains the field descriptions of the sampled soils and includes the following columns:

Publication ID	Sample identification: The first two letters in the sample labels represent the region of study, Innoko Flats (IF). The next two letters represent the site type. Site types include unburned wet (UW), young bog (YB), intermediate bog (IB), old bog (OB), drying margin (UD), and intermediate collapse-scar fen (IF). The number that follows these four characters indicates the profile number. A decimal point separates the profile number from the basal depth of the sample (in cm).
Basal Depth	Indicates the basal depth, in cm, of sampling increment.
Field Horizon Code	Horizon type of the sample, as defined in the field. L = live moss, LN = lichen, D = dead moss, F = fibric organic matter (OM), M = mesic OM, H = humic OM, A = A mineral soil horizon, C = C mineral soil horizon, , La = limnic horizon, and X = unknown horizon. Ob represents a buried organic horizon. A lower case ‘f’ before a horizon code indicates that the sample was frozen when sampled.

Sample Description	A brief description of the sample.
Roots	Root abundance and size using conventions of USDA-ARS (Staff 1998).
pH	pH value of mineral soil measured in the laboratory. Deionized water was added to create a soil slurry (50% soil, 50% water) prior to measurement.
Moist Munsell Color	Munsell color value according to the Munsell Soil Color Chart.
Von Post or Texture Class	If organic soil, the classification using a modified version of the von Post scale of humification (Damman and French 1987). If mineral soil, the soil texture class as described in the field, following conventions of USDA-ARS (Staff 1998).
Height above mineral	Height of each basal depth above the mineral soil boundary. Therefore, the bottom organic layer is at zero and all mineral horizons are negative numbers.
Decomposition State	
Proportion of Amorphous	
Water	

InnokoFlats_Physical

This file contains physical data such as bulk density, volumetric moisture content, and particle size analysis. Column definitions are as follows:

Publication ID	Sample identification: The first two letters in the sample labels represent the region of study, Innoko Flats (IF). The next two letters represent the site type. Site types include unburned wet (UW), unburned old bog (OB), unburned intermediate bog (IB), unburned young bog (YB), unburned drying margin (UD), and unburned collapse-scar fen (IF). The number that follows these four characters indicates the profile number. A decimal point separates the profile number from the basal depth of the sample (in cm).
Basal Depth	Indicates the basal depth, in cm, of sampling increment.
Field Horizon Code	Horizon type of the sample, as defined in the field. L = live moss, LN = lichen, D = dead moss, F = fibric organic matter (OM), M = mesic OM, H = humic OM, A = A mineral soil horizon, C = C mineral soil horizon, , La = limnic horizon, and X = unknown horizon. Ob represents a buried organic horizon. A lower case ‘f’ before a horizon code indicates that the sample was frozen when sampled.
Sample Description	A brief description of the sample.

Date Sampled	Date during which the sample was taken (month/day/year).
Thickness	Thickness of soil horizon.
>2 mm in Sample	Dry weight percent of soil particles not passing through a 2 mm sieve after gentle crushing.
>1 cm in Sample	Dry weight percent of roots larger than 1 cm in diameter in the sample.
Bulk Density (OD; <2 mm)	Grams of oven-dried soil per cubic centimeter, with soil particles greater than 2 mm and roots greater that 1 cm diameter removed.
Bulk Density (OD; all)	Grams of oven-dried soil per cubic centimeter for the entire soil sample with no fractions excluded. Calculated similarly to Bulk Density (< 2 mm) except the weight of particles greater than 2 mm and roots greater than 1 cm diameter have been included.
Volumetric Field Moisture (OD)	The percent water in the sample, by volume.
Moisture in Air-dry Sample	Percent, by weight, of moisture remaining in a sample after air-drying to constant weight as determined by subsequently oven-drying the sample.

InnokoFlats_Chemistry

This file contains chemical data obtained from the elemental analyzer (EA) and the elemental analyzer mass spectrometer (EA/IRMS). Column definitions are as follows:

Publication ID	Sample identification: The first two letters in the sample labels represent the region of study, Innoko Flats (IF). The next two letters represent the site type. Site types include unburned wet (UW), unburned old bog (OB), unburned intermediate bog (IB), unburned young bog (YB), unburned drying margin (UD), and intermediate collapse-scar fen (IF). The number that follows these four characters indicates the profile number. A decimal point separates the profile number from the basal depth of the sample (in cm).
Basal Depth	Indicates the basal depth, in cm, of sampling increment.
Field Horizon Code	Horizon type of the sample, as defined in the field. L = live moss, LN = lichen, D = dead moss, F = fibric organic matter (OM), M = mesic OM, H = humic OM, A = A mineral soil horizon, C = C mineral soil horizon, , La = limnic horizon, and X = unknown horizon. Ob represents a buried organic horizon. A lower case ‘f’ before a horizon code indicates that the sample was frozen when sampled.

Sample Description	A brief description of the sample.
Total carbon %C	Percent by weight of total carbon in an oven-dried soil sample with material >2 mm or 1 cm diameter removed.
Total nitrogen %N	Percent by weight of total nitrogen in an oven-dried soil sample with material >2 mm or 1 cm diameter removed.
LOI	Loss-on-ignition value.
Bulk sample: Fraction Modern (FM)	Fraction modern for bulk soil sample
Bulk sample: $\Delta^{14}C$ (%)	$\Delta^{14}C$ value for bulk soil sample.
Bulk sample: ± $\Delta^{14}C$	Standard deviation of $\Delta^{14}C$ value for bulk soil sample.
Bulk sample: ^{14}C age (yrs)	Radiocarbon age of bulk soil sample.
Datable material: Fraction Modern (FM)	Fraction modern value for datable material (e.g. char, woody debris).
Datable Material: $\Delta^{14}C$ (%)	$\Delta^{14}C$ value for datable material (e.g. char, woody debris).
Datable Material:	Standard deviation of $\Delta^{14}C$ value for datable material (e.g.

± Δ ^{14}C (%)	char, woody debris).
Datable material: ^{14}C age (yrs)	Radiocarbon age of datable material (e.g. char, woody debris).
Datable material: ^{14}C age error (yrs)	Standard deviation of radiocarbon age for datable material (e.g. char, woody debris).
Notes	Description of sample or datable material.

APPENDIX C

DATA STRUCTURE AND CONTENT OF ALL SUPPORTING AND ADDITIONAL DATA STORED ON THE EWING LAB SERVER

Alaska Project
- AGU
  - Abstract Drafts
    - *Drafts for AGU abstract*
  - Presentations
    - *All presentation drafts*
  - *Oral Session Presenter Guidelines*
  - *Torre-Jorgenson-Permafrost Landscapes*
- APEX
  - APEX paper drafts
    - *Drafts for manuscript*
  - APEX-(hardrive from Fairbanks)
    - '*Turetsfield'* hardrive from APEX with all the things you need to know to work at APEX. Eaten By a Bear is the title of folder used to orient new APEX workers
  - Beta manipulation data
    - *Data used for Lillian Aoki's project dealing with the water table manipulation*
  - Bubbles
    - *Data files involving the processing of bubble data before transferred over to a summary data file.*
  - Dailies
    - *Data sheets used to collect daily environmental data measurements*
  - Dating
    - *Data from Miriam Jones for the radiocarbon dating of bog features*
  - Field notes
    - *Scanned copy of both notebook and field sheet notes taken at APEX*
  - Figure Summary Files
    - *Location of the excel sheet used to make manuscript figures*
  - Fluxes
    - *Static chamber flux data files*
  - Gas flux calculation
    - *How we calculated gas fluxes*
  - Hydrophones
    - *Raw hydrophone sound files from download 1*
  - Manual Data Measurements
    - *Files regarding the daily physical data measurements*
  - Methods
    - *Ebullition method drafts*
  - Pictures
    - *Field pictures from Carmel and Rebecca*

Plants
Species composition at APEX sites
Presentations
Drafts for the August presentation to APEX PIs and field crew
Protocol
Field protocols for hydrophones, bubble funnels, and veg survey
Radiocarbon
Necessary paperwork to submit radiocarbon samples
Site Diagram
Powerpoints of APEX site layout..
Summary Report
Field Notebooks
Innoko May2011
Innoko July 2011
Innoko September 2011
Ewing Innoko field notebooks
Innoko
CESU
Coordinates
Discharge Data
Fluxes
Raw data downloaded from IRGAs and very first flux analysis files
For Aiden
All data and information that Ewing lab is sharing with Aiden Johnson
HOBO Dataloggers
HOBO Data
Raw download data files from temperature probes, pressure transducers, and microstations
HOBO Data Crunch
Exported CSV files and the beginning of data analysis
Innoko files SE
Innoko Working Files
Age Model
Dating information from Jen and Miriam
Albedo
Filtered albedo data
Aquastar
Aquastar data files and worked up files
Dissolved Gas-Wickland
Wickland dissolved gas data for Innoko manuscript
ET
Experiment with ET graphs for Innoko manuscript
Figure Summary File

Innoko consolidated file for all data used to make manuscript images.

- Fluxes
    - Gas Flux Calculation
    - NEE modeling
        - *Matlab code and csv files for creating Matlab plots of NEE*
    - *Innoko flux summary datasheets before dumped into Figure Summary Files*
- Harden files Sept-Oct 2012
    - *Age estimate data and peat age models from Jen*
- Hydrophones
    - *Innoko hydrophone data from Ruth*
- Maps
- OC stocks
    - *Jorgenson data for total carbon stocks at Innoko*
- Rain Gauge
    - *Tipping bucket data files*
- Stratigraphy
    - *JH Stratigraphy file*
- Survey
    - *Workup of survey points and elevations of Innoko*
- Temperature
    - *Focused and Complete temperature records*
- Vegetation
- Water level-PTD
    - *Water level data workup before being plugged into Figure Summary file*
- Water Samples
- Wickland Incubation Data
    - *Wickland soil incubation data for Innoko manuscript*

Methane paper drafts
- Author Guidelines
- Coauthor feedback
- Old editions

Microlysimeters

Pictures
- *All Innoko pictures*

Posters & Presentations
- *Presentations from lab members and colleagues*

Radiometer data

Remote Sensing
- *Aiden's projects and Carmel's coursework*

Schedules
Johnston Thesis
Committee Feedback
Literature
Presentation
Thesis Drafts
Thesis Figures
OFR
Jon O'Donnell
Files for Jon O'Donnell's open file data report
Innoko
The beginning of an Innoko OFR

APPENDIX D

SUPPLEMENTAL INFORMATION FOR CHAPTER 2:

BOOTSTRAP VALIDATION OF A RANDOM FOREST ANALYSIS IN THERMOKARST DISTURBED PERMAFROST LANDSCAPE

4.2 Introduction

4.2.1 Permafrost Thaw and Methane Emissions

Permafrost is thawing at an alarming rate, and nearly all permafrost is expected to be gone by the end of the 21st century (Lawrence *et al.* 2008). Methane (CH_4) is an important gas to consider with permafrost thaw, as it is a potent greenhouse gas, responsible for about 20% of greenhouse gas forcing. Thermal, hydrologic and vegetative changes are also known to occur with permafrost thaw (Johnston *et al.* in review., Jorgenson *et al.* 2001, in revision, Turetsky *et al.* 2002, 2008). Warmer soil temperatures and shallower water tables yield greater CH_4 flux and can teeter with the balance between net C sink or source (Johnston *et al.* in review., Turetsky *et al.* 2008, 2002; Treat *et al.* 2007). One of the limitations of on the ground studies is that it is difficult to take numerous measurements because it is often problematic and cost prohibitive to get to remote locations.

This project examined the use of a bootstrap validation of random forest regression to predict CH_4 emissions from a field site in the interior of Alaska. I used field measurements of vegetation cover type and multiple scenes of Landsat throughout the 2011 growing season to run a series of models of observed vs. predicted values. I hypothesize that the true means of observed and predicted values for this methodology would be significantly different from one another (H_0: $\mu_1=\mu_2$, where μ_1 represents the mean observed value, and μ_2 represents the mean predicted value, using a paired t-test). The main objective was to thoroughly analyze this methodology and determine if it could be an effective method for predicting CH_4 emissions in remote areas where field data is less than easy to come by.

4.2.2 Current State of Remote Sensing of Methane Emissions And Boreal Vegetation

Methane production is related to the energy balance at the land surface through the thermal properties of vegetation and soil surfaces that dictate soil temperature and moisture. Remote sensing can detect and monitor changes in land surface structure and function across spatial and temporal scales that cannot be achieved by field measurements, particularly in Arctic regions where areas of interest are not easily accessible (Stow *et al.* 2004). Many studies have looked at the connection between permafrost thaw, vegetation changes, CH_4 flux, and the surface energy balance, but few studies have utilized spatial sciences to scale field observations to broader regions.

Many sensor types can be used to make inferences about land surface features, particularly detecting wetlands and different vegetation types within wetlands (Anderson *et al.* 2010, Anisimov 2007). High resolution imagery is often the best to work with when trying to detect changes at a fine scale; however it is not always possible to obtain such imagery for remote study locations (Anderson *et al.* 2010). Landsat ETM/TM, provides multi-decadal resolution and data continuity that is rarely achieved by flux towers or other observational platforms. Radiometric calibrations can be applied to the Landsat bands to correct radiance values for atmospheric attenuation and derive surface reflectance. The data can then be converted to many informative products that can tell you something about land surface temperature, albedo, and vegetation (Chander *et al.*

2009; Shauai *et al.* 2011; Li 2004; Harris and Bryant 2009). Landsat land surface temperature varies with landscape unit and is positively correlated with albedo as has been found in numerous vegetation change examples worldwide (Juang *et al.* 2007; Yang and Wang 1995).

Vegetation indices can provide a powerful tool for predicting vegetation cover when limited field measurements are available. The most common utilized in boreal vegetation surveys are indices that incorporate various manipulations of the ratio of near-infrared and red spectral responses, the simple ratio (SR) and normalized difference vegetation index (NDVI) (Harris and Bryant 2009). These indices are very well suited for boreal peatlands due to the vegetation that is often associated with different features. Vascular plants, which are often associated with intact permafrost and drying bog features, have a very different reflectance in the red portion of the spectrum than *Sphagnum* species of mosses, which are often associated with wet, active thaw features (Bubier *et al.* 2005). Ecosystem change in the boreal and arctic region can often be best detected by the change of these vascular plants to vegetation with a very different spectral signature such as saturated thaw features (Stow *et al.* 2004).

4.2.3 Remote Sensing Methodologies

Random forest regression is a method that uses a series of predictor variables to describe a response variable. This has been used in many practical applications from mapping invasive vegetation species and distinguishing between specific land use practices to finding nest sites for cavity nesting birds (Lawrence *et al.* 2006; Watts *et al.* 2011; Cutler *et al.* 2007). This method has not been widely used in boreal regions, but it is a potentially useful tool for analyzing spectral data from remote locations. Making inferences about vegetation cover type by either of bootstrap regression or random forest regression can provide necessary information to infer CH_4 emissions from such vegetation.

Bootstrap regression models can be powerful statistical tools to build a sampling distribution when limited field data is available. The methodology involves having a set number of samples collected (n), running a regression on (n-1) samples, and using that regression to predict the value of the remaining sample. This process is then repeated, each time resampling to leave out a different sample. We test for the difference in the regression coefficients to determine how effective the regression is at predicting the 'unknown' sample (Fox 2002). This methodology is not often used in boreal regions, though it can be valuable as field measurements are often limited by time, inaccessibility, and money. Bootstrap regression can be used both to predict vegetation type (Bremond *et al.* 2005) as well as seasonal carbon fluxes (Lund *et al.* 2009).

4.3 Methods

4.3.1 Study Design

The study region is the Innoko Flats National Wildlife Refuge (63.58˚N, 157.72˚W), in the extensive lowlands developed on lacustrine silts south of the Innoko River, an area of degrading peatlands with a continental subarctic climate (United States Department of Interior 1987; Woodward and Beever 2011). Innoko Flats is the fifth largest NWR in the United States with an area of 15,582 km^2 and has no road access.

Over half the refuge is wetlands and much of the area is underlain by discontinuous permafrost. Field measurements (Johnston *et al.,* in review) were taken during three seasonal campaigns, aimed at capturing spring thaw (early June), peak biomass (mid-July), and fall freeze-up (late September). The spatial extent of the study was approximately a 1km by 1km area.

<u>4.3.2 Ancillary Data</u>

Data collection is described in Johnston *et al.*. (in review). Briefly, to capture lowland permafrost thaw dynamics over millennial timescales, we evaluated trace gas fluxes across five landscape units based on feature size and vegetation: unthawed forested plateaus, ombrotrophic bogs at three stages of thaw, and minerotrophic fens. Three field replicates of each landscape unit were identified, for a total of 15 sites. The GPS location of each feature was recorded along with the dominant vegetation types as a categorical variable (1-5) for the five site types. Methane flux measurements were collected at each site over a range of light and temperature conditions throughout the course of each field campaign. All fluxes were measured in diurnal rounds for each replicate set of sites, with four to six measurements of CH_4 flux during a 24 hour period.

Site name, dominant vegetation category, average CH_4 flux, and surface albedo were compiled into a single Excel sheet for each feature from the three field campaigns.

<u>4.3.2 Remotely Sensed Data</u>

Three Landsat 5 and 7 scenes of the study region were acquired from the United States Geological Survey's (USGS) Earth Explorer and imported into ERDAS Imagine.

Only one cloud-free scene was available within the two weeks of each field campaign, dates of images being May 29, 2011, July 2, 2011, and September 19, 2011. These scenes were overlain with coordinates of each feature, taken with a Trimble GeoXH GPS post processed to within one meter. Digital numbers for the seven bands were extracted using ERDAS Imagine "Convert pixel to ASCII" utility for each pixel that a feature was in for each of the three images. Normalized difference vegetation index (NDVI) and albedo in the shortwave (α) were derived using the following equations (Savage *et al.* 2010, Campbell and Wynne 2011)

$$NDVI = \frac{\alpha_4 - \alpha_3}{\alpha_4 + \alpha_3} \quad (4.1)$$

$$\alpha = 0.356\alpha_1 + 0.130\alpha_3 + 0.373\alpha_4 + 0.085\alpha_5 + 0.072\alpha_7 - 0.0018 \quad (4.2)$$

where $\alpha_{\#}$ refers to the digital number in the designated Landsat band

4.3.2 Remotely Sensed Data

A bootstrap verification of random forest was performed in R statistical package (Team 2012). Thirty nine models were created, each withholding one sample to create a model which was then used to predict methane flux of the withheld sample. Predicted values and observed values were compared using a paired t-test and test statistic to determine if each the predicted was significantly different from the field observed values.

4.4 Results and Discussion

The predicted values were not significantly different from field observed values (accept H_0: $\mu_1=\mu_2$, 2-sided p-value = 0.7754, t=-0.2873; df=38, for a paired t-test). It is estimated that the mean difference in CH_4 flux between predicted and observed measurements is 0.08 mg CH_4-C m^{-2} hr^{-1}. A 95% confidence interval for this difference in flux is from -0.682 to 0.513. Because this was an observational study and randomization was incorporated in the study design, causation cannot be inferred, and these results cannot be extended to any area beyond this study area.

Upon looking at the resulting data, careful consideration needs to be taken when interpreting the statistics. This method dramatically over predicted methane flux at very low observation values and severely underestimated flux at the very large observation values (Figure 4.1). This resulted in a net difference across all measurements being very small, even though most of the predictions were not very accurate. I would not recommend using this method if interested in looking specifically at predicting individual landscape units.

This method does have potential if one is only interested in looking at the landscape as a whole. The observed measurements were not randomly selected, as there are a limited number of features in the area, but they were fairly evenly distributed across the landscape. This method came surprisingly close to predicting the actual observed sum for the number of pixels in the analysis, suggesting that with some adjustment, this could become a useful tool for predicting CH_4 emissions on an average basis. It is possible that this is by coincidence because the landscape is comprised of approximately half high producing areas and half low producing areas, which may equate to an averaging effect across the entire area.

The highest percent of variance in the predicted values was explained achieved with this project was 61.04 which is within the range of other random forest and bootstrap analyses (Lawrence *et al.* 2006). Other methods such as cluster analysis, exploratory factor analysis, or confirmatory factor analysis may provide more convincing predictive outcomes than the method tested here.

Table 14 Comparison of observed and predicted CH_4 flux values for each site type.

Site	Slope	Intercept	r^2
Frozen Plateau	-3.29	0.51	0.10
Young Bog	12.28	0.17	0.21
Intermediate Bog	-0.07	2.12	0.04
Old Bog	0.21	0.54	0.00
Fen	0.05	0.59	0.02
All Sites	0.13	0.79	0.06

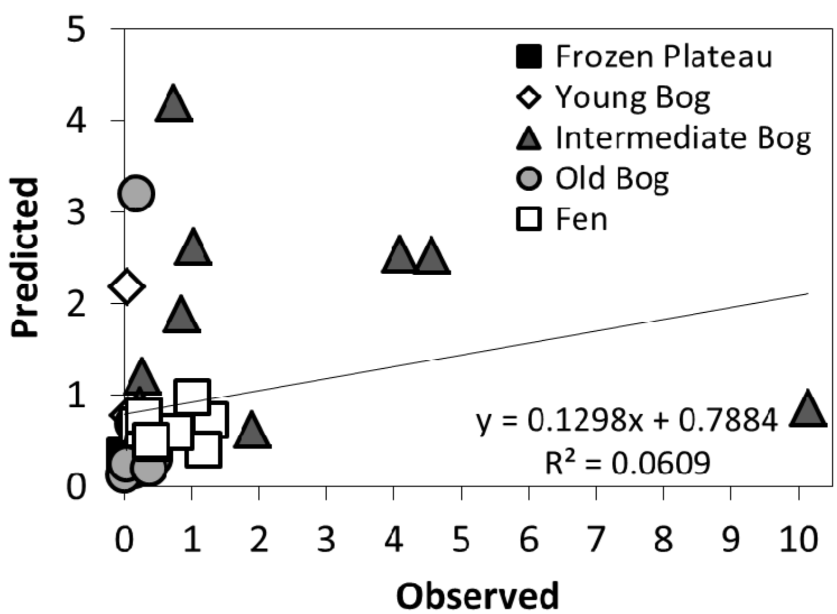

Figure 22. Comparison of observed and predicted CH_4 flux values for each site. Symbols represent similar site types. The best fit line represents a linear fit to the entire data set of observes and predicted values.

APPENDIX E

SUPPLEMENTAL INFORMATION FOR CHAPTER 2:

DRAFT SOIL DATA FOR A COLLAPSE-SCAR BOG CHRONOSEQUENCE IN INNOKO FLATS NATIONAL WILDLIFE REFUGE, ALASKA

Carmel E. Johnston, Jennifer W. Harden, Kristen L. Maines, Stephanie A. Ewing, M. Torre Jorgenson, Jonathan O'Donnell

Introduction

Permafrost soils cover 16% of Earth's surface, but store over half of the world's total belowground carbon (C) (Tarnocai *et al.* 2009, Hugelius *et al.* in revision). Over timescales of decades to centuries, boreal forests have been acting as slight net sinks for C from the atmosphere to land, but periods of disturbance such as drought and severe fire activity can make these systems net sources of C (Harden *et al.* 2000). In northern peatlands, permafrost degradation reorganizes peat hydrology, thermal regimes, and plant species assemblages (Jorgenson *et al.* 2013). This is of particular concern because the area of near-surface permafrost in Arctic and boreal systems has decreased steadily over the past 100 years, and nearly all permafrost is projected to be gone by the year 2100 (Lawrence *et al.* 2008, Heginbottom *et al.* 2013).

Here, we report soil OC inventories from a collapse-scar bog chronosequence located in a peatland ecosystem at Innoko Flats National Wildlife Refuge in Alaska. We sampled organic and mineral soils in lowland black spruce (*Picea mariana*) stands and from collapse-scar bog sites that vary in age since permafrost thaw. These data were originally reported and used to parameterize a mass-balance model of peatland and permafrost OC dynamics in a study by Jorgenson and Harden (201X). Findings from this study indicate that deep OC stocks harbored in Holocene peatland deposits may be vulnerable to thaw and subsequent loss to the atmosphere as CH_4.

Study Region

We conducted our studies in the Innoko National Wildlife Refuges (NWR)), in the extensive lowlands developed on eolian and lacustrine silts south of the Innoko River (Figure 1). The Innoko NWR covers 15,582 km^2, of which over half is wetlands and much of the area is underlain by discontinuous permafrost (USDOI, 1987; Woodward & Beever, 2011). There are abundant thermokarst features in the region, with a range of post-thaw successional stages within close proximity of each other. The Innoko Flats study area (63.58˚N, 157.72˚W; datum = WGS84) is located ~ 150 km south of Galena, and was accessed via floatplane. Logistical support was provided, in part, from the U.S. Fish and Wildlife Service located in Galena. Mean annual precipitation in this region is 445 mm y^{-1} (1971-2000; Riordan *et al.* 2006). The snow depth in April 2011 was 0.60 ± 0.09 m across 18 locations, consistent with previous observations for the refuge (Woodward and Beever 2011).

To capture thaw dynamics of lowland permafrost over millennial timescales, we measured soil hydrologic, thermal and OC dynamics across a permafrost thaw chronosequence. A thaw chronosequence is a series of locations that have similar factors, such as climate, vegetation, slope, and parent material, but differ in age of the landform. Our chronosequence consisted of sites with frozen permafrost plateaus, drying margins, and collapse-scar bogs that varied with respect to time of permafrost thaw and bog initiation (which we refer to as our young, intermediate, and old bog sites). Bog size was used as a proxy for age during bog selection. While all of our sites had similar climate, slope and parent material, vegetation composition differed across landform ages, limiting our ability to isolate the effect of time from vegetation succession. The age of young bogs ranged from 15 to 34 y, as determined by ^{210}Pb analysis of the contact between collapse-scar bog derived limnic peat and forest derived peat. The age of three intermediate (30-590 y) and old bogs (570-1600 y) were determined by radiocarbon (^{14}C) dating of *Sphagnum* moss leaves, amorphous peat rich in roots, or peat picked free of roots from the contact between collapse-scar bog derived limnic peat and forest derived peat. Drying margin sites are transitional between the permafrost plateau and collapse bog sites, where the permafrost has begun thawing but complte subsidence has not yet occurred.

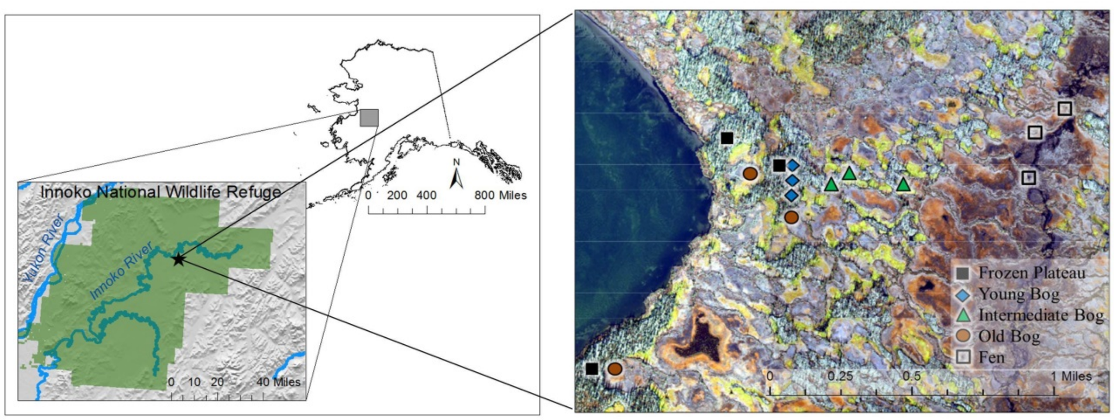

Figure 1. Map of the Innoko National Wildlife Refuge (63.58˚N, 157.72˚W) denoting the position of 2011 field season sampling site located within the refuge (top). Aerial photograph of Innoko study area with locations of each site denoted by symbols. This study area is approximately 24% frozen, 39% bog, 26% fen, and 11% open water, determined by aerial photograph interpretation using a grid overlay.

Vegetation composition varied with landscape position and collapse-scar bog age. Frozen plateaus were dominated by black spruce and and understory of *Ledum* *decumbens, Rubus chamaemorus Sphagnum fuscum,* and *Cladonia* spp. Drying margins of collapse-scar bogs were dominated by *Cladina* spp. (*C. stellaris*, *C. arbuscula*, *C. rangiferina*, *C. mitis*) and *L. decumbens*. Young and intermediate bogs were dominated by *Eriophorum scheuchzeri* and *Sphagnum* spp., including *S. riparium*, and *S. lindbergii*. Old bogs were dominated by *Carex limosa, C. rotundata, Eriophorum scheuchzeri, S. papillosum, and S. majus.*

Soil Sampling

In August and September 2009, we described and sampled soil horizons across a collapse-scar bog chronosequence following USDA-NRCS (Soil Survey Staff, 1998) and Canadian (Soil Classification Working Group, 1998) methodologies. We sampled soil from replicate sites at frozen plateaus (n = 3 sites; site ID = IFUW), drying margins of permafrost plateaus (n = 3; IFUD), young bogs (n = 3; IFUY), intermediate bogs (n = 3; IFIB), old bogs (n = 3; IFOB) and a collapse scar fen (n = 2; IFIF). In collapse-scar bogs, we identified forest peat as organic matter derived from *S. fuscum* and *P. mariana* ecosystems commonly observed on permafrost plateaus, and bog peat as organic matter derived from *Sphagnum spp.* commonly observed at the surface of young, intermediate and old bogs (Figure 1). Fen peat horizons were typically composed of slightly decomposed moss and plant parts, such as *Drepanocladus spp*., *Calliergon* spp., *Menyanthes trifoliata* and *Carex limosa*. Mineral soil horizons (A, B, C) were characterized for texture and the presence of buried organic material. We also described and sampled lacustrine (or limnic) sediment below peat deposits. We used modified soil horizon codes according to the following scheme:

L Live moss, which are green and generally contain some leaf and needle litter.

D Dead moss, which is comprised of non- or slightly-decomposed dead moss. The dead moss layer is characterized by fibric organic horizons that contain more moss than roots.

F Fibric (according to Canadian soil system) or fibrous organic layers, which vary in degree of decomposition but in which roots are more abundant than recognizable moss parts. In most cases these layers would be considered Oi layers (U.S. soil system) or upper duff (U.S.F.S. system).

M Mesic (according to Canadian soil system) organic layers, which are moderately decomposed with few if any recognizable plant parts other than roots. M layers are generally Oe horizons (U.S. soil system) or lower duff layers (U.S.F.S. system).

H Humic (Canadian soil system) or sapric organic layers, which are highly decomposed. This layer generally smears upon squeezing and has no recognizable plant parts. H layers are generally Oa horizons (U.S. soil system) or lower duff (U.S.F.S. soil system) layers.

A Mineral soil that forms at the surface or below organic horizons (U.S. and Canadian soil system), with less than 20% organic matter, as judged in the field.

B Mineral soil that has formed below an A horizon (U.S. and Canadian soil system), with little or none of its original rock structure.

C Mineral soil that has been little affected by pedogenic processes (U.S. and Canadian soil system).

LT Litter layer (dead leaves, twigs, etc.)

LN Lichen

La Limnic sediments

DN Dead lichen, which is comprised of non- or slightly-decomposed dead lichen. The dead moss layer is characterized by fibric organic horizons that contain more lichen than roots.

Frozen samples were described with a lower case "f" preceeding the horizon code. All horizons within a soil profile were sampled for bulk density, analytical purposes, and to determine moisture content.

At all sites, organic soil was sampled using a variety of soil knives, scissors and corers, in order to obtain a sample of known volume. For easily compressible, low-density samples, soil blocks were cut with scissors or serrated knives and dimensions were measured with a ruler. For less compressible shallow soils, samples were obtained with a 50 mm diameter corer rotated with a portable electric drill (Nadler and Wein, 1998). For deeper unfrozen peats we used a 70 mm diameter by 130-cm-long tube that was pushed and rotated into the peat by hand. A rubber cap was tightened over the corer to maintain a vacuum in the corer during extraction. At permafrost plateau sites, permafrost cores (up to 5 m) were obtained using a SIPRE (Snow, Ice, and Permafrost Research Establishment) corer (7.5 cm inside diameter) with a Tanaka power head. We sampled peat until either a basal mineral or limnic horizon was encountered to allow calculation of OC stocks relative to a standard basal layer across sites. Samples were placed in clean ziplock bags and shipped soon after collection to USGS laboratories in Menlo Park, CA.

Soil Sample Preparation and Drying

Upon arrival of samples to the laboratory, samples were inventoried using the field sheets. All samples were placed on open shelves in an isolated room and allowed to air dry to a constant weight, as determined by weights obtained at least one week apart. Temperature during air-drying ranged from 20 to 30 °C. After air-drying, samples were oven dried for 48 hours in a forced-draft oven. Samples that were classified as organic soil horizons (e.g., moss, litter) were oven dried at 65 °C to avoid loss or alteration of organic matter by oxidation or decomposition. The remaining samples were oven dried at 105 °C.

After oven-drying, samples were thoroughly mixed, then split into subsamples for analysis and archiving (archive fractions of most of the samples described here are available by contacting J. Harden at the Menlo Park, CA office of USGS). These samples were then processed one of two ways, depending on horizon code. Mineral samples were gently crushed using a mortar and pestle, being careful to break only aggregates, and then sieved using a 2 mm screen. Soil particles not passing the 2 mm screen were removed, weighed, and saved separately. Soil passing the 2 mm screen was then ground by hand using a mortar and pestle to pass through a 60 mesh (0.246 mm) screen. The ground material was mixed and placed in a labeled, glass sample bottle for subsequent analyses. Organic samples were weighed and roots greater than 1 cm in diameter were removed, weighed, and saved separately. The remaining sample was then milled in an Udy Corporation Cyclone mill (Ft. Collins, CO) to pass through a 0.5 mm screen. The milled sample was thoroughly mixed and a representative sample placed in a labeled, glass sample bottle for analytical chemistry.

Soil Carbon and Nitrogen Measurements

A Carlo Erba NA1500 elemental analyzer (EA) was used to determine total C and total N. We analyzed soil samples for total carbon and nitrogen using a Carlo Erba NA1500 elemental analyzer. We assumed that total carbon was equal to organic carbon, given the low pH of soil samples (pH < 6). Samples were combusted in the presence of excess oxygen. The resulting sample gasses were swept in a continuous flow of helium through an oxidation furnace, followed by a reduction furnace, to yield CO_2, N_2 and water vapor. Water was removed by a chemical trap and CO_2 and N_2 were chromatographically separated before the quantification of C and N (Pella, 1990a, b).

All samples were compared to a main working standard, ethylene diamine tetra-acetic acid (EDTA), which has been calibrated through a set of international standards. The chemical formula for this compound corresponds to a C concentration of 41.09 percent and N concentration of 9.59 percent Additional working standards were analyzed as samples in all runs to check consistency and overall precision. Peach tree leaves (SRM-1547), issued by the National Institue of Standards and Technology (NIST), were included in runs comprised of organic soil. A marine sediment (MESS-1), issued by the Chemistry Division of the Canadian National Research Council, were included runs comprised of mineral soils. Certified values for these standards were obtained from Becker (1990) and Govindaraju (1989), respectively.

Radiocarbon measurements

We analyzed radiocarbon (^{14}C) content on a subset of soil samples to evaluate accumulation rates and turnover times of organic carbon, to determine the age of intermediate and old bog formation, and to determine the basal age of peat across study sites. When possible, we collected *Sphagnum spp*. moss parts for ^{14}C analysis. To determine carbon accumulation rates in permafrost plateaus, we analyzed the ^{14}C content of 12 organic matter samples spanning depths of 2 cm to 405 cm below the ground surface. To age collapse-scar bogs, we analyzed ^{14}C content of organic matter at the interface of peat derived from forest and collapse-scar bog vegetation. When field sampling permitted, we also analyzed ^{14}C content of the lacustrine sediments (limnic, silt) beneath peat deposits. Graphitization at the USGS in Reston, VA, then samples were sent to the Center for Accellerator Mass Spectrometry (CAMS) at Lawrence Livermore National Laboratory in Livermore, CA for analysis as described in Southon *et al.*., 2004. Organic matter was combusted at 900°C in evacuated, sealed quartz tubes in the presence of cupric acid (CuO) and silver (Ag) wire. Following cryogenic purification, carbon dioxide was reduced to graphite in a reaction at 500-550 °C using the sealed tube Zn reduction method. Radiocarbon data are reported as $\Delta^{14}C$, or the per mil deviation of the $^{14}C/^{12}C$ ratio in the sample from that of an oxalic standard that has been decay corrected to 1950 (Stuiver and Polach, 1977). The $\Delta^{14}C$ values we report have been corrected for mass-dependent fractionation using the *in situ* simultaneous AMS $\delta^{13}C$ measurement.

Age interpretation of organic matter samples with modern $\Delta^{14}C$ signatures typically requires additional information, given the non-uniqueness of calculated turnover times and ages.

Data-set descriptions

There are three separate downloadable files containing the soil data collected from the sites described in this report. Appendix 2 describes in detail the data within the following three spreadsheet files: (1) InnokoFlats_Field, contains field descriptions, such as root abundance, color, and soil texture, of the sampled soils; (2) InnokoFlats_Physical contains physical descriptions of the samples, such as volumetric field moisture and bulk density, (3) InnokoFlats _Chemistry contains elemental C, elemental N, $\Delta^{14}C$ of soil organic matter, and loss on ignition (LOI) values.

Acknowledgements

We thank, Misha Kanevskiy and Kim Wickland for their assistance in the field and Xiaomei Xu for analysis of soil samples for radiocarbon at the Lawrence Livermore National Labs. This research was funded by the United States Geological Survey, the Bonanza Creek LTER (Long-Term Ecological Research) program (funded jointly by NSF grant EAR #0630319 and DBI #1021095). Additional assistance was provided by the North and West Alaska Cooperative Ecosystems Studies Unit, and crucial logistical support by the US Fish and Wildlife Service

REFERENCES CITED

Anderson K, Bennie J J, Milton E J, Hughes P D M, Lindsay R and Meade R 2010 Combining LiDAR and IKONOS data for eco-hydrological classification of an ombrotrophic peatland. *Journal of environmental quality* **39** 260–73

Anisimov O a 2007 Potential feedback of thawing permafrost to the global climate system through methane emission *Environmental Research Letters* **2** 045016

Appleby P G and Oldfield F 1978 The calculation of lead-210 dates assuming a constant rate of supply of unsupported ^{210}Pb to the sediment *Catena* **5** 1–8

Becker, D.A., 1990, Homogeneity and evaluation of the new NIST leaf certified reference materials, in Nuclear analytical methods in the life sciences, Gaithersburg, MD, National Institute of Standards, p. 571-577.

Bonan G B, Pollard D and Thompson S L 1992 Effect of boreal forest vegetation on global climate *Nature* **359** 719–718

Bremond L, Alexandre A, Peyron O and Guiot J 2005 Grass water stress estimated from phytoliths in West Africa *Journal of Biogeography* **32** 311–27

Briegleb B and Ramanathan V 1982 Spectral and Diurnal Variations in Clear Sky Planetary Albedo *Journal of Applied Meteorology* **21** 1160–71

Bubier J L, Moore T, Savage K and Crill P 2005 A comparison of methane flux in a boreal landscape between a dry and a wet year *Global Biogeochemical Cycles* **19** 1–11

Camill, P. 2005. Permafrost thaw accelerates in boreal peatlands during late-20th century climate warming. Climatic Change 68: 135-152.

Campbell J B and Wynne R H 2011 *Introduction to Remote Sensing*

Cao M, Marshall S and Gregson K 1996 Global carbon exchange and methane emissions from natural wetlands: Application of a process-based model *Journal of Geophysical Research* **101** 14,399–14,414

Carroll P and Crill P M 1997 Carbon balance of a temperate poor fen period *Global Biogeochemical Cycles* **11** 349–56

Chander G, Markham B L and Helder D L 2009 Summary of Current Radiometric Calibration Coefficients for Landsat MSS, TM, ETM+, and EO-1 ALI sensors *Remote Sensing of Environment* **1** 1–24

Christensen T R and Panikov N 2003 Biotic controls on CO_2 and CH_4 exchange in wetlands – a closed environment study *Biogeochemistry* **64** 337–54

Coakley J A 2003 Reflectance and albedo, surface *Encyclopedia of the Atmosphere* 1914–23

Committee, C.A.S.C. The Canadian system of soil classification. Ontario (Canada): NRC Canada Research Press. p. 1-187.

Cronk J and Fennessy M 2001 *Wetland plants: biology and ecology* (CRC Press LLC)

Cutler D R, Edwards T C, Beard K H, Cutler A, Hess K T, Gibson J and Lawler J J 2007 Random forests for classification in ecology. *Ecology* **88** 2783–92

Dise N B, Gorham E and Verry E S 1993 Environmental factors controlling methane emissions from peatlands in northern Minnesota *Journal of Geophysical Research* **98** 10583

Dunn A L, Barford C C, Wofsy S C, Goulden M L and Daube B C 2007 A long-term record of carbon exchange in a boreal black spruce forest: means, responses to interannual variability, and decadal trends *Global Change Biology* **13** 577–90

Fox J 2002 Bootstrapping Regression Models *An R and S-PLUS Companion to Applied Regression* pp 1–14

Froese D G, Westgate J A, Reyes A V., Enkin R J and Preece S J 2008 Ancient permafrost and a future, warmer Arctic. *Science* **321** 1648

Frolking S, Talbot J, Jones M C, Treat C C, Kauffman J B, Tuittila E and Roulet N 2011 Peatlands in the Earth's 21st century climate system *Environmental Review* **19** 371–96

Goodrich J P, Varner R K, Frolking S, Duncan B N and Crill P M 2011 High-frequency measurements of methane ebullition over a growing season at a temperate peatland site *Geophysical Research Letters* **38** 1–5

Gorham E 2013 Northern peatlands: role in the carbon cycle and probable responses to climatic warming *Ecological Society of America* **1** 182–95

Govindaraju, K., 1989, Compliation of working value and sample description for 272 geostandards: Geostandards Newsletter, v. 13, p. 1-113.

Grosse G, Harden J, Turetsky M, McGuire A D, Camill P, Tarnocai C, Frolking S, Schuur E A G, Jorgenson T, Marchenko S, Romanovsky V, Wickland K P, French N, Waldrop M, Bourgeau-Chavez L L and Striegl R G 2011 Vulnerability of high-latitude soil organic carbon in North America to disturbance *Journal of Geophysical Research* **116** 1–23

Harden J W, Mark R K M, Sundquist E T and Stallard R F 1992 Dynamics of soil carbon during deglaciation of the laurentide ice sheet. *Science (New York, N.Y.)* **258** 1921–4

Harden J W, Trumbore S E, Stocks B J, Hirsch A, Gower S T, O'Neill K P and Kasischke E S 2000 The role of fire in the boreal carbon budget *Global Biogeochemical Cycles* **6** 174–84

Harris A and Bryant R G 2009 Northern Peatland Vegetation and the Carbon Cycle : A Remote Sensing Approach *Geophysical Monography Series* **184** 79–98

Heginbottom, J. A., Brown, J., Humlum, O., & Svensson, H. (2013). *State of the Earth's Cryosphere at the Beginning of the 21st Centry: Glaciers, Global Snow Cover, Floating Ice, and Permafrost and Periglacial Environments- Permafrost and Periglacial Environments* (pp. 1–78).

Heikkinen J E P, Maljanen M, Aurela M, Hargreaves K J and Martikainen P J 2002 Carbon dioxide and methane dynamics in a sub-Arctic peatland in northern Finland *Polar Research* **21** 49–62

Heyer J, Berger U, Kuzin I L and Yakovlev O N 2002 Methane emissions from different ecosystem structures of the subarctic tundra in Western Siberia during midsummer and during the thawing period *Tellus* **54** 231–49

Hinzman L D, Bettez N D, Bolton W R, Chapin F S, Dyurgerov M B, Fastie C L, … Yoshikawa K 2005 Evidence and Implications of Recent Climate Change in Northern Alaska and Other Arctic Regions *Climatic Change* **72** 251–98

Hinzman L D, Viereck L A, Adams P C, Romanovsky V E and Yoshikawa K 2006 Climatic and Permafrost Dynamics of the Alaskan Boreal Forest *Alaska's Changing Boreal Forest* ed F S C III, M W Oswood, K V Cleve, L A Viereck and D Verbyla (Oxford, United Kingdon) pp 39–61

Hua Q and Barbetti M 2004 Review of tropospheric bomb ^{14}C data for carbon cycle modeling and age calibration purposes *Radiocarbon* **46** 1273–98

Hugelius G, Tarnocai C, Bockheim J, Camill P, Elberling B, Grosse G, Harden J, Johnson K, Jorgenson T, Koven C, Kuhry P, Michaelson G, Mishra U, Palmtag J, Ping C-L, O'Donnell J, Schirrmeister L, Schuur E, Sheng Y, Smith L, Strauss J and Yu Z Short communication: A new dataset for estimating organic carbon storage to 3 m depth in soils of the northern circumpolar permafrost region *Earth System Science Data Discussions* **6**

Johnston C E, Ewing S A, Harden J W, Stoy P C, Ruth R K, Wickland K P, Koch J C, Fuller C C and Jorgenson M T Effect of permafrost thaw on CO_2 and CH_4 exchange in a western Alaska peatland chronosequence *Environmental Research Letters*

Johnson K D, Harden J W, McGuire A D, Clark M, Yuan F and Finley A Permafrost and organic layer interactions over a climate gradient in a discontinuous permafrost zone *Environmental Research Letters* in review

Jorgenson M T, Harden J, Kanevskiy M, Donnell J O, Wickland K, Ewing S, Manies K, Zhuang Q, Shur Y, Striegl R and Koch J 2013 Reorganization of vegetation , hydrology and soil carbon after permafrost degradation across heterogeneous boreal landscapes *Environmental Research Letters* **8** 1–13

Jorgenson M T, Harden J, Kanevskiy M, Donnell J O, Wickland K, Ewing S, Manies K, Zhuang Q, Shur Y, Striegl R and Koch J 2013. Reorganization of vegetation , hydrology and soil carbon after permafrost degradation across heterogeneous boreal landscapes. *Environmental Research Letters*, *8*(035017), 1–13. doi:10.1088/1748-9326/8/3/035017

Jorgenson M T and Osterkamp T E 2005 Response of boreal ecosystems to varying modes of permafrost degradation *Canadian Journal of Forestry Research* **35** 2100–11

Jorgenson M T, Racine C H, Walters J C and Osterkamp T E 2001 Permafrost degradation and ecological changes associated with a warming climate in central alaska *Climate Change* **48** 551–79

Jorgenson M T, Romanovsky V, Harden J, Shur Y, O'Donnell J A, Schuur E A G, Kanevskiy M and Marchenko S 2010 Resilience and vulnerability of permafrost to climate change *Canadian Journal of Forestry Research* **40** 1219–36

Juang J-Y, Katul G, Siqueira M, Stoy P and Novick K 2007 Separating the effects of albedo from eco-physiological changes on surface temperature along a successional chronosequence in the southeastern United States *Geophysical Research Letters* **34** 1–5

Kane E S, Chivers M R, Turetsky M R, Treat C C, Petersen D G, Waldrop M P, Harden J W and McGuire A D 2013 Response of anaerobic carbon cycling to water table maniplation in an Alaskan rich fen *Soil Biology and Biochemistry* **58** 50–60

Kanevskiy M, Jorgenson T, Shur Y, O'Donnell J, Harden J, Zhuang Q and Fortier D Cryostratigraphy and Permafrost Evolution in Lacustrine Lowlands of West-Central Alaska *Permafrost and Pariglacial Processes* in review

Kanevskiy M, Shur Y, Fortier D, Jorgenson M T and Stephani E 2011 Cryostratigraphy of late Pleistocene syngenetic permafrost (yedoma) in northern Alaska, Itkillik River exposure *Quaternary Research* **75** 584–96

Koven C D, Ringeval B, Friedlingstein P, Ciais P, Cadule P, Khvorostyanov D, Krinner G and Tarnocai C 2011 Permafrost carbon-climate feedbacks accelerate global warming. *Proceedings of the National Academy of Sciences of the United States of America* **108** 14769–74

Lawrence D M, Slater A G, Romanovsky V E and Nicolsky D J 2008 Sensitivity of a model projection of near-surface permafrost degradation to soil column depth and representation of soil organic matter *Journal of Geophysical Research* **113** 1–14

Lawrence, D. M., Slater, A. G., Romanovsky, V. E., & Nicolsky, D. J. (2008). Sensitivity of a model projection of near-surface permafrost degradation to soil column depth and representation of soil organic matter. *Journal of Geophysical Research*, *113*(F2), 1–14. doi:10.1029/2007JF000883

Lawrence R L, Wood S D and Sheley R L 2006 Mapping invasive plants using hyperspectral imagery and Breiman Cutler classifications (randomForest) *Remote Sensing of Environment* **100** 356–62

Li F 2004 Deriving land surface temperature from Landsat 5 and 7 during SMEX02/SMACEX *Remote Sensing of Environment* **92** 521–34

Limpens J, Berendse F, Blodau C, Canadell J G, Freeman C, Holden J, Roulet N, Rydin H and Schaepman-Strub G 2008 Peatlands and the carbon cycle: from local processes to global implications – a synthesis *Biogeosciences* **5** 1475–91

Lohila A, Aurela M, Regina K and Laurila T 2003 Soil and total ecosystem respiration in agricultural fields : effect of soil and crop type *Plant and Soil* **251** 303–17

Lund M, Lafleur P M, Roulet N T, Lindroth A, Christensen T R, Aurela M, Chojnicki B H, Flanagan L B, Humphreys E R, Laurila T, Oechel W C, Olejnik J, Rinne J, Schubert P and Nilsson M B 2009 Variability in exchange of CO2 across 12 northern peatland and tundra sites *Global Change Biology* **16** 2436–48

MacDonald G M, Beilman D W, Kremenetski K V, Sheng Y, Smith L C and Velichko A a 2006 Rapid early development of circumarctic peatlands and atmospheric CH_4 and CO_2 variations. *Science (New York, N.Y.)* **314** 285–8

Mastepanov M, Sigsgaard C, Dlugokencky E J, Houweling S, Ström L, Tamstorf M P and Christensen T R 2008 Large tundra methane burst during onset of freezing *Nature* **456** 628–30

Myers-Smith I H, Harden J W, Wilmking M, Fuller C C, McGuire A D and Chapin III F S 2008 Wetland succession in a permafrost collapse : interactions between fire and thermokarst *Biogeosciences* **5** 1273–86

Nadler, I.A., and Wein, R.W., 1998, A new forest floor corer for rapid sampling, minimal disturbance and adequate precision: Silva Fennica, v. 32, no. 4, p. 373-381.

O'Donnell J A, Aiken G R, Kane E S and Jones J B 2010 Source water controls on the character and origin of dissolved organic matter in streams of the Yukon River basin, Alaska *Journal of Geophysical Research* **115** 1–12

O'Donnell J A., Harden J W, McGuire A. D, Kanevskiy M Z, Jorgenson M T and Xu X 2011b The effect of fire and permafrost interactions on soil carbon accumulation in an upland black spruce ecosystem of interior Alaska: implications for post-thaw carbon loss *Global Change Biology* **17** 1461–74

O'Donnell J A, Harden J W, McGuire A D and Romanovsky V E 2011a Exploring the sensitivity of soil carbon dynamics to climate change, fire disturbance and permafrost thaw in a black spruce ecosystem *Biogeosciences* **8** 1367–82

O'Donnell J A, Jorgenson M T, Harden J W, McGuire a. D, Kanevskiy M Z and Wickland K P 2011 The Effects of Permafrost Thaw on Soil Hydrologic, Thermal, and Carbon Dynamics in an Alaskan Peatland *Ecosystems* **15** 213–29

Olefeldt D, Turetsky M R, Crill P M and McGuire a D 2012 Environmental and physical controls on northern terrestrial methane emissions across permafrost zones *Global Change Biology* **19** 589–603

Olefeldt D, Turetsky M R, Crill P M and McGuire a D 2012 Environmental and physical controls on northern terrestrial methane emissions across permafrost zones *Global Change Biology* **19** 589–603

Oleson K W, Lawrence D M, Bonan G B, Drewniak B, Huang M, Koven C D, Levis S, Li F, Riley W J, Subin Z M, Swenson S C, Thornton P E, Bozbiyik A, Fisher R, Heald C L, Kluzek E, Lamarque J-F, Lawrence P J, Leung L R, Lipscomb W, Muszala S, Ricciuto D M, Sacks W, Sun Y, Tang J and Yang Z-L 2013 Technical Description of Version 4.5 of the Community Land Model (CLM) *NCAR/TN-503+STR* pp 1-434

Osterkamp T 2005 The recent warming of permafrost in Alaska *Global and Planetary Change* **49** 187–202

Osterkamp T E, Jorgenson M T, Schuur E A G, Shur Y L, Kanevskiy M Z and Vogel J G 2009 Physical and ecological changes associated with warming permafrost and thermokarst in Interior Alaska *Permaforst and Periglacial Processes* **256** 235–56

Payette, S., Delwaide, A., Caccianiga, M., Beauchemin, M. 2004. Accelerated thawing of subarctic peatland permafrost over the last 50 years. Geophysical Research Letters 31: doi:10.1029/2004GL020358.

Pella, E., 1990a, Elemental organic analysis. Part 1: Historical developments: American Laboratory, v. 22, no. 2, p. 116-125.

Pella, E., 1990b, Elemental organic analyzer. Part 2: State of the art: American Laboratory, v. 22, no. 12, p. 28-32.

Potter C S 1997 An ecosystem simulation model for methane production and emission from wetlands *Global Biogeochemical Cycles* **11** 495

Qin D, Manning M, Marquis M and Averyt K 2007 *Climate Change 2007: The Physical Science Basis* (Cambridge University Press)

Reichstein M, Stoy P C, Desai A R, Lasslop G and Richardson A D 2012 Chapter 9 Partitioning of Net Fluxes *Eddy Covariance: A Practical Guide to Measurement and Data Analysis* ed M Aubinet, T Vesala and D Papale (Dordrecht: Springer Netherlands) pp 263–89

Reimer P J, Brown T A and Reimer R W 2004 Discussion : Reporting and calibration of post-bomb 14C data *Lawrence Livermore National Labs*

Riordan B, Verbyla D and McGuire A. D 2006 Shrinking ponds in subarctic Alaska based on 1950–2002 remotely sensed images *Journal of Geophysical Research* **111** 1–11

Roulet N T, Lafleur P M, Richard P J H, Moore T R, Humphreys E R and Bubier J L 2007 Contemporary carbon balance and late Holocene carbon accumulation in a northern peatland *Global Change Biology* **13** 397–411

Savage S L, Lawrence R L, Custer S G, Jewett J T, Powell S L and Shaw J a. 2010 Review of Alternative Methods for Estimating Terrestrial Emittance and Geothermal Heat Flux for Yellowstone National Park Using Landsat Imagery *GIScience & Remote Sensing* **47** 460–79

Schuur E A. G, Abbott B W, Bowden W B, Brovkin V, Camill P, Canadell J G, … Zimov S A. 2013 Expert assessment of vulnerability of permafrost carbon to climate change *Climatic Change* **119** 359–74

Schuur E A G, Bockheim J G, Canadell J G, Euskirchen E, Field C B, Goryachkin S V., Hagemann S, Kuhry P, Lafleur P M, Lee H, Mazhitova G, Nelson F E, Rinke A, Vladimir E, Shiklomanov N, Tarnocai C, Venevsky S, Vogel J G and Zimov S A 2008 Vulnerability of permafrost carbon to climate change : implications for the global carbon cycle *Bioscience* **58** 701–14

Shauai Y, Masek J G, Gao F and Schaaf C B 2011 An algorithm for the retrieval of 30-m snow-free albedo from Landsat surface reflectance and MODIS BRDF *Remote Sensing of Environment* **115** 2204–16

Smith L C, MacDonald G M, Velichko A A, Beilman D W, Borisova O K, Frey K E, Kremenetski K V and Sheng Y 2004 Siberian peatlands a net carbon sink and global methane source since the early Holocene. *Science (New York, N.Y.)* **303** 353–6

Staff, S.S. 1998. Keys to Soil Taxonomy. Blacksburg (VA): Pocahontas Press, Inc. 599 p.

Strack M and Waddington J M 2007 Response of peatland carbon dioxide and methane fluxes to a water table drawdown experiment *Global Biogeochemical Cycles* **21** GB1007

Stow D a, Hope A, McGuire D, Verbyla D, Gamon J, Huemmrich F, Houston S, Racine C, Sturm M, Tape K, Hinzman L, Yoshikawa K, Tweedie C, Noyle B, Silapaswan C, Douglas D, Griffith B, Jia G, Epstein H E, Walker D, Daeschner S, Petersen A, Zhou L and Myneni R 2004 Remote sensing of vegetation and land-cover change in Arctic Tundra Ecosystems *Remote Sensing of Environment* **89** 281–308

Stoy P C, Street L E, Johnson A V., Prieto-Blanco A and Ewing S A 2012 Temperature, heat flux, and reflectance of common subarctic mosses and lichens under field conditions: might changes to community composition impact climate-relevent surface fluxes? *Arctic, Antarctic, and Alpine Research* **44** 500–8

Stuvier, M., and Polach, H.A., 1977, Discussion: reporting of ^{14}C data: Radiocarbon, v. 19, p. 355-363.

Talling F 1961 Photosynthesis under natural conditions *Annual Review Plant Physiology* **12** 133–54

Tarnocai C, Canadell J G, Schuur E A G, Kuhry P, Mazhitova G and Zimov S A 2009 Soil organic carbon pools in the northern circumpolar permafrost region *Global Biogeochemical Cycles* **23** 1–11

Tarnocai, C., Canadell, J. G., Schuur, E. A. G., Kuhry, P., Mazhitova, G., & Zimov, S. A. (2009). Soil organic carbon pools in the northern circumpolar permafrost region. *Global Biogeochemical Cycles*, *23*(2), 1–11. doi:10.1029/2008GB003327

Tokida T, Miyazaki T, Mizoguchi M, Nagata O, Takakai F, Kagemoto A and Hatano R 2007a Falling atmospheric pressure as a trigger for methane ebullition from peatland *Global Biogeochemical Cycles* **21** GB2003

Tokida T, Mizoguchi M, Miyazaki T, Kagemoto A, Nagata O and Hatano R 2007b Episodic release of methane bubbles from peatland during spring thaw. *Chemosphere* **70** 165–71

Torn M and Chapin III F S 1993 Environmental and biotic controls over methane flux from arctic tundra *Chemosphere* **26** 357–68

Treat C C, Bubier J L, Varner R K and Crill P M 2007 Timescale dependence of environmental and plant-mediated controls on CH_4 flux in a temperate fen *Journal of Geophysical Research* **112** 1–9

Turetsky M R, Treat C C, Waldrop M P, Waddington J M, Harden J W and McGuire A D 2008 Short-term response of methane fluxes and methanogen activity to water table and soil warming manipulations in an Alaskan peatland *Journal of Geophysical Research* **113** 1–15

Turetsky M R, Wieder R K and Vitt D H 2002 Boreal peatland C fuxes under varying permafrost regimes *Soil Biology and Biochemistry* **34** 907–12

United States Department of Interior 1987 Innoko National Wildlife Refuge Comprehensive Consrevaation Plan, Environmental Impact Statement, Wilderness Review *Fish and Wildlife Service*

Viereck, L.A., Dyrness, C.T., Batten, A.R., and Wenzlick, K.J., 1992, The Alaska Vegetation Classification: General Technical Report PNW-GTR-286, U.S. Department of Agriculture, Forest Service, Pacific Northwest Research Station.

Waldrop M P, Harden J W, Turetsky M R, Peterson D G, McGuire A D, Briones M J, Churchill A C, Doctor D H and Pruett L E 2012 Bacterial and enchytraeid abundance accelerate soil carbon turnover along a lowland vegetation gradient in interior Alaska *Soil Biology and Biochemistry* **50** 188–98

Watts J D, Powell S L, Lawrence R L and Hilker T 2011 Improved classification of conservation tillage adoption using high temporal and synthetic satellite imagery *Remote Sensing of Environment* **115** 66–75

Whalen S C 2005 Biogeochemistry of methane exchange between natural wetlands and the atmosphere *Environmental Engineering Science* **22** 73–94

Wickland K P, Striegl R G, Neff J C and Sachs T 2006 Effects of permafrost melting on CO2 and CH4 exchange of a poorly drained black spruce lowland *Journal of Geophysical Research* **111** 1–13

Wille C, Kutzbach L, Sachs T, Wagner D and Pfeiffer E-M 2008 Methane emission from Siberian arctic polygonal tundra: eddy covariance measurements and modeling *Global Change Biology* **14** 1395–408

Williams M, Street L E, Wijk M T and Shaver G R 2006 Identifying differences in carbon exchange among arctic ecosystem types *Ecosystems* **9** 288–304

Woodward A and Beever E A 2011 Conceptual Ecological Models to Support Detection of Ecological Change on Alaska National Wildlife Refuges *United States Geological Survey*

Yang J and Wang Y Q 1995 Estimation of land surface temperature using Landsat-7 ETM+ thermal infared and weather station data

Zak D R and Kling G W 2006 Microbial Community Composition and Function across an Arctic Tundra Landscape *Ecological Society of America* **87** 1659–70

Zhuang Q, Melillo J M, McGuire A D, Kicklighter D W, Prinn R G, Steudler P A, Felzer B S and Hu S 2007 Net emissions of CH_4 and CO_2 in Alaska: implications for the region's greenhouse gas budget *Ecological Applications* **17** 203–12